Cooperative Mobile Robot and Manipulator System for Autonomous Manufacturing

MANMAN YANG

Department of Design, Manufacturing and Engineering Management
University of Strathclyde, Glasgow

A thesis presented in partial fulfilment of the requirements for
the degree of Doctor of Philosophy

May 10, 2024

Declaration

This thesis is the result of the author's original research. It has been composed by the author and has not been previously submitted for examination which has led to the award of a degree.

Copyright Statement

Signed: Manman Yang Date: May 10, 2024

Abstract

Autonomous manufacturing is broadly defined as a set of manufacturing practices with the wide adoption of advanced autonomous technologies, e.g., autonomous robotic systems. With the purpose of shaping future manufacturing operations, autonomous manufacturing plays a pivotal role on the fourth industrial evolution. In advanced manufacturing contexts, fixed, static and inflexible transportation systems such as conveyor belt refrain the greater performances and efficiency of large-scale fixed-base robotic manipulators in autonomous manufacturing. Mobile robots, as flexible and movable platforms, can be cooperated with the fixed-base robotic manipulator to perform both material transportation and material handling tasks at production lines. However, due to the many technologies involved, material transportation by the mobile robot and material handling by the fixed-base robotic manipulator have not been studied on how to develop a holistic, integrated, cooperative and autonomous robotic system. To solve this challenging issue, a strategy that is capable of seamlessly integrating different modules into a cooperative mobile robot and manipulator system (Co-MRMS) and provides autonomous material transportation with sufficiently accurate and robust capabilities for material positioning, is required to investigate. This thesis deals with the system integration and performance improvement for a Co-MRMS which contains a fixed-base robotic manipulator and a mobile robot. Compared to previous works, this research is focused on the specific challenges arising from heterogeneous robots that must be coordinated along with the complex set of

tasks required for autonomous manufacturing applications.

In this thesis, a new integrated simulation framework is proposed to comprehensively demonstrate the cooperative concepts of the whole proposed Co-MRMS which integrates a mobile robot with a fixed-base manipulator. Furthermore, to validate the feasibility of the proposed Co-MRMS, a case study on robotic material transportation and composite lay-up, which is based on a real-world scenario commonly found in advanced composite manufacturing, is investigated. The simulation-based results demonstrate promising features of the proposed Co-MRMS.

From this simulation-based case study, a flexible and efficient interaction mode is designed for the proposed Co-MRMS and a novel positioning system is developed for the relative positioning between the mobile robot and the fixed-base robotic manipulator. In the developed positioning system, a new two-stage positioning framework with multi-sensor fusion positioning is proposed, which contains two different kinds of localization approaches for the robotic manipulator continually perceiving the mobile robot. One positioning approach is ultrasonic sensors fused with an inertial measurement unit (IMU) by using the filtered extended Kalman filter (EKF) algorithm and another positioning approach is vision-based positioning by identifying ArUco marker. Crucially, to ensure the robustness of positioning, a seamless switching strategy for the robotic manipulator to relocalize the mobile robot is presented for the case in which the vision sensor fails.

Another contribution in this thesis is the performance improvement of advanced visual-based simultaneous localization and mapping (SLAM) system in scenarios that contain blurred frames by integrating an efficient image deblurring framework, which can be used for the phase of autonomous material transport. The conventional localization systems in manufacturing rely on external setups

such as ArUco marker, lacking of sufficient flexibility to adapt to autonomous manufacturing of the future. Visual-based SLAM enables autonomous robotic behaviors which allow the mobile robot to adequately handle dynamic environments by visual sensors. It takes advantage of the natural markers from the around environment and allows the mobile robot to move autonomously toward the target. However, challenges arise when applying visual-based SLAM in the practices of autonomous manufacturing. Particularly, blurred images that exist in visual-based SLAM can result in low-quality outcomes and are thus studied in this work. The proposed efficient image deblurring framework is feasible in real-world scenarios and incrementally enhances the positioning accuracy of visual-based SLAM according to the results in the TUM RGBD dataset and TUM Visual-Inertial dataset.

At last, a physical prototyping Co-MRMS, which is basically comprised of a fixed-base robotic manipulator and a mobile robot was developed. Cooperative behaviors and handling tasks to advance composite manufacturing serve as a case study. Abundant evaluations through a series of tasks were performed to evaluate the performance of individual components of the proposed Co-MRMS through a small-scale robotic cell consisting of a 6 degrees of freedom manipulator and a Turtlebot3 Burger mobile robot. An effective machine vision system has been developed to support the robotic tasks described above by providing the capabilities for object detection, localization and fiber orientation detection and dealing with uncertainties such as size and shape of fiber plies. In conclusion, by exploiting the availability of the proposed Co-MRMS, it is possible to implement a flexible system that provides autonomous material transportation and sufficiently-accurate material handling capabilities that extend beyond what is currently adopted in the industry.

Acknowledgements

In the process of my PhD study, I would like to express my thanks to all those who have helped me.

Firstly, I would like express my gratitude to my supervisor Erfu Yang who gave me kind encouragement and invaluable instruction all through my period of PhD study. I am extremely lucky to have a supervisor who cared so much about my study, provided me with to expand my horizon in the world of research and took a lot of effort to get the necessary equipment to conduct important experiments for my research. Without his continual support, my PhD study could not be completed.

I would like to thank Cuebong Wong, Carmelo Mineo and Leijian Yu for their valuable advice and involvement in the case study reported in Chapter 3 and Chapter 6 of this thesis. Their contributions in the area of machine vision, path planning and KUKA robot controller make it possible to develop a working physical system. Additionally, when I encountered problems in my research, Cuebong and Leijian always discussed with me and generously helped me to find solutions patiently.

I would like to acknowledge to Quang-Cuong Pham and Vuong-Quoc Nghia for hosting my visit to their research group at Nanyang Technological University (NTU), Singapore, and providing their experimental equipment for my research.

Nghia has helped me significantly in both theoretical and experimental studies during the visit.

I am also very grateful to Iain Bomphray and Ruoyu Huang from the Lightweight Manufacturing Centre and Remi Zante and Scott Brady from the Advanced Forming Research Centre for the provision of research funds through the Route to Impact scheme, which has supported my research work in NTU and the case study in my thesis.

I would also like to thank Xiu-Tian Yan and Cong Niu for providing me with the OptiTrack to conduct important experiments for my research.

My colleagues and friends in DMEM have also helped me a lot during this period of time. I am grateful to Beiya Yang, Dino Bertolaccini, Neil Shepherd for their valuable advice and generous help in performing real robot experiments reported in Chapter 4.

Lastly, I would like to give special thanks to my husband Deqiang Wang and my family for their great support and encouragement when undertaking my research.

Without these people, I cannot be where I am today. Many thanks.

Contents

List of Figures

List of Tables

List of Acronyms

AFP: Automated Fiber Placement

AGVs: Automated Guided Vehicles

ANN: Artificial Neural Networks

AR: Augmented Reality

ATE: Absolute Trajectory Error

ATL: Automated Tape Laying

CAD: Computer-aided Design

CDF: Cumulative Distribution Function

Co-MRMS: Cooperative Mobile Robot and Manipulator System

CPU: Central Processing Unit

DFT: Discrete Fourier Transforms

DSO: Direct Sparse Odometry

DoF: Degrees of Freedom

DTAM: Dense Tracking and Mapping

EID: Efficient Image Deblurring

EKF: Extended Kalman Filter

ELM: Extreme Learning Machine

FAST: Features from Accelerated Segment Test

GAN: Generative Adversarial Networks

GPS: Global Positioning System

GPU: Graphics Processing Unit

HMM: Hidden Markov Models

ICP: Iterative Closest Point

IDFT: Inverse Discrete Fourier Transforms

IFR: International Federation of Robotics

IMU: Inertia Measurement Units

IOT: Internet of Things

ITRA: Interfacing Toolbox for Robotic Arms

KF: Kalman Filter

LOS: Line-of-sight

MAE: Mean Absolute Error

MAP: Maximum-a-Posteriori

MAVs: Micro Aerial Vehicles

MBA-VO: Motion Blur Aware Visual Odometry

MEMS: Micro-electro-mechanical Systems

ORB: Oriented FAST and Rotated BRIEF

PDF: Probability Density Function

PSF: Point Spread Function

RMSE: Root Mean Squared Error

ROS: Robot Operating System

RRT: Rapidly-exploring Random Tree

SLAM: Simultaneous Localization and Mapping

SRN-DeblurNet: Scale-recurrent Network

STD: Standard Deviation

ToF: Time-of-flight

UDP: User Datagram Protocol

VI-SLAM: Visual-inertial SLAM

VINS-Mono: Monocular Visual-Inertial System

VR: Virtual Reality

VSLAM: Visual SLAM

List of Symbols

Roman symbols

$\widetilde{a}$	Acceleration
$\widetilde{a_n}$	Nominal acceleration
a_m	Motion component
a_g	Gravitational component
ε_a	Measurement noise
b_a	Bias of acceleration
b_ω	Gyro bias
B	Base station
d_{cc}	Distance between the centre of the material and the marker
d	Distances between the target point and the base stations
D	Distances of the object that projects into the camera
$f(i,j)$	Gray values of the denoised image
$f_{d(t)}$	Desired image with clear edges
$f_{(t)}$	Original image
$prior(f)$	Prior items of image content
F_i	Jacobian matrix of prediction model

$\hat{F}_{(f)}$	Discrete Fourier transforms
$g(i,j)$	Gray values of the original image
$g_b(t)$	Captured blurred image
$g_{(t)}$	Observed degraded image
$prior(h)$	Prior items of blurring kernel
$h_b(t)$	Degradation kernel
$h_{(t)}$	Blurring kernel
H_i	Jacobian matrix of the measurement model
I_p	Gray value of p
I_x	Intensities of image patch p at pixel x
I_y	Intensities of image patch p at pixel y
$k(f,g)$	Data fidelity term
K	Fixed intrinsic camera matrix
M_p	Number of pixels in the length of the image
$n_{(t)}$	Noise term
N_p	Number of pixels in the width of the image
$p_{(x_0)}$	Prior probability
$p_{(y_n\|x_n)}$	Emissions
$p_{(x_n\|x_{n-1})}$	Transition dynamics
$p_{(x_i\|y_{1:i-1})}$	Prediction of the belief
p_i	Estimated pose obtained from the SLAM system
Q_i	Ground truth of pose in frame i
$R(\Theta)$	Rotation matrix
s_n	Displacements
S	Similarity transformation matrix from the calculated pose to the ground truth
t	Threshold value
T	Transformation matrix
$\vec{T}$	Transitional distance of the camera

Δt	Integration time
ΔT	Sampling time interval
u	Control vector
v_n	Velocities
v_0	Initial velocity
$w_{(t)}$	Convolutional function
$\hat{x}_i$	Estimated pose of the ith image frame in the sequence
x_i	Ground truth
(x_{mar}, y_{mar})	Positions of Aruco marker
(x_{mat}, y_{mat})	Positions of the material centroid
X	State vector
$\hat{X}$	Estimate of the state vector
$\tilde{\omega}$	Measured angular velocity
η_ω	Additive measurement noise
θ'	Angle between the positive x-axis and the normal to the line
μ	Gaussian mean
μ_f	Spatial frequencies
σ	Standard deviation
ε	System noise
υ	Measurement noise
ρ'	Distance from the origin to the line
ρ	Adjustment factor

Unit symbols

cm	Centimeter meter
Hz	Hertz
kHz	Kilohertz
m	Meter
mm	Millimeter
N	Newton
s	Second
$\circ$	Degree

Publications Arising from this Thesis

Articles

[J1] Yang, M., Yu, L., Wong, C., Mineo, C., Yang, E., Bomphray, I., & Huang, R. (2021). A cooperative mobile robot and manipulator system (Co-MRMS) for transport and lay-up of fibre plies in modern composite material manufacture. The International Journal of Advanced Manufacturing Technology, 1-17.

- This paper presents the use of the Co-MRMS in modern composite material manufacture that reported in Chapter 6. My contributions as the first author are as follows: I contributed to the initial idea and built up the Co-MRMS, prepared the manuscript drafts and conducted all experiments.

[J2] Yang, M., & Yang, E. (2023). Two-stage multi-sensor fusion positioning system with seamless switching for cooperative mobile robot and manipulator system. International Journal of Intelligent Robotics and Applications, 7(2), 275-290.

- This paper presents the work reported in Chapter 4. My contributions as the first author are as follows: I designed the interaction mode and positioning system, conducted all experiments and prepared the manuscript drafts.

Conference proceedings

[C1] Yang, M., Yang, E., Zante, R. C., Post, M., & Liu, X. (2019, September). Collaborative mobile industrial manipulator: a review of system architecture and applications. In 2019 25th International Conference on Automation and Computing (ICAC) (pp. 1-6). IEEE.

- This paper presents a detailed review on the system architecture and industrial applications of collaborative mobile industrial manipulator as summarised in Chapter 2. My contributions as the first author are as follows: I conducted all literature review activities and prepared the manuscript drafts.

[C2] Yang, M., Yu, L., Wong, C., Mineo, C., Yang, E., Bomphray, I., ... & Brady, S. (2021). Comprehensive simulation of Co-MRMS for advanced composite manufacturing: a case study. In Advances in Manufacturing Technology XXXIV (pp. 105-110). IOS Press.

- This paper presents the integrated simulation of Co-MRMS for composite material transport and lay-up that reported in Chapter 3. My contributions as the first author are as follows: I integrated the subsystems of Co-MRMS in simulation environment, prepared the manuscript drafts and conducted all simulation-based experiments.

Chapter 1

Introduction

1.1 Background and Motivation

In modern society, robots play an increasingly vital role in almost all areas of life, including applications in medical health, autonomous manufacturing and intelligent services. For decades, robotic systems have been used in manufacturing to replace human workers to do several tasks that are dangerous or include high volumes of materials [1]. Even in the short term, employees can experience fatigue or become distracted due to the repetitive nature of their work, leading them to make errors. Due to the dexterity and high levels of machine learning, robots can avoid the common failures of human workers such as fatigue and distraction, which have become commonplace in industry context [2]. According to the International Federation of Robotics (IFR), about 3 million industrial robots were applied in worldwide manufacturing in the year 2021, demonstrating the flourish of industrial robots [3]. Due to the widespread use of robotic systems, numerous studies have been carried out on enhancing the capability of robots to execute various manufacturing tasks, e.g. material handling, transporting and assembly [4–6].

Over the recent years, manufacturing has developed rapidly with the changing environment in the form of huge demand for customers, growing global competition, etc. To tackle these challenges and survive in the intensely competitive environment, manufacturing is paying increasing attention to flexibility, efficiency and other manufacturing characteristics [7–10]. Therefore, the comprehensive elements, such as automation, flexibility, efficiency and informatization, have gradually become critical points to improve in the manufacturing context. Until now, automation has been involved in several stages of manufacturing, replacing the operations that purely rely on humans. With this trend, industrial robotic manipulators and mobile robots are widely utilized in manufacturing to perform 4D tasks, namely dumb, dangerous, dull, and/or dirty [11]. Thus, industrial robots are indispensable parts of advanced manufacturing.

Generally, traditional automated robotic systems are built with the purpose of a particular process in manufacturing. For example, the conventional fixed-base robotic manipulators are generally involved in custom-designed fixtures that are caged within a secure enclosure to ensure the safety of workers. Whereas, the challenges to manufacturing such as fierce competition stimulate the development of robots and thus multiple forms of robots have been employed except the conventional fixed-base robotic manipulator. A few examples of using various forms of robotic systems in manufacturing are given here [12–18]. Collaborative robots have attracted manufacturers for their capability in interacting with humans to perform tasks that contain direct physical contact, e.g. assembly and disassembly [12]. Mobile robots have been developed in quantity to transport large loads within manufacturing environments [13]. In manufacturing environments that contain large parts located at multiple stationary stations such as the shipbuilding industry or aerospace industry, industrial mobile manipulators are being developed as they are economical solutions and are allowed to work in different stations with the same tasks [14]. Multiple mobile manipulator systems

have been studied for the assembly of a large structure, i.e., airplane wing [15]. Industrial manipulators, usually attached to a fixed basement and consisting of multiple jointed arms and end-effectors, have been used predominantly in the automotive industry for important operations, e.g. welding, painting and material handling [16]. A robotic system containing multiple mobile robots has found significant importance in inspecting and maintaining equipment located at a large number of distributed servicing points in various manufacturing and industrial scenarios [17]. Multiple robotic manipulators have shown notable advantages in performing cooperative tasks such as peg-in-hole as well as handling large and heavy objects [18].

Indeed, during the past decades, the interest in developing different robotic systems in a manufacturing context has significantly increased and significant milestones have been achieved. However, there still are abundant challenges and technological bottlenecks that need to be solved before robots can completely replace humans to perform manufacturing tasks as expected now.

1.1.1 Robotic Systems in Advanced Manufacturing

Mobile robots and robotic manipulators are the most common robotic systems employed in advanced manufacturing, playing different roles for scheduled tasks on the basis of their own characteristics [19]. Mobile robots can move around without needing a fixed physical location. As material transport is a typical task in manufacturing, deploying mobile robots to perform such a task can reap various crucial benefits such as flexibility, safety, and efficiency. By contrast, robotic manipulators are usually attached to a fixed physical location, constructed by multiple linked manipulators and end-effectors for performing various manufacturing tasks such as assembly and material handling. To date, both of these two different types of robots have been studied as independent robotic systems respec-

tively and extensively, and a large number of researchers have been dedicated to improving the performance of robotic systems in terms of flexibility, autonomy and versatility [6, 13]. Meanwhile, various robotic systems have emerged and can be broadly classified into single and cooperative robotic systems without former reference. The cooperative robotic system, which integrates more than one robot, is becoming competitive and has been widely applied in advanced manufacturing to perform cooperative tasks such as material transportation and handling at production lines [15,17,18]. Compared to a single robotic system, multiple robots work together as a single robotic system, presenting and combining a number of advantages such as versatility and efficiency.

Moreover, the cooperative robotic system has several different forms like multiple mobile robots, multiple robotic manipulators and mobile manipulators. Without the formal classification from the existing literature, cooperative robotic systems are broadly divided by the author into cooperative homogeneous robotic systems and cooperative heterogeneous robotic systems. A cooperative homogeneous robotic system generally consists of the same type of robot, performing a similar task with a single robotic system. For example, a cooperative mobile robotic system is composed of groups of mobile robots. It has been studied extensively for a manufacturing task that needs more than one mobile robot, such as lifting and transporting heavy objects in advanced manufacturing.

A cooperative heterogeneous robotic system generally consists of different types of robots. For example, a mobile robotic manipulator is a typical cooperative heterogeneous robotic system that integrates a robotic manipulator into a mobile platform. Advantages offered by the robotic manipulator such as dexterity and benefits provided by the mobile platform such as mobility, are combined into a single robotic system. Thus, the work area of the mobile robotic manipulator is extended and the system is allowed to work in different locations, making it flexible to perform several manufacturing tasks. In the framework of Industry 4.0,

mobile robotic manipulator is a reality available and enable to execute mechanical and repetitive tasks. However, the tasks that are performed by this system are limited due to the light load and speed of the attached robotic manipulator [20].

Compared with the integrated mobile robotic manipulator, this thesis is concerned with another type of cooperative heterogeneous robotic system that contains a mobile platform and a fixed-base robotic manipulator, namely cooperative mobile robot and manipulator system (Co-MRMS), which has been relatively unexplored in literature. The fixed-base robotic manipulator is responsible for demanding manufacturing tasks such as performing heavy loads and complex assignments, while the mobile robot is used as the intermediate to supply materials. As this robotic system fundamentally consists of two different and separate robots, both the independent and interactive behaviors of robots will be investigated in this thesis.

1.1.2 Limitations and Opportunities

As is mentioned above in Section 1.1.1, a large variety of robotic systems have emerged within advanced manufacturing context, which can be categorized into the following mainstream classes: single robotic system (single mobile robot and single robotic manipulator) and cooperative robotic system (mobile manipulator system, multiple mobile robots system and multiple robotic manipulators system) [12–18]. However, these robotic systems have not yet covered all the circumstances in manufacturing. For large-scale industrial robotic systems, heavy fence guarding is generally required to ensure the safety of human workers. Traditional material transport systems for the fenced robotic manipulator such as conveyor belts, are fixed, static and inflexible, reducing the flexibility of manufacturing as well as consuming lots of workspace [16]. By contrast, mobile robots have been widely used as a platform for material transport due to their flexibility

and mobility, which creates opportunities for further cooperation with the fixed-base robotic manipulator [17]. In this case, the fixed-base robotic manipulator and the mobile robot can be cooperated and integrated as a single robotic system to perform both material transport and handling tasks at production lines. This new type of cooperative robotic system has received little attention, which is challenging to build owing to the incorporation of different types of robots and the involvement of many technologies such as material detection and localization.

In addition, when the cooperative robotic system is put into practical applications within the manufacturing context, other challenges are as well introduced. For example, current manufacturing is facing fierce competition and has been developed rapidly with the changing environment. Therefore, the robots in manufacturing are required to not only work in a stable environment but also enable to adapt to dynamic and incompletely structured environments [19]. A stable environment means that the environment remains static and unchanged over time. The past few years have seen the rapid development of robots within a stable environment, especially in manufacturing industry. The robots are usually programmed offline and the path is planned in advance based on a structured environment [21]. However, dynamic conditions are unavoidable, i.e. the operation environment is changed or dynamic with unexpected cases. This potentially leads to the failures of robots. Thus robots are required to become autonomous and enable to adapt to complex, uncertain, dynamic and incompletely structured manufacturing environments. Compared with the traditional robotic system working in a stable environment, autonomous robotic systems are intelligent to deal with small variations and adapt to changing environments in a task, thereby executing high-level tasks without planned and predefined programming [7].

From the technology standpoint, integrating a fixed-base robotic manipulator and a mobile robot as a single robotic system is challenging as the system requires the integration of multiple sub-systems and robotic capabilities. In addition, the

scientific challenges of this research mainly focused on building a new form of a complete cooperative robotic system and conducting experiments to validate the proposed system's capabilities.

Motivated by these challenges and opportunities, a cooperative robotic system that contains a fixed-base robotic manipulator and a mobile robot involved with many technologies for autonomous manufacturing, namely is presented in this thesis. Different components are integrated for intelligent and flexible material transportation and handling. Multi-sensor fusion positioning system and an improved visual-based SLAM algorithm are proposed to further improve the robotic behaviors of a whole robotic system. In this thesis, the described cooperative robotic system is industrially relevant, seeking to provide a strategy that combines different modules in a flexible system, providing autonomous material transport as well as accurate and robust material handling capabilities.

1.2 Research Aim, Questions and Objectives

1.2.1 Research Aim

This research investigates a cooperative mobile robot and fixed-base robotic manipulator system, involving related positioning problems for material handling and SLAM problems for autonomous material transport.

In advanced manufacturing, material transport and handling have not been integrated into a single autonomous robotic system, which is challenging due to the many technologies involved, including path planning, material detection and localization, etc. To achieve autonomous material transportation as well as accurate and robust material handling, the development of combining different components is required.

In addition, conventional material transport techniques for the fixed-base robotic manipulator by mobile robot commonly require predefined offline programming. These two robots work independently with relatively little interaction. In this scenario, any changes to the process can lead to the failure of material transport and require considerable offline programming effort, lacking the anticipated flexibility and efficiency. Consequently, material transport techniques for the fixed-base robotic manipulator by mobile robot have traditionally been limited to little interaction with minimal reliance on sensing technologies.

Visual-based SLAM enables autonomous robotic behaviors, allowing the mobile robot to adequately adapt to a dynamic environment and mainly depends on visual sensors [22]. However, challenges arise when applying visual-based SLAM in the practices of autonomous manufacturing. Particularly, blurred images that exist in visual-based SLAM can result in low-quality outcomes. The research on combining image deblurring and visual-based SLAM has not received significant attention in the literature and is studied in this work.

The aim of this research is to investigate a new form of cooperative robotic system that enables to perform material transport and handling tasks autonomously and flexibly in advanced manufacturing.

1.2.2 Research Questions

The scope of this research is advanced manufacturing. In order to develop a cooperative mobile robot and fixed-base robotic manipulator system for performing material transport and handling tasks in advanced manufacturing, several research questions are formulated in the beginning phase of the literature review and real industrial scenarios, which are listed below. Research question 1 addressed the overall background of using Co-MRMS in advanced manufacturing while Research question 2, Research question 3 and 4 addressed some technical

problems in the proposed Co-MRMS. Each of these questions is complex to address when a strategy is required to perform both autonomous material transport and flexible material handling in a single robotic system. By addressing these research questions, the proposed Co-MRMS achieves the aim of this research successfully and makes new knowledge contributions in robots for autonomous manufacturing.

1 What is the current situation of using cooperative robotic manipulators and mobile robot systems in advanced manufacturing?

2 How to use the cooperative fixed-base robotic manipulator and mobile robot system to realize both autonomous material transport and flexible handling?

3 How to achieve accurate and robust positioning in the proposed Co-MRMS?

4 How can the proposed Co-MRMS transports the material in a fast-changing environment?

1.2.3 Research Objectives

To meet the above research aim and answer the research questions, the following objectives have been set:

1. Perform a comprehensive literature review on the state-of-the-art techniques of robotic systems in advanced manufacturing as well as positioning and SLAM methods, and identify the limitations of existing works in relation to applying a cooperative mobile robot and robotic manipulator system in autonomous manufacturing.

2. Develop a cooperative mobile robot and robotic manipulator system to serve as a promising strategy for autonomous material transfer and handling tasks in autonomous manufacturing.

3. Conduct an integrated simulation based on Objective 2 to comprehensively demonstrate the feasibility of the proposed robotic system.

4. Develop a sensing system for accurate and robust identification and positioning.

5. Develop a new approach that allows the mobile robot to transport the material autonomously in a dynamic manufacturing environment.

6. Evaluate the quantitative performance of the techniques developed in Objective 4 and Objective 5, the feasibility and effectiveness of the proposed Co-MRMS in Objective 2.

1.3 Research Methodology

A research methodology is a way to systematically resolve a research problem. It defines the components of research activity and states the adopted strategy and rationale of different steps [23]. Research philosophy is the fundament of research methodology, which provides guidelines about choosing suitable research strategies or methods [24]. Generally, four philosophical approaches to research are acknowledged: positivism, constructivism, post-positivism and interpretivism [25]. Positivism uses data to verify hypotheses, requiring quantitative analysis [26]. Constructivism emphasizes on individual beliefs and experiences, solving research problems via constructing models, diagrams, etc [27]. Post-positivism lies between positivism and constructivism. It not only emphasizes the independence of observation but also asserts that the observation is affected by the values and experiences of the researcher [28]. Interpretivism is commonly used in social science without gathering data to interpret the research object by social constructions. In interpretivism, qualitative analysis is emphasized over quantitative analysis [29].

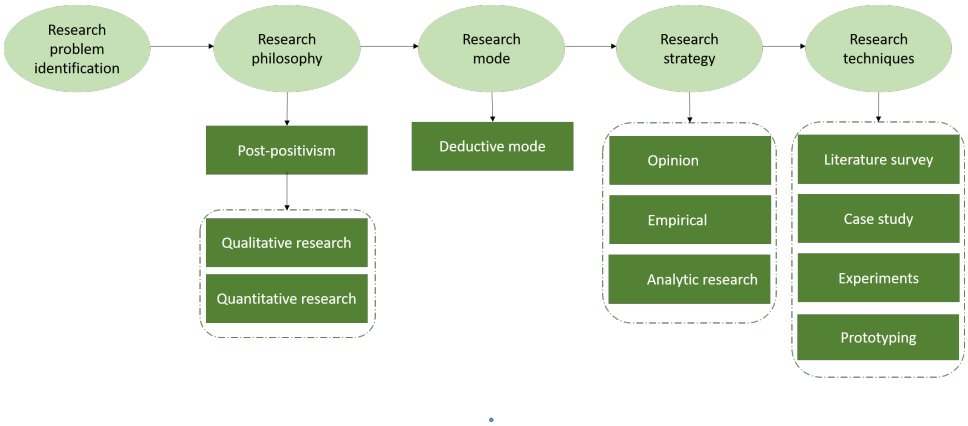

Fig. 1.1. The framework of research methodology.

Fig. 1.1 shows the framework of the adopted research methodology. Firstly, the research problem is identified. This research addresses a new form of cooperative robotic system and its performance in advanced manufacturing. The main issues dealt with are developing a novel Co-MRMS and optimizing the subsystems for autonomous operations. Secondly, the adopted research philosophy in this work is determined, which is post-positivism. Thus both qualitative and quantitative analysis are used. Deductive research is a method that tests a prior hypothesis or theory by collecting data and empirical observation [26]. It is used as the research mode in this work. Three research strategies adopted are opinion, empirical and analytic research [30]. Opinion strategy is used for obtaining other people's views while empirical strategy is used for observation [30]. An analytic research strategy is adopted for analyzing the obtained information [30]. For research techniques, literature surveys, case studies, experiments and prototyping are employed in this work to collect data. The investigations and developments have been broken down into several smaller studies that focus on one or more of the research questions introduced in Section 1.2.2, which are described as follows.

1.3.1 Literature Review

Literature review is performed in this thesis to provide a critical analysis of the cooperative mobile robot and manipulator system in advanced manufacturing, as well as the current state-of-the-art technology including robotic positioning and SLAM, which can be integrated into Co-MRMS to improve the performance of the whole system. With the purpose of identifying the limitations of existing state-of-the-art techniques and improving the autonomy and flexibility of Co-MRMS, the crucial knowledge gaps in the literature are determined and have been addressed subsequently in this research. As is shown in Fig. 1.2, the literature review process can be divided into five steps. The first step is the research question definition. Then, based on the specific research question, the advantages and disadvantages of the general techniques are known according to a substantial amount of literature review. Afterward, the literature review is narrowed down depending on the chosen approach. Finally, the knowledge gaps are determined through an in-depth literature review.

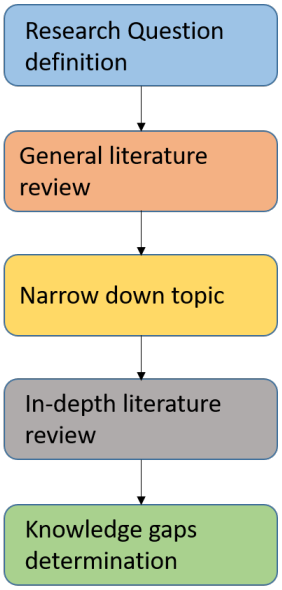

Fig. 1.2. Literature review process.

1.3.2 A Simulated Case Study in Composite Manufacture

An integrated simulation framework is investigated to comprehensively demonstrate the concepts of the whole proposed Co-MRMS, given that applying the proposed robotic system to a real scenario directly is time-consuming, expensive and difficult.

Material transportation and composite material lay-up tasks in composite manufacture are chosen as an application example for the proposed Co-MRMS as it provides the opportunity to investigate the feasibility of the proposed Co-MRMS. This case study will primarily seek to address Research Question 2 (see Section 1.2.2). Moreover, the development of approaches for enhancing the performance of the proposed Co-MRMS studied in this thesis is driven by the findings in this case study.

1.3.3 Positioning Design for the Proposed Co-MRMS

The first development for enhancing the performance of the proposed Co-MRMS is the positioning. In this thesis, the positioning problem studied addresses that the fixed-base robotic manipulator can have accurate and robust interaction with the mobile robot by using sensing technologies. The attention given to this problem is derived from the simulated case study in composite manufacture and observation of material transport in real industrial scenarios. The mobile robot with material is generally driven to the predefined stop location, then the fixed-base robotic manipulator executes material handling by offline programming without identifying the position of the material. These two robots work independently with relatively little interaction, lacking the anticipated autonomy and flexibility. This investigation addresses the problem of robotic interaction when the mobile robot transports material to the fixed-base robotic manipulator. To achieve the

robotic interaction, robustly and accurately perceiving the positions of the mobile robot is necessary for the fixed-base robotic manipulator. This needs to explore the benefits of combining multiple sensors into a single positioning system for the fixed-base robotic manipulator to perceive and estimate the positions of the mobile robot. The performance of the positioning system is evaluated through a series of physical static and dynamic experiments. I go on to identify the positioning system that enables the robotic manipulator to estimate the positions of the mobile robot in the case of visual sensor failure. The output of this work is a two-stage positioning strategy, allowing seamless switching between different sensor suites based on sensor state for the robotic manipulator relocalising the mobile robot. This work addresses Research Question 3 (see Section 1.2.2) for accurate and robust positioning in the proposed Co-MRMS.

1.3.4 Autonomy Enhancement for the Proposed Co-MRMS

The second development for enhancing the performance of the proposed Co-MRMS is the autonomy of the system. Owing to the techniques of SLAM, the mobile robot in the proposed Co-MRMS is able to work in a dynamic and changing environment, which significantly enhances the autonomy of the proposed Co-MRMS. In this thesis, the study of SLAM seeks to apply an advanced SLAM algorithm to the phase of autonomous material transport in a manufacturing environment and addresses the problem of blurred images. This problem is investigated by integrating the advanced SLAM algorithm and image deblurred algorithm to incrementally enhance the SLAM accuracy for autonomous material transport by a mobile robot. The performances are evaluated on the mobile robot in the real world as well as the famous TUM RGB-D dataset [31] and TUM Visual-Inertial dataset [32]. This work addresses Research Question 4 (see Section 1.2.2) for autonomous material transport by a mobile robot in manufacturing.

1.3.5 Prototype Verification of the Proposed Co-MRMS

As a simulated case study in composite manufacture has been conducted, a prototype is built up to verify the feasibility and cooperative behaviors of the proposed Co-MRMS in the real world. Similar to the simulated case study, material transfer and handling operations in advanced composite material manufacturing are chosen as applied tasks since composite material manufacturing mainly relies on manual labor and individual skills, especially in transport and lay-up processes. Comprehensive physical experiments conducted with a 6 Degree-of-Freedom (DoF) serial manipulator and a two-wheeled differential drive mobile robot, demonstrate the efficient interaction and high performance of the Co-MRMS for autonomous material transportation, material localization, fiber orientation detection and grasping of material. This real-world case study further seeks to address Research Question 2.

1.4 Thesis Organisation

This thesis is composed of seven chapters and the remainder of this thesis is organized as follows.

Chapter 2 critically reviews the existing research in the area of cooperative robotic manipulators and mobile robot systems and covers the state-of-the-art in robotic positioning and SLAM. Within the scope of the contributions of this thesis, the knowledge gaps are discussed and the limitations of the current techniques are identified.

Chapter 3 proposes an integrated simulation framework to comprehensively demonstrate the cooperative concepts of the whole proposed Co-MRMS. In addition, a case study on robotic material transportation and composite material

lay-up, which is based on a real-world scenario commonly found in advanced composite manufacturing, is investigated to validate the feasibility of the proposed Co-MRMS in a simulation-based environment.

Chapter 4 investigates the interaction and positioning problem of the proposed Co-MRMS by sensing techniques with the consideration of unavailable sensors. An interaction mode is designed and a novel positioning system comprised of two different kinds of positioning methods is developed for the relative positioning between the mobile robot and the fixed-base robotic manipulator. Additionally, to ensure the robustness of the positioning system, a seamless switching strategy for the fixed-base robotic manipulator relocalizing mobile robot, is presented for the case in which the vision sensor fails.

Chapter 5 addresses the problem of blurred images that exist in visual-based SLAM, decreasing the quality of autonomous navigation for mobile robots. An efficient image deblurring framework is introduced to incrementally enhance the SLAM accuracy for the autonomous navigation of mobile robots.

Chapter 6 describes a prototype system to validate the feasibility of the proposed Co-MRMS through a case study on material transportation and handling tasks in advanced composite manufacturing. Adequate experimental results are provided to illustrate the capabilities of material transportation and accurate material handling of the proposed robotic system.

In the end, **Chapter 7** provides the conclusions drawn from this thesis and a collective discussion on the research findings obtained from each of the studies with regard to the overall research aim and objectives. Then, the individual contributions to knowledge made in this thesis are summarised and presented. Limitations of the reported work are described and possible directions for future work are discussed based on the current research findings.

The logic behind the thesis organization design is finding the knowledge gap and solutions from the literature review first and then using simulation-based experiments to initially demonstrate the solutions. The submodules are then verified and an integrated demonstrator is set up and validated in the real world. Therefore, the layout and organization of the thesis are shown in Fig. 1.3. The underlying research questions addressed and the focal points of each chapter are displayed on a chapter-by-chapter basis.

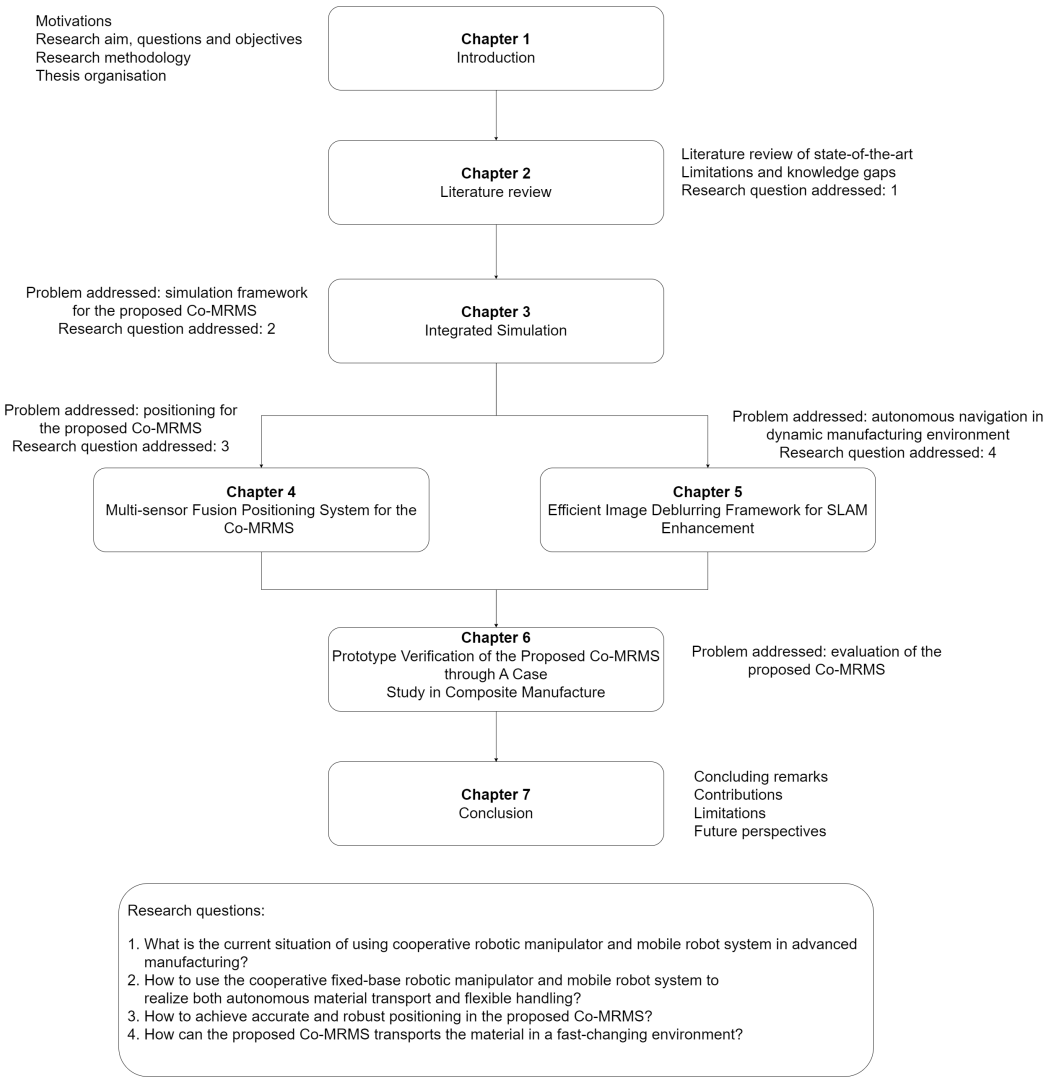

Fig. 1.3. Organisation of the thesis.

Chapter 2

Literature Review

This chapter gives a literature review of the Co-MRMS in advanced manufacturing, as well as the current state-of-the-art technology including robotic positioning and SLAM, which can be applied into the Co-MRMS to improve the performance of the whole system. The chapter is comprised of three sections covering the review of the Co-MRMS, robotic positioning and SLAM techniques. A summary of reviewed literature is provided to highlight the current knowledge gaps, their limitations and how these problems are addressed in this thesis.

2.1 Cooperative Mobile Robot and Manipulator System

Due to the increasing competition in a globalized environment, manufacturers need to constantly evolve their production systems to accommodate the changing requirements of markets. Nowadays, production is transforming the paradigm from a great deal of ready-made products to mass-customized production. One of the impacts of this tendency on production systems is that the manufacturing process is required to be more flexible and can promptly adapt to handle more production variation and smaller batch sizes [19]. Since robot-based production

has been an indispensable part of advanced industrial manufacturing, another impact is that more and more robotic systems will be deployed in the manufacturing industry along with substantial investigation of the robots [7]. With the coming of Industry 4.0, robotic systems can significantly promote the manufacturing process and thus a growing number of tasks will be performed by robots in the future [33]. Different types of robots that are deployed in industry generally include large-scale industrial robotic manipulators with fences, mobile manipulators, small-scale stationary robotic manipulators and mobile platforms. On one hand, these robots can replace humans in carrying out repetitive manual tasks. On the other hand, they can enter into more hazardous environments to fulfill several dangerous tasks.

Normally, robotic manipulators that are used prevalently in manufacturing, are statically placed in a guarded cell to continuously repeat a delicately predefined sequence of actions without changes for decades. It is not surprising that these typical robotic manipulators cannot provide considerable flexibility and thus transformable production systems to such a degree lack adequate capabilities of current production systems [21]. While traditional robotic manipulators are automated to a large degree but are difficult to reconfigure, manual labors are flexible to perform various tasks in a manufacturing environment but are uneconomical for large-scale production, especially in countries that lack human power. For the next generation of manufacturing, mass customization requires combining high flexibility with a high degree of automation [34]. To achieve this goal, robotic manipulators are expected to be one of the promising enablers of this transition to a transformable future factory. In order to reach the demanded level of flexibility, robots need to possess more autonomy and cope with dynamic environments. Another kind of robot that has been widely employed in advanced manufacturing environments is mobile robot. Owing to their mobility, mobile robots have been extensively utilized in a variety of tasks such as material transport and

part-feeding. Michael and Roger et al. in [35] stated that the number of mobile robots will increase in manufacturing and more complex tasks are expected to be accomplished by mobile robots.

The aforementioned two different types of robots, mobile robots and robotic manipulators, are distinct robots and possess expertise in different aspects within the manufacturing environments. Due to the limitation of single robots, different cooperative forms of robotic systems have emerged [17, 18]. For example, in Fig. 2.1, two different cooperative forms between a mobile robot and a robotic manipulator are shown. As is the most typical cooperative form of a mobile robot and a robotic manipulator, mobile manipulators have been extensively investigated because of their mobility, collaboration and flexibility [14, 15]. Mads et al. [36] focused on mobile industrial manipulator applications and surveyed 12 general industrial application requirements, which combines academic research and industrial applications. However, little emphasis has been placed on the importance of system architecture. Additionally, a number of issues of mobile manipulators proposed in previous literature have been solved since then. New techniques have emerged and can be integrated into the system to improve its performance. This section overviews the typical framework of mobile manipulators including hardware and software components, and the applications of systems in industry to gain a full understanding of the system.

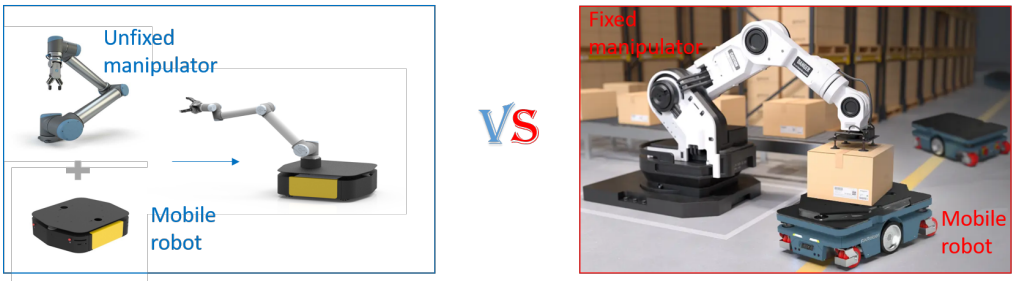

Fig. 2.1. The different cooperative forms between a mobile robot and a robotic manipulator.

2.1.1 System Overview of Mobile Manipulator

It remains challenging for a mobile manipulator to cope with the relationship between modularity and integration. On one hand, modularity decomposes the whole complex into several subsystems, which will be easier to build up. On the other hand, the synergies of the integrating systems are as well need to be considered to ensure that the incorporation of the components will make the whole system work effectively [37]. In this thesis, the components of the mobile manipulator system will be introduced and are divided into two subsystems: hardware module and software module. The typical framework of a mobile manipulator involving system components is displayed in Fig. 2.2.

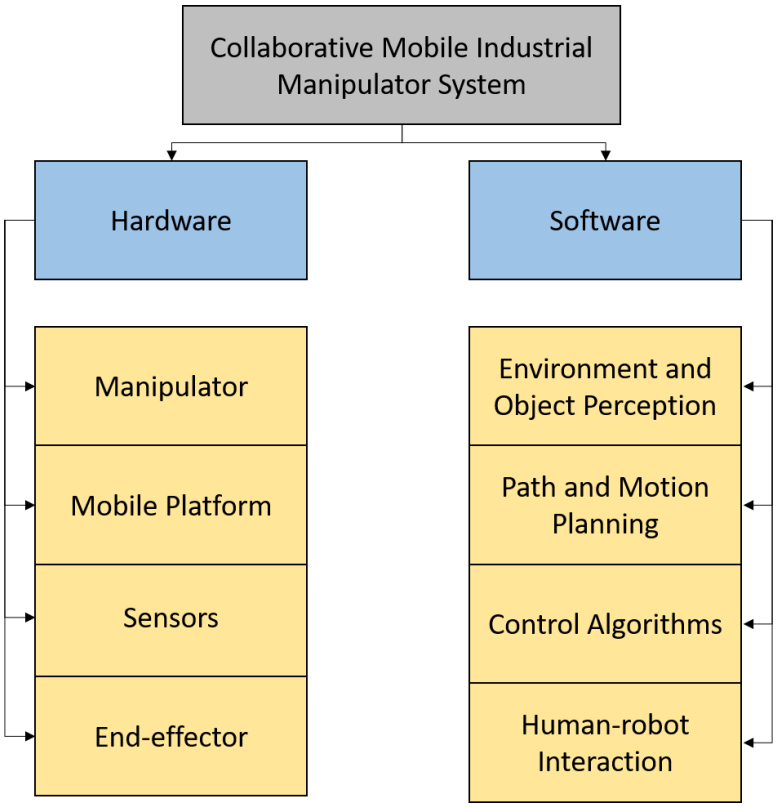

Fig. 2.2. The framework of mobile manipulator system.

2.1.1.1 Typical Hardware Modules

The hardware module of a typical mobile manipulator contains four parts, which are a mobile platform, a robotic manipulator, multiple sensors ad an end-effector of the manipulator. Simply put, the mobile platform is used for movement. The end-effector is generally integrated with the robotic manipulator for manipulation and performing operational tasks such as pick-and-place. Sensors are used for perceiving the environment or objects. These components can be modular, which allows being combined together arbitrarily and flexibly to build up the mobile manipulator system.

1) Mobile platform

For a mobile manipulator, the mobile platform is generally used for navigation and localization because of its mobility. The platform normally works in the plane and thus its DoFs are 3, which are the positions of the robot center and rotation angle. For mobile platforms using omnidirectional wheels, which can move into any direction directly without turning on the ground, the platform is holonomic. Based on this, different modes of autonomous control systems have been designed [38]. Nowadays, there are a number of companies focusing on the development of mobile platforms, which leads to the widespread adoption of mobile platforms in a variety of areas.

2) Manipulator

In advanced industry, there are two main kinds of robotic manipulators. One is large-scale but has to be fenced because its working velocity is relatively high, which is dangerous for humans. It has extensive applications in industry, such as metal cutting and forging. However, this kind of robotic manipulator is normally pre-programmed to repeat the same tasks. The size of another kind of manipulator is comparatively small and thus is compatible with human interaction. In

general, its work velocity and payload are quite low but it can be mounted into a mobile platform to perform more complex and flexible tasks. Usually, manipulators are equipped with end-effectors to achieve complex tasks. Manipulators with different DoFs have been designed and adapted to different tasks and scenarios. Manipulators with 3 or 6 DoFs are commonly introduced. The former is similar to a human's arm and thus generally used in humanoid robots while the latter has been employed extensively in advanced industry due to its advantages of simplicity and flexibility. In [39], both the flexible arm and rigid arm have been designed and cooperated with a mobile platform to work in different scenarios.

3) Sensors

A variety of sensors such as cameras and wheel encoders have been used in a robotic system for obtaining the desired information. For example, a head sensor in the robot is analogous to a human's eyes and normally mounted on the pan-tilt of a robot to perceive the information around the environment. Another example is using a force/torque sensor that is mounted on the end-effector of a robotic manipulator to stop the system operation if the detected force exceeds the threshold. If multiple sensors are utilized in a robotic system, the fusion method must be considered to acquire reliable and accurate data. In [40], a workspace monitoring system, which contains three stereo cameras and one time-of-flight camera, is used in the VALERY project for protecting the tool of a mobile manipulator and has proven its effectiveness. Besides, sensor data generally contains noise, which can be reduced by numerous methods such as the Kalman filter and particle filter [41]. Overall, sensors are vital for robotic systems as they can provide crucial information for the key behaviors of robots such as path planning and controlling.

4) End-effector

The end-effector of the robotic manipulator is equivalent to a human's hand and

has been broadly used for grasping assignments. The shape of the end-effector changes according to the specific task. For example, a cable-driven gripper with internal sensors has been designed for picking strawberries in [42]. Nowadays, some bionics end-effectors like the shape of an eagle's claw have been designed for improving grasping performance. As mentioned before, some sensors have been employed and combined with end-effectors for safety considerations or to provide assistance to perform tasks. In [43], sensitive force feedback sensors were built up with end-effectors to stop the system automatically if the detected force exceeds the threshold. In [44], aided by other modules and components such as controller and sensors, the robotic manipulator with end-effector was set up to accurately and reliably perform tasks such as object handling.

2.1.1.2 Typical Software Modules

For a mobile manipulator system, the software module involves multiple parts, which combine disciplines of environment and object perception, path and motion planning, system control and human-robot interaction. In general, depending on the requirements of a specific task, different software structures and strategies are adopted to adapt to the task. In the following part, the fundamental software modules in a mobile manipulator system are introduced.

1) Environment and Object Perception

Perceiving information about the environment to avoid collision is the first step in operating a software module, which is closely related to using various sensors. Until now, a number of vision-based sensor systems have been extensively employed for detecting objects and humans to avoid a collision. In [45], a thermal vision system based on a thermal camera and neural network technology was utilized for environment detection by acquiring the temperature image. The system is robust, reliable and not easily affected by the light or skin colour of

humans. To avoid the collision, authors in [46] used a torque sensor to detect the external forces, which are then integrated into the admittance controller for rapidly responding to the collision forces. Meanwhile, as using visual sensors for perception has been one of the popular research fields in the last decades, a number of techniques have been adopted to process the obtained images. Liu et al. [47] utilized extreme learning machine (ELM) face recognition with Microsoft Kinect sensors for fast perception, which has been implemented on a four-wheeled mobile robot and achieved good performance in terms of speed and accuracy. Researchers in [48] used a deep learning approach to accurately detect the target while researchers in [49] used visual saliency modeling for object recognition. Bonn et al. [50] used detect architecture based on a deep neural network to find the tools and complete the challenge well in the Mohamed Bin Zayed international robotics challenge 2017. To get a better understanding of the environmental scene, image segmentation that partitions a digital image into multiple image segments has received more and more attention [51].

2) Path and Motion Planning

Mobile manipulator planners usually contain two parts: motion planning for the manipulator and path planning for the mobile platform. The algorithms used in both planning parts can be the same or different. The common planning algorithms can be divided into preprogrammed planning and real-time planning, which depends on whether the environment map is known or unknown. In previous works, there was plenty of research based on structured environments, which means that mobile manipulators can achieve localization and navigation by preprogramming. Nowadays, the trend of robotic planning is transformed into a more flexible mechanism, requiring the robotic system to have the capability of dealing with a dynamic environment. SLAM is one common solution that allows the system to perform real-time planning by mapping the environment

and localizing itself simultaneously. To achieve successful path and motion planning, localization is indispensable and various localization approaches have been investigated and used in industry, such as odometry-based methods, ape-based methods, bar code methods and laser triangulation methods [35]. Moreover, owing to the unstable environment or dynamic obstacles, collision avoidance is an important factor that needs to be considered when designing the planning [52].

3) Control Algorithms

From the perspective of development history, a robotic control system has gone through the stages of semi-automated control and automated control and gradually moved towards the stage of autonomous control. A semi-automated control system enables the robotic system to perform tasks with partial automation but has to involve human intervention in many cases. In comparison, automated control, based on predefined heuristics, allows the robotic system to work independently but cannot deal with changing environments. An autonomous control system can learn and adapt to changing environments, and evolves as the environment with no need for human intervention, which has been the practical way to achieve a completely intelligent industry.

The control system that includes controller and control algorithms aims to make the whole system perform better in tracking, disturbance rejection, robustness and so on. Controlling for mobile manipulators is a complex problem because the system involves both manipulator and mobile platform. In the past, a number of research has been done on the whole body control [53], which means that both mobile platforms and robotic manipulators move at the same time. The discretization method has been as well used for mobile manipulator controlling, where the mobile platform and manipulator adopt different and respective control methods [54]. For a system combining a non-holonomic mobile platform and a holonomic manipulator in [55], a robust adaptive controller considering the

coupling was proposed by designing Lyapunov functions of subsystems relatively and the disturbance rejection ability of the designed controller was proved by simulation but lacks physical experimental results. Nowadays, some researchers are considering using the damping controller to improve the interaction between the mobile manipulator and other objects. In this case, the mobile platform moves unless it reaches a set of constraints such as the singularity, minimum of manipulability, distance to objects and angular deviations. In a real environment, the situation is more complicated and these four constraints can not ensure all fully intuitive collaborations and thus more control constraints are required to be studied in the future [56].

4) Human-Robot Interaction

Safety and interaction methods are two key factors in the way of realizing human-robot collaboration. The interaction can be divided into two ways, contact and contactless operation. Contact operation has traditionally been the standard approach for human-robot interaction. This allows direct contact with the machine (e.g. via joystick) and requires extensive training to familiarize with the system. To date, a number of contactless interaction methods have been introduced, such as pose, speech and brain waves. The contactless methods above are simple for workers to use but have not been applied widely. Additionally, intuition is the tendency of human-robot interaction, where the robot can forecast the human's following movement based on the movement library and extensive training. MIT (Massachusetts Institute of Technology) team [57] presented a data-driven approach and built a human motion library, which can reach 70% or higher correct classification on predicting human trajectory. Therefore, it can be concluded that contactless and intuitive operations are the tendency of human-robot interaction. Besides, both mental and physical factors need to be considered to make the robotic system safe and comfortable for humans. In the future, human operators can interact with the robotic system easily and naturally

without abundant professional knowledge.

2.1.2 Applications in Industry

Both hardware and software components in mobile manipulators have been introduced individually in the above sections. These components can be integrated into a whole robotic system to implement several tasks and one of the significant application areas for the mobile manipulator is industry. In fact, the sales of mobile manipulators have increased rapidly in recent years, especially in the industry area. Until now, mobile manipulators have been successfully applied in logistics for object transport and handling. Other industrial applications such as painting for large equipment and homokinetic joint assembly [58] have been researched as well. It can be predicted that the sales of mobile manipulators will still have a considerable increase for achieving Industry 4.0 and several key techniques such as autonomous control and dealing with dynamic environments will get major breakthroughs in the next decades. At present, since mobile manipulators are suitable for both transporting objects and performing pick-and-place tasks, this robotic system has been mainly applied to two industrial areas, which are logistics and manufacturing.

1) Logistics

Logistics is an area that calls for a vast mobile manipulator because it has a high volume of transferring tasks. The operating environments for mobile manipulators such as factories and warehouses are generally stable and unchanged. Extensive research regarding mobile manipulators with object-transferring capabilities has been conducted. Robotics-enabled logistics and assistive services for the transformable factory of the future [59], a project founded by European Commission, aims to realize a robotic system not only used in the intelligent automatic logistic systems but also used in some assistant services such as preparing and

assembly. As one of the achievements of the project, Madsen et al. [60] applied two mobile manipulators into the real industry environment for pump production, where one of them mainly worked as a logistics robot for transporting the rotor from one workstation to another while another mobile manipulator was used as an assistant for assembly and quality control. Although the two mobile manipulators cooperated well, the experimental results indicated that several problems existed with this technology. For example, the hardware setup of the system is quite time-consuming and some navigation errors often occur. Additionally, the speed and safety of the system need further investigation before the technology can be truly applied in the real environment.

2) Manufacturing

Except for the area of logistics, manufacturing is another area in which mobile manipulators have shown high potential in different fields of manufacturing. For example, as mentioned in the previous section, Madsen et al. [60] investigated using two mobile manipulators (Omni Rob and Little Helper) in water pump manufacturing [60]. Researchers in [61] proposed a mobile manipulator for collaborative autonomous kitting in car manufacturing. For some manufacturing tasks that require high precision such as drilling and screwing, a stationary manipulator has been widely applied as it is not difficult for the fixed robotic system to guarantee demanding accuracy and performance while a mobile manipulator cannot easily achieve this owing to its multiple modules and complex control mechanism. Nevertheless, Guo et al. [62] successfully applied a mobile manipulator in aerospace manufacturing for drilling work which requires both high accuracy and flexibility. In addition, plenty of experiments have been conducted to validate the feasibility of the system. Paul et al. [63] applied a mobile manipulator to a screwing task and the experimental results showed that the system and human work together well and it can be extended into other industrial

areas in the future.

Assembly is a common task in manufacturing and stationary robotic manipulators have been greatly deployed in fixed assembly lines. However, advanced manufacturing is faced with mass-customized production, addressing the demand for changeable assembly lines and flexible robotic systems. Compared to stationary manipulators, mobile manipulators are more flexible and adaptive, contributing to more production and less cost in the industry. Researchers in [64] developed a mobile manipulator for automated structure assembly. The system is capable of performing a series of tasks for the brick building in a semi-structured environment.

2.1.3 Key Findings

Robotic systems have promoted the development of industry majorly in the last decades. Due to the extensive research and increasing knowledge of robotic systems, various robotic systems are now being applied in a variety of settings. Among the various kinds of robots, a mobile platform with a manipulator is a practical robotic system since it can move flexibly and handle stuff easily, which is suitable for work in industry for a variety of tasks such as transporting and pick-and-place. Through the overall literature review of mobile manipulator's research, framework and applications in recent years, the key issues based on the findings are outlined below.

Firstly, Co-MRMS generally refers to a single robotic system, namely a mobile manipulator, where the robotic manipulator is mounted on the mobile robot and these two distinct robots are coupled as a whole. To date, the mobile manipulator has been substantially investigated and widely used in industry but the tasks that are performed by this system are limited due to the light load of robots. Mobile manipulator is mainly used for material transport and simple manipulation in in-

dustry. In the real industrial environment, the situation is quite complicated. For instance, some tasks are demanding for robotic systems to possess superior capabilities such as performing heavy loads and super-accurate assignments. There are currently a large number of robotic manipulators that are fixed for complex and heavy tasks, using mobile robots as intermediates to supply the materials. In this case, the fixed-base robotic manipulator and the mobile robot can be regarded in the same robotic framework, where two robots are loosely coupled. This kind of Co-MRMS has received little attention, lacking sufficient investigations. Additionally, the interaction between the fixed-base robotic manipulator and the mobile robot is one of the crucial issues. To realize a successful interaction, perceiving the state of a mobile robot accurately and robustly is necessary for the fixed-base robotic manipulator, which is still an open research question.

Secondly, in general, the current mobile manipulators are automated systems with pre-programming, while the industry environment requires that the robotic system be applied to dynamic and changeable scenes with real-time programming. Until now, the system has not reached a sophisticated level of intelligence yet. For example, in some cases, the system meets a number of problems or ambiguous information that it cannot handle independently, requiring intervention from human operators. Based on the literature review above, fully autonomous robotic systems that can complete the entire task independently, will be the future direction of research work. Thus, the autonomy of robotic systems needs to be further investigated.

Thirdly, techniques used in other areas will be more and more adopted in the development of mobile manipulators. For example, researchers in [48] used deep learning which is mainly used in the computer vision field to detect and pick up garbage. According to the experimental results, the recognition is relatively effective and accurate, revealing the potential in cleaning lawns. In the future, an increasing number of research used in other areas will be combined with the

mobile manipulator to explore more application possibilities.

2.2 Positioning Approaches in Robotics

With the development of the Internet of Things (IOT) in recent years, robots have been widely used in many indoor scenarios such as factories and airports. To determine their own positions in the environment, positioning has become an essential component and numerous sensors have been deployed for indoor positioning. For example, Automated Guided Vehicles (AGVs) have been generally applied in industry for several tasks such as transporting material from one place to another. Aided by the visual sensors, AGVs can easily and accurately navigate in the building by detecting the artificial markers that are set in the environment. As one of the most important components for a robot's autonomous navigation, positioning in robotics has been extensively researched and a variety of methods have been proposed [65].

Classified by the obtained positioning information, positioning methods can be further divided into absolute positioning method and relative positioning method [66]. The absolute positioning method uses external devices and the absolute position information can be acquired while positioning information needs to be derived and calculated from the data of sensors such as inertial sensors and encoders in the relative positioning method. Additionally, according to the usages and principles of sensors, the methods of positioning can be divided into two categories, which are single sensor positioning method and multi-sensor fusion positioning method. For the single sensor positioning method, the positions of the agent are estimated depending on a single sensor, among which LiDAR and cameras are universally utilized with specific advantages and limitations. The visual sensors are low-cost and can provide high performance. However, the

performance of perception is easily affected by changes in environments such as illumination variation. By contrast, high-frequency data can be obtained from LiDAR but the data resolution is usually not adequate and the content information needs to be converted into more intuitive information. Compared with the single sensor positioning methods, multi-sensor fusion positioning methods improve the robustness as well as the accuracy of positioning greatly by collecting and fusing the environmental information from different types of sensors. Additionally, for the sake of using multiple sensors for positioning, it is possible that the robotic system contains two or more positioning methods to adapt to different scenarios, allowing switching among different sensor suites. Thus, the auxiliary positioning method can be used as a substitute if the primary positioning method is unavailable in some cases. Based on these advantages, the related research in multi-sensor fusion positioning methods has become an important focus in the study of state estimation.

The first part of this section reviews and presents the state-of-the-art indoor environment positioning methods by a standalone sensor, covering the fundamental positioning principle of widely used sensors including camera, IMU and ultrasonic sensors. The second part of this section introduces the multi-sensor fusion positioning methods by using multiple sensors. Furthermore, the multi-sensor fusion methods are broadly classified into traditional methods (Kalman Filters, Bayesian network and Particle filter) and learning-based methods. Lastly, based on the employment of multiple sensors, literature works in repositioning by switching different sensor suites are introduced.

2.2.1 Single Sensor Positioning

In indoor positioning systems, cameras are usually used as a standalone tool or combined with other types of sensors for identification, tracking, and navigation

in indoor environments [67–70]. By collecting the information from cameras and deploying a set of image processing techniques, this approach has a distinct growing application. For visual indoor positioning methods, cameras are either fixed in the environment to track mobile entities such as robots and people or affixed on the mobile entities. In the first category, object tracking is performed with no need for the mobile entities to load any device. Methods in the second category use cameras for monitoring and capturing image frames from the user's perspective. The collected image frames are usually mapped with the obtained image frames from the configuration stage or acquired during the space reconstruction. The visual positioning systems are allowed to adopt various cameras (e.g. monocular cameras, stereo cameras, RGB-D cameras) for identifying artificial markers like ArUco marker and natural markers that belong to parts of the environment. In [71], a standalone vision system with a neural networks-based algorithm was researched for object detection and tracking. Shahjalal et al. [72] used a set of fixed cameras in indoor environments to reduce the rate of mobile robot's location errors and built an application that can be used in the Android platform to receive images obtained from several different simultaneous transmission links. Experimental results showed that the distance error margin is mitigated to 0.10 m by using a set of four cameras for positioning. Diop et al. [73] attached two visual cameras on a wheeled mobile robot, where one was located in the front-looking direction while another was located in the downward-looking direction. With the developed image processing algorithm, the mobile robot's positions and orientations can be yielded. Experimentally, the real-world effective test on a wheeled mobile with two cameras demonstrated that the vision odometer is 10 times better than the wheel odometer in the accuracy of traveled distance estimation. However, the visual method suffers accumulation errors in long-term traveling. In the last part of the research, a framework of unique artificial landmarks was proposed to minimize the accumulation error.

Owing to the recent advances in manufacturing and hardware designing, IMU has become ubiquitous due to its low cost and lightweight. Additionally, it enables high-accuracy positioning especially for micro aerial vehicles (MAVs) and mobile devices, possessing enormous potential in large-scale emerging applications such as autonomous driving, virtual reality (VR) and augmented reality (AR) [74–76]. Over the years, inertial sensors have been extensively deployed for the positioning of robotic systems, especially in GPS-denied scenarios such as indoor environments.

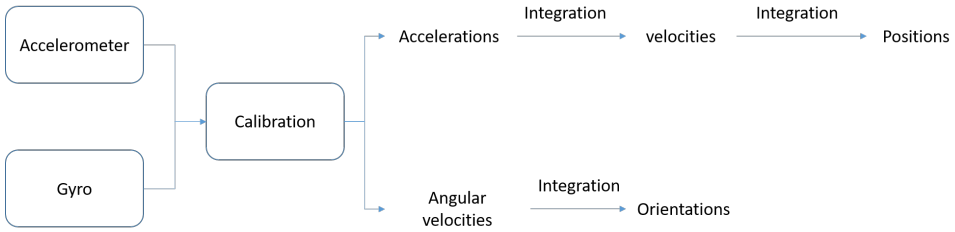

Fig. 2.3. Structure of IMU.

As a commonly used relative positioning method, IMU generally contains a triaxial accelerometer that measures accelerations and a triaxial gyroscope that measures angular velocities. The structure of IMU that includes an accelerometer and a gyroscope is shown in Fig. 2.3. Typically, each sensor can provide three measurement values defined for x-axis, y-axis, and z-axis while acceleration values and angular velocity are kept separately [77]. Through the process of calibration, more accurate measurement data can be obtained from IMU. Afterward, velocities, positions and orientations can be gained by one or more integrations. This positioning method has the advantages of low cost and easy implementation. Nevertheless, positions, velocities and attitude are gained by accumulating the inertial data from IMU while the errors of state estimation are as well accumulated over time, which can cause huge drift although each error of IMU measurement is minor.

Mathematically, acceleration is integrated once for obtaining velocity and twice for obtaining positions. Acceleration provided by the accelerometer contains three acceleration components that correspond to motion, gravity and error. The source of acceleration measurement error involves deterministic elements such as axis misalignment, bias and random elements [78]. In the following equation [79], the acceleration $\widetilde{a}$ is given as a combination of a motion component a_m, a gravitational component a_g, the bias b_a and measurement noise ε_a.

$$\widetilde{a} = a_m + a_g + b_a + \varepsilon_a \tag{2.1}$$

Since only the accelerations caused by motion rather than gravity have to be integrated, the velocities v_n at time n can be estimated by accumulating motion accelerations [79]:

$$\widetilde{v_n} = v_0 + \sum_{k=1}^{n} a_{m,k}\Delta t \tag{2.2}$$

where v_0 is the initial velocity and Δt is the integration time. Similarly, the displacements s_n at time n can be estimated by accumulating velocities [79]:

$$\widetilde{s_n} = s_0 + \sum_{k=1}^{n} v_k\Delta t \tag{2.3}$$

For gyro in IMU, the measurement model can be expressed as follows [79].

$$\tilde{\omega} = \omega + b_\omega + \eta_\omega \tag{2.4}$$

, of which $\tilde{\omega}$ is the measured angular velocity while ω is the true angular velocity. b_ω and η_ω are gyro bias and additive measurement noise respectively. Therefore, the orientation can be derived from gyro measurements by using Taylor expansion [79]:

$$\theta_{(t+\Delta t)} \approx \theta_{(t)} + \omega\Delta t \tag{2.5}$$

For outdoor positioning, the global positioning system (GPS) is the most popular system used in outdoor environments for position determination. However, GPS cannot be deployed in indoor environments due to the requirement of line-of-sight (LOS) when connecting the satellites with the handset. Thus, "indoor GPS" po-

sitioning system, which contains a receiver, pseudolites and other transmission devices, has been adopted as an independent positioning system. The core concept of the "indoor GPS" is that the receiver continuously receives the signal through indoor transmitters, which is similar to the outdoor GPS positioning system.

Ultrasound defines the spectrum of sound waves with high frequency that is beyond human perception (more than 20 kHz). Since the technology does not require direct visibility between signal readers and transmitters, it is considered as a more effective positioning solution than GPS. As a type of "indoor GPS", ultrasonic positioning system has been widely used in a variety of economic sectors such as warehouses and healthcare owing to its centimeter-level positioning precision. The flow chart of the positioning principle based on the ToF (Time-of-flight) method is displayed in Fig. 2.4, where the signal propagation time between the "base station" and signal receiver is measured and the corresponding distance is obtained by applying tags that transmit ultrasound impulses. The receivers scan ultrasonic signals and send information to the central system for position calculation by multilateration method.

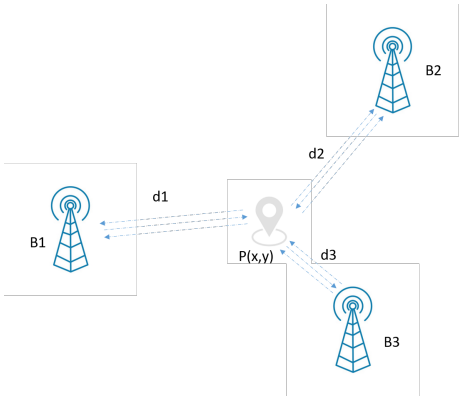

Fig. 2.4. Positioning by range-based method.

In the algorithm of planar positioning, there requires at least three anchor nodes with known locations to calculate the location of the target point by distances

from anchor nodes to the target point. Assume that the positions of target point P is (x, y) and the base stations B_1, B_2 and B_3 are located at fixed positions (x_1, y_1), (x_2, y_2) and (x_3, y_3) respectively. The distances between the target point and the base stations are d_1, d_2 and d_3 respectively, which can be known by the speed of the ultrasonic wave and ToF [80]:

$$\begin{cases} d_1 = \sqrt{(x - x_1)^2 + (y - y_1)^2} \\ d_2 = \sqrt{(x - x_2)^2 + (y - y_2)^2} \\ d_3 = \sqrt{(x - x_3)^2 + (y - y_3)^2} \end{cases} \tag{2.6}$$

Then the positions (x, y) of target point P can be derived from the above equation and shown in the following equations [80]:

$$\begin{bmatrix} x \\ y \end{bmatrix} = \begin{bmatrix} 2(x_1 - x_3) & 2(y_1 - y_3) \\ 2(x_2 - x_3) & 2(y_2 - y_3) \end{bmatrix}^{-1} \begin{bmatrix} x_1^2 - x_3^2 + y_1^2 - y_3^2 + d_3^2 - d_1^2 \\ x_2^2 - x_3^2 + y_2^2 - y_3^2 + d_3^2 - d_2^2 \end{bmatrix} \tag{2.7}$$

2.2.2 Multi-sensor Fusion Positioning

The sensors introduced above have commonly existed in indoor positioning literature and numerous research about robotic positioning have been conducted relying on a single sensor [81]. Nevertheless, introducing an additional sensor modality can assist the indoor positioning system to obtain more information about the state of the agent or the around environment, which has become an important direction in the research field of robotic positioning. By relying on more than one sensor modality, the positioning system can possess plenty of distinct advantages such as accuracy and robustness improvement [82]. In the last few decades, multi-sensor fusion approach which integrates multiple information sources to obtain robust and reliable sensing performance has been extensively researched as a typical option for accurate and robust robot state estimation [83]. A number of positioning techniques based on multi-sensor fusion have been presented to date [84, 85]. According to the classification in [86], the multi-sensor fusion methods can be divided into traditional methods and learning-based meth-

ods. Traditional fusion methods involving the Kalman filter, Bayesian network and Particle filter, have been studied and extensively used for decades while the learning-based sensor fusion approach is still in its infancy and has not been widely adopted since many challenges in this research area remain to be solved.

2.2.2.1 Traditional Multi-sensor Fusion Methods

In this subsection, three traditional typical multi-sensor fusion methods, which are Kalman filter, Bayesian network and Particle filter, are introduced respectively.

Since the formulation of the Kalman filter (KF) allows multiple sensor modalities to be arbitrarily fused, KF has been extensively applied in sensor fusion systems. Additionally, the algorithm is able to perform in real-time, which as well increases its popularity. Usually, the KF formulation contains a prediction process corresponding to a form of state-space modeling and followed by a correction process. As a non-linear formulation of the KF, the extended Kalman filter (EKF) approximates the models of state transition through linearisation and is commonly used in literature. Researchers in [87] proposed a positioning system based on the multi-sensor fusion of radar, ultrasonic and odometry data, using the EKF algorithm to determine the positions and orientation of a mobile robot in an indoor environment. The work in [88] utilized an EKF approach to integrate IMU and vision data extracted from sped-up robust feature and random sample consensus algorithms to estimate the mobile robot pose in an indoor environment. Authors in [89] proposed a hybrid modes data fusion approach. The IMU data was fused with ultrasonic data by EKF when it was available while the trained least squares support vector machine corrected the inertia navigation system during outages. In [90], the researchers applied EKF to fuse the wheel encoder and computer vision system with augmented reality code. In a simulation environment, the approach can successfully deal with unknown initial

positions and robot kidnapping problems. Likewise, EKF can be incorporated with the SLAM technique, which is known as EKF-SLAM. Gao et al. [91] used an enhanced EKF-SLAM based on directional endpoint features extracted from laser data for an indoor navigation task of mobile robots. In [92], the relative performance of two filter works Particle filter and EKF, were compared in terms of performances in positioning and tracking. The experimental results concluded that they have similar tracking accuracy but the Particle filter is much more demanding than EKF in computation cost.

Bayesian network, known as Belief network or directed acyclic graphical models, are a subset of probability graph models. For a multi-sensor fusion system, the nodes of the graph mean modeled variables while the connections between the nodes represent their conditional dependencies. Simply put, by using the directed acyclic graphical models and connecting all the involved random variables of the system according to their conditional independence, the Bayesian network is then formed. For random variables, the expression of the joint probability distribution can be given by the following equation [93].

$$p_{(x_1,\ldots,x_k)} = \prod_{i=1}^{k} p_{(x_i|pa_{x_i})} \tag{2.8}$$

where x denotes a set of nodes and pa_{x_i} means all the parents node of node x_i.

Overall, this approach can combine multiple pieces of evidence to give the expression of uncertainty and thus is generally used in fusing several sensor data for obtaining reliable estimation. Each sensor data is taken as a Bayes estimation and then the joint posterior probability distribution of a multi-sensor system can be obtained by incorporating the associated probability distribution of individual objects. By minimizing the likelihood function of the joint posterior probability distribution, the fusion value of a multi-sensor setting is acquired. Hidden Markov Models (HMM), which are based upon dynamic Bayesian network, are a popular example used in evaluating temporal processes such as speech recognition. The

evaluating joint probability between the states x and observations y during the overall process can be described as follows [94].

$$p_{(x_{1:n},y_{1:n})} = p_{(x_0)} \prod_{i=1}^{n} p_{(y_n|x_n)} p_{(x_n|x_{n-1})} \tag{2.9}$$

In above equation, $p_{(x_0)}$ is the prior probability. $p_{(y_n|x_n)}$ represents the emissions such as likelihood and $p_{(x_n|x_{n-1})}$ represents the transition dynamics.

Many examples of Bayesian fusion can be found in multi-sensor fusion literature. He et al. [95] used an HMM approach to obtain the probabilistic fusion of multiple modalities for the indoor positioning of a mobile device. A graph structure was proposed to store the information from multiple sensors for the offline processing phase while a multi-modal particle filter was utilized to fuse the information seamlessly for the online processing phase. The designed system and proposed algorithm were evaluated on the iOS platform and showed robust, accurate, highly-integrated positioning results.

Basically, Particle filter is a branch of Bayesian estimation methods, which recursively estimates the posterior probability of the state involved with some observations from sensors. Particularly, this approach builds up the probability density function of the state by considering all previous sensor observations. To estimate the state, the prediction of the belief $p_{(x_i|y_{1:i-1})}$ is firstly calculated and the formal expression is given as follows [96].

$$p_{(x_i|y_{1:i-1})} = \int p_{(x_i|x_{i-1})} p_{(x_{i-1}|y_{1:i-1})} d_{x_{i-1}} \tag{2.10}$$

where x_i is the state estimation at step i and $y_{1:i-1}$ are all the observations of sensor data from step 1 to step $i-1$.

Then, the posterior probability of the state estimation is updated recursively by Bayes' theorem which is based on probabilistic inferences. The update equation is shown below [96]:

$$p_{(x_i|y_{1:i})} = \frac{p_{(y_i|x_i)} p_{(x_i|y_{1:i-1})}}{p_{(y_i|y_{1:i-1})})} \tag{2.11}$$

A great deal of literature in terms of multi-sensor fusion by using the Particle filter method can be found in applications ranging from robotic area to motion recognition. To estimate the location of the humans in indoor environments, Pham et al. [97] used a Particle filter module to fuse the motion information from wearable IMU that was attached to human subject passive and location information from infrared sensors distributed in the environment.

2.2.2.2 Learning-based Multi-sensor Fusion Methods

Owing to the advances of machine learning in recent years, a great deal of research works have been conducted on the usage of tailored artificial neural networks (ANN) for sensor fusion [98,99]. Although there exists a large number of literature dedicated to using ANN algorithms for objective specific sensor fusion, learning-based method still remains extensively unexplored and the standardization among the positioning methods is lacking [86].

Generally, ANN is used in the processing process before implementing actual fusion [100–102]. To estimate the roll angle which is used as a "pseudo-measurement" for the following steps, the authors in [100] firstly used a neural network module, which is based on the widely-used method Back-Propagation algorithm and IMU data. Then the pseudo roll angle was utilized into a Linear Kalman Filter algorithm for the state estimation of a vehicle. Wang et al. [101] used Channel State Information and deep learning-based algorithms for indoor positioning applications. By using the neural network method, the features of wireless channel information were explored and the optimal weights were trained and obtained as fingerprints, which were used for the feature extraction of positioning. To reduce the computational complexity of the neural network method, a greedy learning algorithm was incorporated into the system. The weights gained from the offline training phase were then fused together within a probabilistic

method in the online stage for location estimation. Jamil et al. [102] proposed using learning to prediction model and sensor fusion method for position estimation in indoor environments. In the sensor fusion module, for the sake of obtaining the noise-free and drift-free orientation matrix of the object, Kalman filter was used in fusing three 3-axis sensors of IMU, which are, accelerometer, gyroscope, and magnetometer. The positions of the object were then gained through the integration of linear acceleration. In the learning to prediction model, the prediction based on Kalman filter is tuned by the learning module to improve the performance of the prediction algorithm, while the learning module based on an ANN framework continuously receives the output data from the Kalman filter as feedback to determine the external parameters and assess the performance of the prediction algorithm.

2.2.2.3 Repositioning in Multi-sensor Fusion Positioning System

For the sake of multi-sensor fusion positioning, sensor suites switching can be used and validated to perform robust state estimation [103]. Authors in [104] indicated that MEMS-based inertial sensors such as IMU are suitable for pose estimation in environments where GPS signals are unstable. In the case of GPS failure, camera is an excellent substitute to aid inertial navigation owing to its low cost and high-dimensional information. Thus, a measurement model was derived first, where geometric constraints are defined when a static feature is observed from several camera poses. This model was then combined into an EKF-based algorithm for state estimation without involving the 3D feature position to reduce the computational complexity of the system. According to the experiments in indoor and outdoor environments, the proposed vision-aided inertial navigation system can handle different cases and achieve accurate, robust and real-time state estimation.

In [105], the researchers investigated a multi-sensor fusion approach to improve the robot navigation performance in accuracy and robustness. EKF-based framework involving multiple sensors was presented to seamlessly handle additional or lost sensor signals. The modular design allows for deploying a limitless number of sensor types and sensors with the scheme of online self-calibration of the sensor suite. In addition, re-linearization of the state prediction was achieved by Iterated EKF and a state buffering scheme for dealing with highly nonlinear systems. To demonstrate the efficiency of state estimation framework, different types of sensors including a GPS receiver, visual sensor, inertial sensor and pressure sensor were combined into a robotic system for indoor and outdoor navigation. The experimental SLAM results indicated that the proposed method can efficiently and seamlessly switch between different sensor elements, which improves the system performance in robustness and fail-safety, especially in long-term tasks.

The failure of GPS receivers or dynamic maneuvers containing challenging motion might result in the loss of important information such as attitude and heading, which leads to a disastrous scene. Similar to [105], researchers in [106] adopted a backup scheme for state estimation to handle the scenario of GPS failures. If the GPS is available, the normal operation that fuses GPS, static pressure, inertial sensors and three-axis electronic compasses, is performed and the position update from GPS is applied to EKF. Otherwise, the navigation system switches to backup operation, where the filter update employs airspeed vector measurement in place of the position update. From the simulated flight test, the EKF-based inertial navigation system with the proposed backup algorithm can provide continue orientation estimation even in the case of GPS failures and a seamless switch from backup operation to normal operation once the GPS signal is recovered.

Hausman et al. [103] fused multiple sensors including GPS, ultra-wideband

range measurements, visual sensor and IMU measurements into an integrated multi-sensor fusion system for state estimation. The positioning system allows seamless switching between different sensor modalities according to the statistical signal quality analysis. Additionally, self-initializing and self-calibrating approaches were introduced for escaping external calibration or initialization as well as handling erroneous measurements. The evaluation on a real robotic system indicated that the design of seamless sensor suites switching enhances the robustness of systematic state estimation.

2.2.3 Key Findings

Visual sensors have been extensively deployed in robotic positioning owing to their high accuracy and precision, but the performance is easily affected by a variety of factors such as confined view. To ensure the robustness of positioning, fusing more than one sensor for positioning is a common practice. For the multi-sensor fusion approach, an ANN-based sensor fusion algorithm usually requires a large computational load and training process, which is not suitable for real-time performance. In traditional fusion methods, EKF can deal with the nonlinear system through Taylor expansion while ensuring computational efficiency for providing real-time state estimation.

2.3 Image Deblurring in SLAM

In the last decades, the research on mobile robots, especially in the aspect of autonomy improvement, has attracted considerable attention from worldwide researchers and brought about major progress and breakthroughs [107,108]. Presently, mobile robots possess the capability to perform complex tasks with partial autonomy, whereas input and interaction from humans are needed in the past to

ensure the system can be operated properly. By now, mobile robots have been applied to diverse fields including manufacturing. It is expected that mobile robots have more autonomy and can perform complex tasks independently in dynamic environments without human intervention [109]. To achieve autonomous navigation and path planning, it is necessary and challenging that robots can update the environment map and positioning themselves in the environment. This challenge has been greatly investigated and numerous approaches have been proposed. Simultaneous localization and mapping (SLAM) is an important solution that was formulated in the 1980s [110, 111]. The concept of SLAM is defined as follows: when the robot enters into an unknown environment, it can construct a map of the surrounding environment and positioning itself in real time with the aid of external sensors such as camera and LIDAR. The SLAM system aims at obtaining a globally consistent pose estimation of the robot and environmental map. In recent years, visual sensors have been largely applied to SLAM systems owing to their number of advantages such as small volume and richness of information. However, challenges arise when applying visual-based SLAM in the practices of autonomous manufacturing. For example, blurred images that exist in visual-based SLAM can result in low-quality outcomes [22]. Thus, minimizing the effects of blurred images in visual-based SLAM is focused on in this thesis.

In this section, a detailed literature review of the current state-of-the-art in SLAM and image deblurring methods is first provided. Then, the advanced technique of SLAM systems combined with image deblurring methods is reviewed to highlight the knowledge gaps.

2.3.1 Visual-based SLAM System

In the past couple of decades, SLAM has been extensively studied, resulting in many different solutions with the aid of various of different sensors such as Laser

scanners [112] and sonar [113]. Recently, the interest in visual-based SLAM, has enormously increased due to the rich visual information obtained from low-cost video sensors [22]. Owing to the recent advances in Central Processing Unit (CPU) and graphics processing units (GPU) technologies, the major drawback, which is the high computational cost, is no longer an insurmountable problem and thus the real-time implementation of the required sophisticated SLAM algorithms can be performed to process images and extract crucial information. As a matter of fact, various visual sensors such as monoculars and cameras that combine color and depth (RGB-D) have been utilized as promising SLAM solutions.

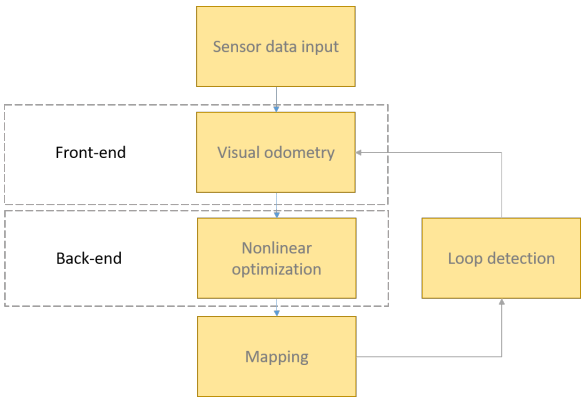

Fig. 2.5. Classical visual SLAM framework.

Visual-based SLAM system usually deploys one or more visual sensors to receive 2D images, which serve as the input of SLAM information. Generally, the visual-based SLAM system can be divided into five main modules: sensor data input, visual odometry, nonlinear optimization, mapping and loop detection [114]. Fig. 2.5 demonstrates a general view of the five main parts normally presented in visual-based SLAM techniques. Visual odometry is a process to estimate the robot's position through the information from sensor input, which is usually called the front-end, while the part of nonlinear optimization is a process to determine the most likely poses of the robot and is called the back-end. The mapping process is responsible for the construction of an environmental map.

The part of loop closure detection enables the SLAM system to correct the accumulated drifts at the end of the trajectory. In visual-based SLAM systems, other different types of sensors such as IMU can be integrated as well, resulting in diverse forms of input data such as image data, IMU data and depth data. In regards to visual-based SLAM, visual SLAM (VSLAM) uses solely cameras and visual-inertial SLAM (VI-SLAM) uses both cameras and IMU, attracting most of the research and giving an excellent illustration of new SLAM strategies. Thus, VSLAM and VI-SLAM are emphatically surveyed in this work.

2.3.1.1 Visual SLAM System

One of the groundbreaking VSLAM solutions, which is known as Mono-SLAM, was introduced by Davison et al. [115] in 2007. In this SLAM system, a single monocular camera is employed to implement the real-time Structure from Motion. By extracting sparse features of the images using a Shi and Tomasi detection operator [116] and matching new features to those already observed using a normalized sum-of-squared difference correlation, the environment map is constructed based on the probabilistic framework. However, using a single monocular camera means that the camera is hard to calibrate and the absolute scale of the system can not be gained. In addition, as an EKF was utilized in the system for state estimation, this SLAM approach can only extract and track a limited number of features to reduce the computational cost of the EKF, which constrained the performance of the system in large scenes.

Newcombe et al. [117] presented a depth-only mapping algorithm using a fully direct method, which is known as dense tracking and mapping (DTAM). This is the first time applying a fully direct method in the literature. The system comprises two main modules, which are dense mapping and dense tracking. In the dense mapping stage, multi-baseline stereo is used for mapping and then the

space continuity is considered to optimize the generated map and compute the 3D coordinates of all pixels. In addition, data cost volume, which represents the average photometric error of multiple frames, is defined to estimate the depth values. Subsequently, the inverse depth of the current frame is derived from the depth values to integrate the reconstruction with minimizing the photometric error. In the second stage, the input image of the current frame is compared and aligned with images generated from the dense reconstructed map. The algorithm presents high accuracy and sufficient information of reconstruction but requires a large computational cost to process and store the data owing to the high level of density reconstruction. Therefore, state-of-the-art GPUs are needed to operate DTAM in real time.

Compared to dense maps, where pixel information of most or all of the image frames is used to reconstruct maps, the sparse method obtained information from a small selected subset of the pixels and mainly focused on trajectory correctness. As a well-known sparse point cloud features-based SLAM, ORB-SLAM was first proposed in 2016 [118]. It works in four parallel threads: map initialization, tracking, local mapping, and loop closure. In the process of map initialization, the initial correspondences are found based on the extracted Oriented FAST and Rotated BRIEF (ORB) features in the current frame and matches search in the reference frame. In parallel threads, a homography and a fundamental matrix are computed to apply relative orientation. The initial map of landmarks or 3D points is created by triangulation. The tracking stage is matching features in the current image frame with previously created keyframes. By applying resection techniques such as the perspective-n-points method, the pose of the robot is estimated as the 3D positions of the matched features have been determined in the previous procedure. As for the back-end step, local mapping uses the current image frame to adjust the pose of the robot and construct new map points. This is achieved by performing bundle adjustment that minimizes the reprojection error

of 3D map points. Loop closure is responsible for the drift error correction in the loop and new loop detection. The loop closure and all the poses are refined by bundle adjustment or graph optimization if the revisited place is detected with the deployment of the bags of words technique.

Originated from monocular feature-based ORB-SLAM, ORB-SLAM2 algorithm [119] extended the application and can be implemented for stereo and RGB-D cameras. Differing from methods based on photometric and depth error or Iterative Closest Point (ICP), the back-end of ORB-SLAM2 adopts bundle adjustment and achieves higher accuracy in RGB-D results. Using monocular observations and stereo points makes the better performance of ORB-SLAM2 than other state-of-the-art direct stereo SLAM algorithms. However, the unidentification of highly similar frames is likely to cause the failure tracking and state loss situation. Additionally, the requirement of keeping the same frame rate between the acquired images and processed images makes it difficult to apply to embedded platforms with real-time operation. In spite of this, there are still several embedded implementations based on CPU or GPU platforms that can be found in the literature.

In 2012, Henry et al. [120] first implemented the SLAM by using a Microsoft Kinect, which is a type of RGB-D camera. The researchers utilize the information obtained from the camera to build a 3D dense model of the environment and estimate the 6 DoFs pose of the camera. The Features from Accelerated Segment Test (FAST) [96] features are extracted from RGB images and subsequently matched with the features obtained from the previous frame via the Calonder descriptors. Then random sample consensus alignment procedure is performed to obtain a subset of feature matches that correspond to a consistent rigid transformation and combine with dense ICP to determine the best frame-to-frame alignment. In addition, sparse bundle adjustment is utilized to improve global optimization for obtaining a globally consistent map. The method of matching the current frame with the previously collected keyframes is utilized for the process of loop

closure detection. Based on this algorithm, a number of variant RGB-D SLAM have been researched. Endres et al. [121] proposed an RGB-D-SLAM that replaces the FAST features with three different features, which are scale-invariant feature transform, speeded up robust features, and ORB feature. The researchers also contributed a 3D pose graph optimization by the g2o framework instead of bundle adjustment for consistent global optimization.

2.3.1.2 Visual-Inertial SLAM System

Although significant improvements have been developed in the research of VSLAM, a key limitation of using VSLAM is the lack of sufficient robustness within challenging environments such as low texture and illumination changes. Numerous researchers have investigated the coupling of cameras and IMUs for solving the robustness problem of VSLAM [122–125].

Qin et al. [122] proposed a real-time monocular visual-inertial state estimator in 2018, which was called Monocular Visual-Inertial System (VINS-Mono). The IMU data between the adjacent frames is pre-integrated and the images from the camera are processed as a measurement process to extract features. Then, an initialization process is performed through a non-linear optimization process that minimizes both the visual and inertial errors to provide the initial guess of states. Also, the VINS-Mono algorithm implements online relocalization and a 4-DoF pose-graph optimization module that fuses the IMU data and features observations from the visual sensor. When compared with other SLAM systems such as Robust Visual Inertial Odometry [123], Visual Inertial ORB-SLAM [124] and Open Keyframe-based Visual-Inertial SLAM, VINS-Mono demonstrates high accuracy yet high memory usage as well. In spite of this, due to the fact that the VINS-Mono system merely considers the latest IMU states such as pose and velocity for the optimization process, this SLAM algorithm still has the advantages

in embedded implementations.

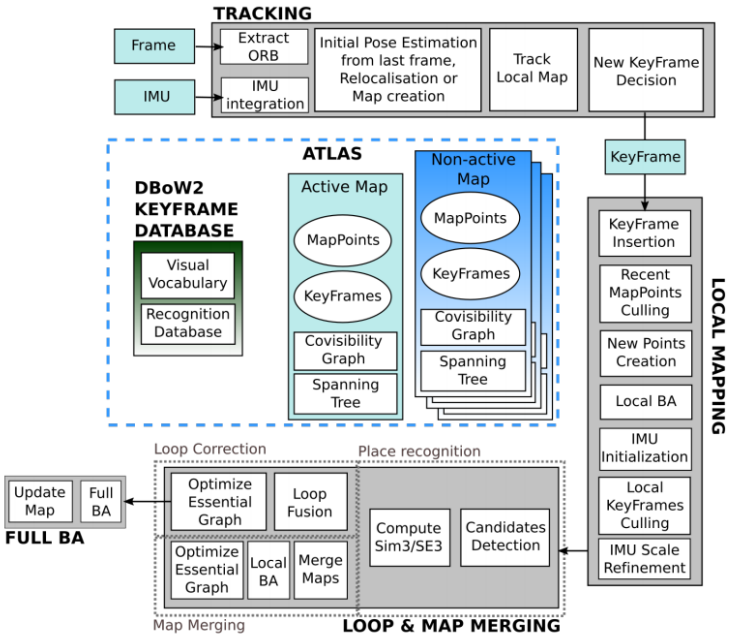

Fig. 2.6. The pipeline of ORB-SLAM3. [125]

On the basis of ORB-SLAM and ORB-SLAM2, the ORB-SLAM3 algorithm was proposed in 2021 [125]. Similar to its predecessors, the algorithm contains three main threads, which are tracking, local mapping, loop closure and map merging instead of loop closure. The framework of ORB-SLAM3 is presented in Fig. 2.6. A multi-map representation called Atlas maintains both active maps and non-active maps. In an active map, the incoming frames are localized by the tracking thread and optimized continuously through the local mapping thread. Non-active maps are stored for relocalization and place recognition, loop closure and map merging. ORB-SLAM3 follows the same principle as VIORB in the threads of tracking and local mapping but adds map merging in the third thread. In the thread of loop closure and map merging, both the active and non-active maps in the atlas are used to detect the common regions. The loop correction is performed if the common area locates at the active map, or maps merge are

conducted to form a single active map.

Another important contribution of ORB-SLAM3 is the visual-inertial initialization method based on the Maximum-a-Posteriori (MAP) estimation. Vision-only and inertial-only MAP estimation are applied respectively and then jointly optimized by a full visual-inertial bundle adjustment. This algorithm is able to work with pure visual modes with sensors such as monocular, stereo and RGB-D or visual-inertial modes. However, the online performance of ORB-SLAM3 is not good, which is demonstrated in [126]. Authors in [127] compared three modern approaches, which are ORB-SLAM3, OpenVSLAM and RTABMap. By performing in several different datasets, the experimental results illustrated that ORB-SLAM3 failed to process in several experiments.

2.3.2 Image Deblurring Methods

Over the years, algorithms have been improved significantly in many fields of our life. It is common that images are acquired as the input data to feed to the system for desired output. To ensure that the images can be well interpreted, image degradation should be handled for better processing of algorithms [128]. Due to the natural scene illumination or the point spread function (PSF), which refers to the response of an imaging system such as a camera to a point object or point source, the captured images inevitably contain blur or noise [129].

Image deblurring is a classical task of image restoration. There are numerous causes that give rise to different types of image blurring such as out-of-focus blur and motion blur. When the object in the scene is located out of the range of depth-of-field, the out-of-focus blurring occurs. Generally, the techniques of out-of-focus deblurring correspond to the extension of the depth-of-field of the camera. Motion blur refers to the obvious streaking of moving objects in image frames, which resulted from the rapid movement of the camera or long exposure

when being utilized for changes recorded of a single exposure [130].

Advanced techniques of image deblurring against motion blur are the most commonplace as motion blur is generally not what the photographer wants to introduce to the captured image [131]. As mentioned before, motion blur occurs due to rapid camera movement or changes in the recorded scene. Capturing an image needs a certain exposure time. During this exposure time, if the movement of an image that projects into the sensor exceeds the size of a single pixel, motion blur arises. The longer the exposure time, the more severe blur appears in the image. The blurring kernel, which is generated by the accumulated motion trajectory of the scenic spots, records the energy distribution in the image and influences the area of the scenic points amid the exposure time [132]. Therefore, the most direct method of reducing the blur phenomenon is shortening the exposure time. For example, when capturing the image using an exposure time that is lower than the shutter, the blur in the image caused by the camera shake can be minimized. Whereas, in some scenarios, decreasing exposure time causes problems as well, such as high noise and color cast. Until now, there are plenty of image restoration approaches that have been developed to solve the blur problem in different scenarios. The image deblurring approaches can be classified in various forms, for instance, blind deblurring and non-blind deblurring according to whether the blur state is known or not [133]. Additionally, the classification can be divided into traditional method methods and learning-based methods in accordance with different restoration principles. The following gives a detailed introduction to deblurring methods by this classification.

2.3.2.1 Traditional Image Deblurring Methods

Generally, the traditional image deblurring technique first builds the model of the blurring process and solves the inverse process with the aid of various mathemat-

ical tools such as the optimization method. The classic form of the traditional deblurring approach is given as follows [134]:

$$g_{(t)} = h_{(t)} * f_{(t)} + n_{(t)} \tag{2.12}$$

$n_{(t)}$ represents the noise term. As the blurred image $g_{(t)}$ is known, the original image $f_{(t)}$ and blurring kernel $h_{(t)}$ can be estimated by the blind deblurring approach. Or $f_{(t)}$ is estimated based on the known $g_{(t)}$ and $h_{(t)}$, which is recognized as a non-blind deblurring solving process.

Since the 1960s, image problems have been transformed into the frequency domain to solve the problem of image deblurring. Classical deconvolution frameworks such as Wiener filter [134] and Lucy-Richardson [135, 136] have been proposed. As one of the most typical techniques in the field of image deblurring, Wiener filter demonstrates substantial capability in dealing with blurred images caused by linear motion or out-of-focus optics. The noise has a great impact on the image deblurring algorithm which is based on the frequency domain. Basically, the main concept of Wiener filter is minimizing the mean squared error between the estimated image and the desired image, which is produced by linear time-invariant filtering of the observed images with stationary known additive noise and signal and noise spectra. In Wiener filter deblurring, an optimal trade-off between noise smoothing and inverse filtering can be achieved because the additive image noise is removed and the blurring is inverted simultaneously. Thus, Wiener filter is a simple and efficient algorithm for image deblurring.

The Richardson-Lucy deconvolution, proposed by William Richardson and Leon Lucy, is an iterative procedure based on Bayes' theorem of conditional probability related to the PSF and degraded image for image deblurring [135, 136]. The main idea of this deconvolution is to represent the blurred image pixels with respect to the known PSF and unknown sharp image. One problem of Richardson-Lucy deconvolution is that an underlying theory is required in the

calculation for determining the size of the blurring kernel. Although the blurring kernel is involved in the deblurring calculation, the size of the blur kernel is assumed to be known, hence making the devolution process non-blind. This algorithm is adequately efficient even in the presence of noise with no need for any prior information from the input image.

In most real-world cases, PSF is unknown and thus the blind deblurring problem is more practical than non-blind deblurring. Based on the traditional devolution algorithms, a number of new blind deconvolution algorithms have been designed and can be found in a variety of literature.

Projection-based blind deconvolution and maximum likelihood restoration are two basic blind deconvolution approaches [133]. The former firstly gives an initial estimation of PSF and then the initial estimation of the sharp image is obtained by non-blind deconvolution. This process is repeated and will cease until the requirement of a predefined convergence criterion is satisfied. This approach is insensitive to noise and robust against inaccuracies of support size. However, it is not unique and errors will be caused if the local minima have been initiated unsuitably. In regards to the latter, parameters such as PSF and covariance matrix are estimated by using maximum likelihood. Owing to the non-uniqueness of PSF estimation, PSF parameters such as symmetry and size can be considered. This approach has the advantage of low computational complexity with obtaining the blur, noise and power spectra of the true image. However, it converges to local minima for solving the estimated cost function.

Authors in [137] combined the Richardson-Lucy deconvolution with a pyramid structure for image restoration. A three-layer pyramid structure was built and the Richardson-Lucy algorithm with different numbers of iterations was used from coarse scale to fine scale. Compared with the Richardson-Lucy deconvolution, less computation time was required by implementing the proposed algorithm.

The performance of image restoration was satisfactory without the ringing effect according to the simulation results.

In [138], the PSF was firstly estimated and then the Wiener filter was performed to deblur the image after obtaining the estimated PSF. Specifically, to accurately estimate the PSF, blur orientation and extent caused by uniform linear motion were obtained by adapting Rekleitis' approach [139] which uses information from the motion blur to estimate the optical flow map. Following this, motion parameters caused by uniform acceleration motion were obtained by using the average autocorrelation function. Based on these motion parameters, the PSF was created and non-blind deconvolution was then implemented.

2.3.2.2 Learning-based Methods

With the rapid development of machine learning, diverse learning-based image restoration methods have emerged in recent years [140–143]. Compared with image restoration tasks such as image denoising and super-resolution, learning-based image deblurring methods started slightly later.

Generative Adversarial Networks (GAN), introduced by Ian Goodfellow et al. [140] in 2014, is a learning method to generate synthetic data that is remarkably similar to real known input data. By using this method, convincing images involving various types of images can be generated and its amazing ability to reflecting higher-order semantic logic has been shown. There are two models involved in GAN: generator network and discriminator network. The generator network takes random input values such as dimensional noise vectors to generate images and assimilate them to the real images by using a deconvolutional neural network. The discriminator network offers a contrast between the generated image and the real image and determines whether they look alike. A GAN model is a method of adversarial learning and various image restoration methods based

on this have been proposed in recent years.

Inspired by the work on image-to-image conversion and image super-resolution in GAN, Kupyn et al. [141] proposed a GAN-based framework: DeblurGAN, which is an end-to-end conditional GAN used for motion deblurring. In the constructed GAN model, both the generator network and discriminator network are trained. During the training phase, the generator network is trained and the discriminator network is introduced as well, where the two networks are trained in a confrontational manner. Through this alternate training approach, the performance of both networks can be improved when continuously competing with each other. Two loss functions, content loss and adversarial loss, are built and combined as the total loss for image deblurring. Generally, the content loss is responsible for recovering the general image content while the adversarial loss is responsible for recovering the image details. The experimental results showed that a blurry image can be transformed into its corresponding sharp version by the trained generator network.

Kupyn et al. further extended this method to a new framework of DeblurGANv2 [142]. Compared with DeblurGAN, the authors adopted a feature pyramid network as the generator while using a relativity discriminator as the discriminator to improve the deblurring efficiency and performance. In the feature pyramid model, a higher spatial resolution is rebuilt from the semantically rich layer by following a top-down path. The top-down and bottom-up paths with high-resolution details are complemented by the horizontal connection between the compartments. Feature maps with different scales are obtained as the output, where all layers of information are integrated to improve the image deblurring performance. The feature semantic information in the low level is relatively small but contains an accurate target location while the feature semantic information in the low level is richer but has a relatively rough target location. Owing to the independence of predictions at different feature layers rather than fused features

for predictions, the feature pyramid network can handle convolution and other processing at different times, which enhances deblurring efficiency and performance.

Scale-recurrent Network (SRN-DeblurNet) is another learning-based approach proposed by Tao et al. [143] for deblurring tasks. Compared to many recent learning-based approaches, SRN-DeblurNet is smaller in structure and number of parameters, which is easier to be trained.

2.3.3 SLAM System Involving Image Deblurring

A massive effort in evaluating the robustness of different SLAM systems has been made but mainly focused on singular specific types of perturbations [144, 145]. Bujanca et al. [146] introduced a systematic evaluation methodology to assess the robustness of different SLAM algorithms such as OpenVINS, ORB-SLAM2, ORB-SLAM3 and FullFusion in scenarios containing singular perturbation or multiple disturbance. The authors illustrated that the camera is widely deployed in SLAM and motion blur that results from the camera's rapid movement hinders both direct alignment and feature detection. Thus, the capability of dealing with motion blur is taken as one of the most significant benchmarks when evaluating the effectiveness of SLAM system. The three baseline datasets, TUM, ICL-NUIM and EuRoC-MAV, are selected and used to thoroughly quantify the evaluation results. From the experimental results, if only a small portion of the blurred image frames are encountered, ORB-SLAM3 can quickly recover from the dynamic scene, otherwise, it will fail to perform mapping and localization.

Guo et al. [147] developed a DeblurSLAM framework based on the Visual SLAM system ORB-SLAM2 and deblurring network DeblurGANv2 to improve the image quality by removing the motion blur in the image. The input images are first delivered to the process of blur detection, where the sharpness of the image

is calculated by the Laplacian algorithm. Then the image is determined as a clear image or blurred image according to the comparison of Laplacian variance and set threshold. If the image is determined as a clear image, the processed image is sent to the SLAM part. Otherwise, the image that is regarded as a blurred image is fed into DeblurGANv2 for deblurring. The ORB-SLAM2 and DeblurSLAM were evaluated by performing on both the TUM and KITTI datasets. The experimental results revealed that DeblurSLAM improves the feature point extraction, matching effect and trajectory accuracy in contrast with ORB-SLAM2. However, the processing time of image deblurring is generally vast, which is not quantified in this research and thus cannot prove the real-time capability of DeblurSLAM.

In [148], Luo et al. improved the ORB-SLAM2 system with a traditional image prepossessing algorithm, which is an adaptive image sharpening adjustment based on information entropy. The SLAM system can deal with the failure of localization and mapping resulting from the raid movement and large-angle rotation of the camera. The adaptive image sharpening adjustment allows to automatically determine the information entropy threshold for the preparation of image sharpening adjustment. The images with information entropy lower than the threshold are sharpened to extract the feature points better. By combining the ORB-SLAM2 system and adaptive sharpening adjustment, the trajectory accuracy is improved without adding too much processing time according to the experimental results obtained from the three sequences of the TUM dataset.

Authors in [131] proposed a novel hybrid visual odometry method on the basis of a deep deblurring network and Direct Sparse Odometry (DSO) to improve the robustness of the system in motion blur scenes. The local motion trajectory of the camera for each frame within the exposure time is calculated while the conventional algorithms estimate the camera pose within a particular point in time. By contrast, the former method allows to model the motion blur in the image explicitly and the model can be utilized in the tracking process. The image de-

blurring is achieved by SRNDeblurNet and combined with DSO as a motion blur aware visual odometry (MBA-VO) system. MBA-VO performs better accuracy and robustness than ORB-SLAM and DSO in the real-world datasets collected from the authors but achieves lower accuracy than ORB-SLAM observed from the three sequences results in the public open-source dataset TUM. Similar to [147], the processing time of MBA-VO is not recorded as a benchmark to assess the real-time capability of the proposed system.

Mustaniemi et al. [149] provided a deblurring thought aided by the inertial information. The motion blur is first estimated and the translation and rotation of the camera can be derived mathematically from inertial measurements. Wiener deconvolution filter is then convolved with the image for the image deblurring. The method was tested on both static and dynamic datasets containing motion blurred images and performed in a scenario of visual reconstruction with traditional feature points detector and descriptor RANSAC. The experimental results illustrated that the approach improves the performance of keypoints detection and localization accuracy of the detector. The capability in dealing with motion blur was validated. However, the approach has not been applied to a complete SLAM system and cannot testify its effectiveness in SLAM applications.

2.3.4 Key Findings

Over the years, the development of SLAM system, especially capabilities in both mapping and localization, has been noticeable. Compared with the initial SLAM which can only map small-scale fields such as small rooms, the current SLAM system can perform on large-scale spaces. Additionally, owing to the advances in sensors, computing systems and machine learning, the utility and research of SLAM have been extended to multiple areas such as semantic mapping and dense 3D reconstruction except the initial landmark-based mapping. Until now, SLAM

system has been applied into different scenarios but there still exist some areas that need to be further improved such as robustness. Robustness is the capability of a system to escape fatal failures with continuous accurate performance and quick recovery ability from nonfatal failures. Once fatal failures happen, the system is unable to perform normal functions without external intervention. Therefore, fatal failures need to be avoided and the robustness of SLAM should be ensured. Commonly, the fatal failures of SLAM systems result from various environmental perturbations such as sudden illumination changes, noise, blurred images and dynamic scene changes. In the current research, the robustness of SLAM is widely considered as the most difficult challenge.

Although learning-based image deblurring has achieved significant development, there are still a number of challenging problems. Specifically, learning-based image deblurring methods require a large set of paired input-output images, making the training process very time-intensive. Additionally, obtaining the paired training data is difficult and expensive in real-world applications. Suffering from interference among different tasks and fatal forgetting of previous learning, most existing image deblurring approaches are unable to be directly extended to multiple tasks as they are built for specific tasks. Designing an individual network for each task is costly in calculation time and memory, which greatly limits its applications. Traditional image deblurring, in contrast, has been developed over the years and a large number of algorithms have been proposed. It can be incorporated with SLAM techniques to improve the robustness and accuracy of SLAM with great adaptability and training time-saving.

2.4 Summary

In this chapter, a literature review on Co-MRMS in manufacturing, robotic positioning and SLAM approaches has been presented to understand the state-of-the-art and identify the knowledge gaps, where both fundamental developments and advanced techniques have been covered.

Section 2.1 comprises the literature review of the collaborative mobile industrial manipulator, where both system architecture and applications have been addressed. Hardware and software components that are involved in the system have been introduced and the industrial applications (logistics and manufacturing) of the robotic system have been surveyed. Findings showed that more research is needed for the collaborative robotic system that contains a mobile robot and a fixed-base robotic manipulator, and the autonomy of the robotic system needs to be enhanced as well. These findings correspond to Research Objective 1 to 3 and serve as motivation for the research work presented in this thesis, which advances the state-of-the-art in applying a cooperative mobile robot and fixed-base robotic manipulator system into manufacturing.

Section 2.2 has been devoted to indoor positioning methods including single sensor and multi-sensor fusion methods. For single sensor methods, three representative sensors IMU, camera and ultrasonic sensors have been introduced, covering their positioning principles and features. Nevertheless, using a single sensor is difficult to meet the requirements of robotic positioning while the application of multi-sensor fusion is the trend of positioning methods. The positioning system that fuses multiple sensors for a fixed-base robotic manipulator to identify the mobile robot in Co-MRMS is lacking, which is one of the knowledge gaps identified in this section, corresponding to Research Objective 4. Another knowledge gap is inadequate consideration about cases that not all the sensors are contin-

uously available. The multi-sensor fusion methods have been categorised under the traditional method and the learning-based methods. The former further comprises of Kalman filter, Bayesian network and Particle filter methods. By building "experience", learning-based fusion methods have demonstrated good potential for positioning accurately online. However, they are heavily limited due to their requirement for a substantial learning phase and poor scalability. Among traditional algorithms, Kalman filter-based algorithms have been extensively used as the more reliable approach for their balance between accuracy and computational efficiency. Considering the necessity for both real-time performance and positioning accuracy, the research in this thesis deploys Kalman filter-based algorithms for sensor fusion.

In Section 2.3, a number of fundamental techniques and developments of SLAM systems and image deblurring methods have been reviewed. Since the accuracy of ORB-SLAM3 greatly exceeds other existing systems, and the system allows for both visual and visual-inertial operation modes with different visual sensors such as RGB-D cameras and stereo, this thesis outlines the problem of blurred frames that are addressed in this work and devotes to further improvement of ORB-SLAM3 in terms of image deblurring, which corresponding to Research Objective 5. The methods in image deblurring were classified into traditional and learning-based methods. As mentioned above, learning-based methods require substantial offline training and are poor in scalability. Whereas, traditional methods have been developed for decades and balance well between deblurring effectiveness and efficiency. These methods have not been integrated with advanced SLAM systems for enhancing the performance of SLAM, which is a knowledge gap in this field. Finally, this chapter reviewed the recent state-of-the-art SLAM system involving image deblurring. Findings showed that ORB-SLAM3 with the traditional deblurring method has not been investigated and thus focused on in this research.

Chapter 3

Integrated Simulation of the Proposed Co-MRMS

3.1 Introduction

As Chapter 2 has illustrated, the Co-MRMS that contains heterogeneous robots has been largely investigated, where a robotic manipulator is mounted on a mobile robot and these two distinct robots are coupled as a whole. In contrast, in the real industrial environment, a fixed-base robotic manipulator and a mobile robot that commonly communicated and cooperated for a series of tasks such as part feeding and handling can also be integrated into a single robotic system but have not been investigated. In advanced manufacturing, a large number of robotic manipulators are generally fixed and fenced to perform various manipulation tasks, requiring a part-feeding system to supply the materials [150].

Nowadays, supplementing materials mainly rely on conveyors and human operators [151]. These feeding solutions lack the anticipated flexibility and efficiency when having to deal with dynamic tasks [152]. Thus, in order to achieve greater flexibility as well as efficient production, it is essential to develop flexible and

autonomous part-feeding systems for advanced manufacturing. Today, mobile robots, as flexible and movable platforms, have been a popular choice at production lines to transport materials. Considerable progress has been made in using mobile robots for fixed-base robotic manipulators to transport and feed part materials. However, in advanced manufacturing, material transport by mobile robots and subsequent operations by fixed-base robotic manipulators are generally separated with few interactions between them. A fixed-base robotic manipulator and a mobile robot have not been integrated into a single robotic system as mobile manipulator systems, which is challenging due to the many technologies involved, including path planning, material detection and localization, etc. Achieving this requires the development of a strategy that combines different modules in a flexible system and provides autonomous material transportation and sufficiently-accurate material handling capabilities. Therefore, a Co-MRMS that contains a fixed-base robotic manipulator and a mobile robot is proposed and investigated in this thesis to improve the flexibility and intelligence of using mobile robots to feed parts to fixed-base robotic manipulators.

In order to validate proposed methods and algorithms before they are applied to a real scenario, simulation is an effective way. This chapter presents a case study in a simulation environment to explore some of the necessary considerations when implementing the system, demonstrating how the proposed Co-MRMS can be utilized in advanced manufacturing for material transport and handling. The case study examined is set in the context of advanced composite manufacturing for several reasons. In the last decades, composite materials have attracted much attention because of their outstanding performance, especially their small weight-to-strength ratio [153]. They are typically made up of multi-directional layers of high-strength fibers, connected by a plastic resin. The manufacturing of composite parts is complex, time-consuming and prone to errors [154]. Currently, it is mostly a manually driven process. The use of robotics in the field of composite

material manufacturing is a technique worthy of investigation.

The remaining parts of this chapter are organised as follows: The integrated simulation of utilising proposed Co-MRMS for composite material transport and pick-and-place operations is presented in Section 3.2. Section 3.2.1 describes the framework of the integrated robotic system in a simulation environment and Section 3.2.2 demonstrates the modeling methods, including the modeling of deformable materials and the simulation of the machine vision module. In Section 3.2.3, the simulation results and their analysis are discussed. Finally, Section 3.3 summarises this chapter.

3.2 Development of the Integrated Simulation Environment

3.2.1 Integrated Robotic System Framework

The proposed Co-MRMS integrates an autonomous mobile robot with a fixed-base manipulator. The mobile robot is responsible for transporting the composite material. With the help of a vision module, the position and orientation of the raw material are sent to the fixed-base robot manipulator. This latter robot is used for grasping each fiber ply and placing it correctly according to the designed lay-up manufacturing specifications. The simulation framework for the proposed Co-MRMS is presented in Fig. 3.1. Robotic path planning for both the mobile and fixed robot platforms was implemented in MATLAB® [155]. A camera was mounted on the end-effector of the fixed-base robotic manipulator to support a machine vision solution. OpenCV [156] was used for image processing. Simulations of the full system were generated in CoppeliaSim.

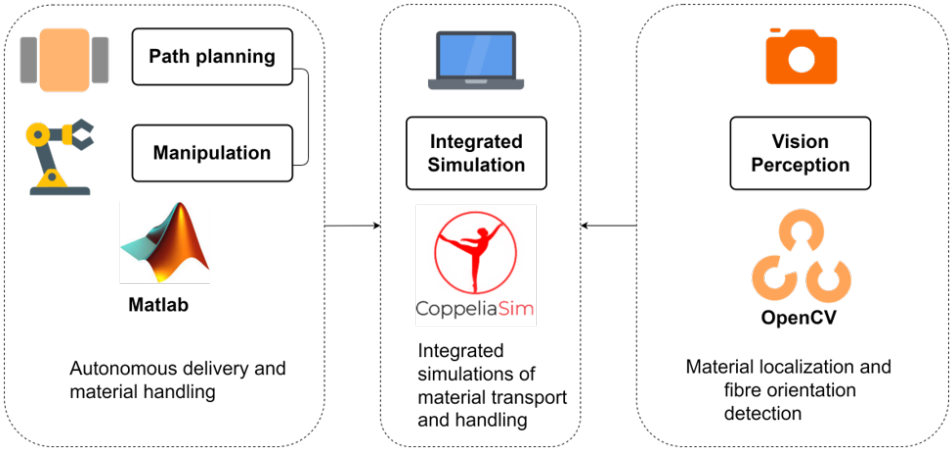

Fig. 3.1. The simulation framework of Co-MRMS.

The simulation framework can be divided into two stages: autonomous raw material transportation and composite material handling. In the first stage, the mobile robot deploys a collision-free path obtained by using a modified variant of the Bi-directional RRT* path planning algorithm based on [157], which enables the robot to autonomously navigate from any start location to a goal location. Once the mobile robot arrives at the goal, the second stage begins. Odometry data of the mobile robot is transmitted to the CoppeliaSim simulation environment through the use of the Robot Operating System (ROS) [158]. Following the reception of the estimated material position, the fixed-base robotic manipulator moves its end-effector, which carries an arrangement of suction cups for grasping operations, from the home position to a standby position above the material. The machine vision module is activated once such position is reached and an image of the scene is captured through the camera. The image is processed in OpenCV to gain a more accurate estimation of the material position and to compute the fiber orientation. Such position is transmitted to CoppeliaSim through UDP (User Datagram Protocol). The fixed robot manipulator adjusts the end-effector position and orientation, according to the received vision data. The end-effector approaches the deformable material, grasps the material and transfers it to the

mould. Finally, the robot returns to its home position.

In this work, the Turtlebot3 Burger differential drive mobile robot was chosen as the mobile robot platform in simulation experiments due to the unavailability of industry-standard mobile robots and the convenience for system validation. The robot setup in the simulation environment is presented in Fig. 3.2.

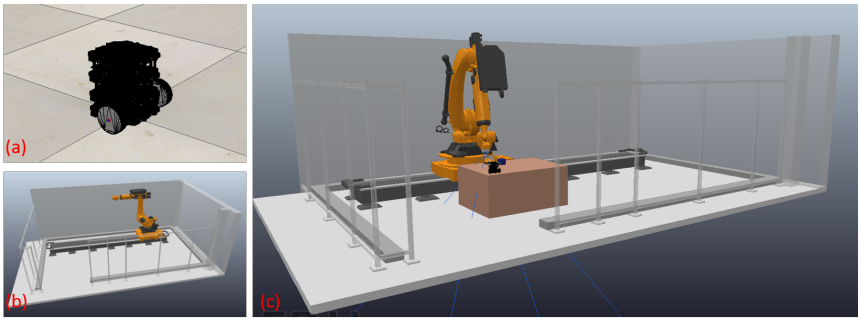

Fig. 3.2. The robotic setup in CoppeliaSim, (a) and (b) are Turtlebot3 Burger and KUKA KR90 R3100 industrial manipulator model respectively while (c) is the integrated simulation environment.

3.2.2 Deformable Object modeling and End-Effector Design

3.2.2.1 Deformable Object modeling

The modeling of the deformable composite material within CoppeliaSim was inspired by the particle-based method described in [159] and consists of representing a sheet material as an array of primitive cuboids. For each individual cuboid within the model, up to four dummy links were attached to the shape at a fixed distance from the outer edges. A simple 3x3 example of a composite material model, consisting of individual cuboids and associated dummies, is shown in Fig. 3.3. Dummies between adjacent cuboids were linked by dynamic overlapping constraints to emulate the stretching and bending behaviors of the material. These dynamic constraints constrain the relative motion between linked dummies. These maintain a connection between adjacent cuboids while permitting distur-

bances to the overall structure of the collection of bodies, which subsequently enable deformation.

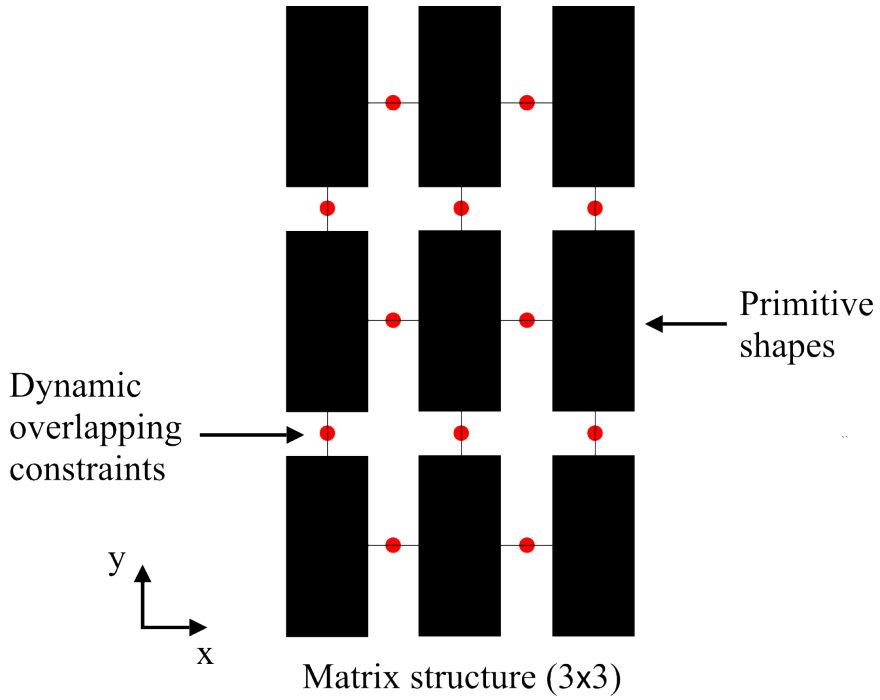

Fig. 3.3. Modeling the non-rigid nature of composite material as an array of dynamically-linked cuboids.

3.2.2.2 End-effector Design

Having developed an approach to model composite material as a non-rigid, deformable body within CoppeliaSim, it is also necessary to develop a model for the vacuum suction-based end-effector. CoppeliaSim's default library provides a simple vacuum suction cup model that enables the simulation of vacuum suction grasping for the manipulation of rigid bodies. However, without any modifications, this model cannot realistically interact with the composite material model as it is developed to grasp only a single rigid body within the simulation environment. When used to grasp the simulated composite material, a numerical-method-induced sagging effect will occur around the vacuum suction cup as the

end-effector will pick up the deformable object from a single point corresponding to one cuboid. In reality, however, a suction cup gripper should maintain contact with the entire region of cloth directly underneath the suction cups. Therefore, the default suction cup model was modified to enable compatibility with the approach to modeling deformable materials by ensuring more proper contact behavior between all elements that lie within the grasp region of a suction cup during grasping operations. The modified suction cup gripper with four suction cups provides a useful simulation component for quickly evaluating different gripper designs comprising an arrangement of multiple suction cups. This is an important resource for future design processes that seek to minimize sagging effects during the transfer of composite material sheets of a known shape and size.

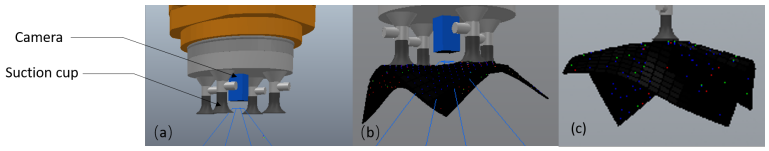

Fig. 3.4. The sagging effects of deformable material handling in CoppeliaSim, (a) End-effector mounted with camera and vacuum suction cup in simulation environment; (b) Image captured from simulation showing the grasping interactions between the vacuum suction cup gripper and composite material model.

The capability of the robot end-effector to deal with ply sagging was tested in a simulation environment. Fig. 3.4 shows images of an example simulation involving the use of a 4-cup and single-cup vacuum suction gripper to transfer a sheet of composite material across the workspace. Compared with single-cup vacuum suction gripper, 4-cup vacuum suction gripper reduced the sagging effects significantly, reaching satisfactory performance in dealing with ply sagging. It should also be noticed that each suction cup maintains complete contact with the material and sagging effects are minimized in the convex region defined by the four contacts between the gripper and the composite material.

3.2.3 Machine Vision Operations

3.2.3.1 Material Localization

In order to localize the position of the material, its geometry information plays a key role. As shown in Fig. 3.5, images captured by the simulated vision sensor are converted to grayscale images to reduce unrelated information. Afterward, a Gaussian blur filter [160] is adopted to smooth the data. The image is then transformed into a binary image and post-processed through morphological operations. Finally, the pose information of the material is obtained by analyzing its shape and area.

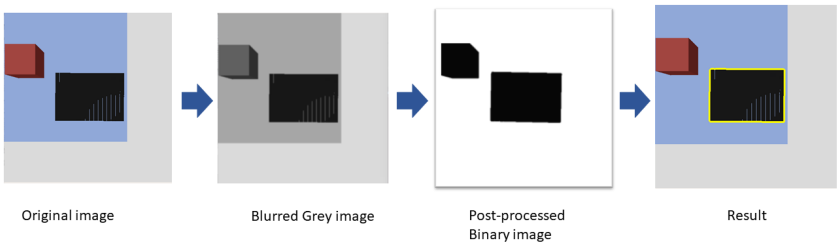

Fig. 3.5. Image processing workflow.

When the relative height between the camera and material is fixed, the scale of image pixels and real-world distance can be calculated in accordance with the pinhole camera theory [161]. Therefore, the real distance between the center of the camera and the surface of the part is inferred.

3.2.3.2 Fiber Direction Identification

In order to detect the texture of the material, the end-effector translates downwards along the z-axis, until the relative height between the material and the camera reaches 100 mm. With a series of pre-processing operations (Gaussian blur and morphological operations), the reflections produced by the fibers are

extracted from the material texture. As the fibers are not perfectively straight, calculating the slope and intercept of the fitting lines is not straightforward. To overcome this, all detected fibers in the image space are transformed into the Hough space [162]. Each line in the image space is represented by a point in the Hough space. As shown in the following equation [162], the formula of the line in the image space is:

$$\rho' = xcos(\theta') + ysin(\theta') \tag{3.1}$$

where ρ' is the distance from the origin to the line, and θ' is the angle between the positive x-axis and the normal to the line. As shown in Fig. 3.6, each point in the image space corresponds with a curve in the Hough space. If points lie in a line in the image space, all the corresponding curves of these points will intersect at a common point in the Hough space. Thus this point can be used to detect the line in the image space.

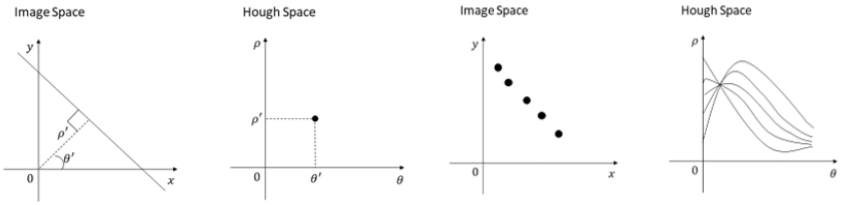

Fig. 3.6. The corresponding between image space and Hough space.

3.3 Simulation-based Experiments

The Co-MRMS, which employs a KUKA KR90 R3100 industrial fixed-base manipulator and a Turtlebot3 Burger differential drive mobile robot, was first modeled in CoppeliaSim to verify the performance in fulfilling the transportation and lay-up task of the proposed system. The simulation results in CoppeliaSim and the view of composite material placed on a mobile robot and mould are presented in Fig. 3.7.

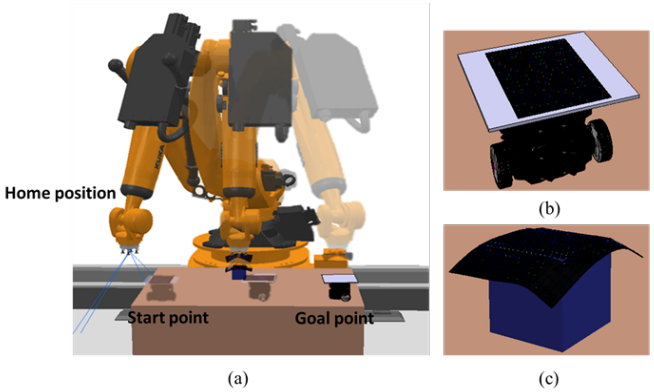

Fig. 3.7. The process of material transport and handling in CoppeliaSim, (a) Simulation environment in CoppeliaSim; (b) and (c) are composite material's placement on mobile robot and mould respectively.

Additionally, an integrated camera and a gripper unit with four suction cups were modeled on the KUKA KR90 end-effector so that the detection and grasping of the material can be simulated. Based on the modeled Co-MRMS, two simulation-based experiments were conducted to evaluate the attainable accuracy of the composite material vision system. First, an experiment evaluating localization accuracy was assessed. Using the modified bi-directional RRT algorithm [157] to compute a collision-free path, the mobile robot drove autonomously to a randomly generated goal within the manipulator workspace. Then, the vision system was employed to correct the simulated error in the wheel odometry-based positioning system by applying the object localization algorithm described in Section 3.3.3.1. To evaluate the repeatability of the localization results, this experiment was conducted 10 times. In addition, to simulate the accumulation of error in wheel odometry observed in real environments, Gaussian noise was introduced and superimposed with the simulated wheel odometry measurement of the mobile robot's position relative to its starting position. Gaussian noise has generally been used in signal processing to deal with uncorrelated random noise and is also commonly adopted in neural networks for modeling uncertainties [163]. It is statistically defined by a probability density function (PDF) that is equivalent to

a normal distribution (also known as Gaussian distribution). In other words, the odometry error due to wheel slippage was assumed to be Gaussian-distributed.

Table 3.1: Localization and fiber orientation detection error in simulation environment.

		MAE	RMSE
Material localization	Wheel odometry/mm	158.48	121.21
	Vision/mm	11.53	9.00
Fiber orientation detection	Vision/degree	0.70	0.048

Setting the mean and standard deviation of the Gaussian distribution to 100 mm and 70 mm, respectively, the wheel odometry position error in x and y are given by:

$$\begin{aligned} Error(x) &= \frac{1}{\sqrt{2}\sigma\pi} e^{\frac{-(x-\mu)^2}{2\sigma^2}} \\ Error(y) &= \frac{1}{\sqrt{2}\sigma\pi} e^{\frac{-(y-\mu)^2}{2\sigma^2}} \end{aligned} \tag{3.2}$$

where μ is the Gaussian mean and σ is the standard deviation. With the material position data obtained from the machine vision system and wheel odometry, the localization accuracy can be evaluated through Mean Absolute Error (MAE) and Root Mean Squared Error (RMSE). Here the ground truth was retrieved from the simulation. The results are presented in Table 3.1, where the MAE and RMSE of wheel odometry were 158.48 mm and 121.21 mm, respectively, while the MAE and RMSE of the vision system were 11.53 mm and 9.00 mm, respectively. Compared to the wheel odometry-based estimation, the proposed machine vision system reduced the localization error by 93% and demonstrated its ability in improving the localization accuracy.

In the second experiment, the fiber orientation detection algorithm was evaluated by comparing the output of the algorithm against the ground truth. Here the orientation of the material was incremented by 10 degrees between the range of [0°, 180°] relative to the camera frame. Like before, the accuracy is expressed by the MAE and RMSE and is shown in Table 3.1. The MAE and RMSE for fiber

orientation detection were found to be 0.70° and 0.048°, respectively. Since the experiments were conducted in a simulation environment, the lighting conditions in the scene can be controlled, which shows that under ideal conditions, the fiber orientation detection algorithm can provide accurate estimates.

In real world composite manufacturing, the placement and orientation of plies greatly determine the properties of composite material parts. For example, a 5° misalignment of ply cause 20% strength degradation [164]. For plies that are larger than the size of the designed composite material part, there are no specified requirements about the positional accuracy as plies can be trimmed for the designed part. For plies that require no trimming, the tolerance of position depends on the specified working instructions. Therefore, there is no uniform requirement for positioning accuracy. For fiber orientation deviation, it is required to be less than 3° [165]. In this research, the fiber orientation detection error in the simulation environment is 0.70°, which meets the required standards.

3.4 Summary

In this Chapter, the proposed Co-MRMS consisting of a fixed-base robotic manipulator and a mobile robot was established in a simulation environment to evaluate its feasibility and accuracy. In CoppeliaSim, a material transfer operation that involves the use of a mobile robot to transport composite material to a fixed-base robotic manipulator is first simulated and then the transported material is handled to a mould in a simulation environment, proving the feasibility of the proposed robotic system. In addition, as validated in multiple simulations, the MAE and RMSE for material localization can be drastically reduced by using machine vision to correct odometry errors. The fiber orientation can also be accurately estimated within suitable tolerances through the use of machine vision

techniques, validating the accuracy of the proposed Co-MRMS for the composite material layup.

The machine vision-based positioning approach presented here is limited by the requirement of strong differences between the target and background. In Chapter 4, a further investigation into perceiving the positions of objects by a fixed-base robotic manipulator is provided to show how it can be extended to enable accurate and robust positioning.

Chapter 4

Multi-sensor Fusion Positioning System for the Co-MRMS

4.1 Introduction

The developments reported herein stem from the proposed Co-MRMS for material transport and operations in manufacturing. Generally, the stoppage of a mobile platform is scheduled to feed parts for the fenced industrial robotic manipulators on production lines. To enhance the flexibility and efficiency of production, a flexible part-feeding scheme allowing interactions between the fixed-base robotic manipulator and the mobile robot is considered but involves several challenging tasks. For instance, when the mobile robot moves around the fixed industrial robotic manipulator, one of the key problems is that the positions of the mobile robot must be perceived by the manipulator accurately and robustly before performing other tasks such as grasping. Therefore, an important concern for the cooperative robotic system is that the fixed-base robotic manipulator can robustly and accurately perceive and track the mobile robot, as otherwise it will undermine the performance of handling objects. Additionally, the positioning

approach for the proposed Co-MRMS is required to be considered. Owing to the rapid development of machine vision techniques, an image-based positioning system using cameras has been developed as a promising positioning solution for industrial applications, as well as robot positioning [166]. Nevertheless, there are no limitation-free sensors. On one hand, it has been demonstrated that the vision-based positioning system can provide accurate and reliable information about the state, especially with fiducial visual markers, which have been widely used in literature. The well-known "ArUco" visual marker, developed by Garrido-Juradoetal et al. [167] in 2014, has been used extensively as a low-cost and straightforward solution to obtain position information. In [168], the authors tested the positioning accuracy of ArUco marker. The conducted experiments demonstrated that the positioning error is less than 0.005m by using a webcam when the distance between the camera and the marker is less than 1.2m. Thus, the vision-based positioning system using the ArUco marker has been verified as a superb accurate positioning method and is used in this work. On the other hand, there are some challenges for visual positioning methods, such as a random blocked view and low-quality and distorted images, which result in the failure of visual positioning. In this case, it is reasonable to combine vision system with other sensors for robot positioning [169]. An IMU can offer a robust signal with a high sampling rate while suffering from accumulated errors owing to the integration during state estimation. Ultrasonic sensor system is superior in accuracy for indoor environment positioning but work at a slow rate with random outliers. To address limitations and utilise the specific features of standalone sensors, IMU and ultrasonic sensors are fused to provide auxiliary state estimation for positioning. Benefiting from the design of a backup positioning system, seamless switching positioning is allowed and thus robust repositioning of the mobile robot can be achieved for the fixed-base robotic manipulator.

In the proposed Co-MRMS, a fixed-base robotic manipulator and a mobile

robot are coupled as a whole and have a shared workspace. In this case, the interaction model and coordinated control are significant for a workspace sharing system especially one that contains moving agents. Liu and Tomizuka [170] established the workspace sharing interaction model between a robot and a human to perform collaborative tasks. In [171], the kinematic modeling between a human and exosuit was established. To adapt to different terrains, impedance learning was utilized in the inner loop to regulate the impedance parameters of the exosuit while human-in-the-loop was deployed in an external loop to adjust speeds. Yu et al. [172,173] used visual and force sensors to obtain human motion and the interaction force for human–robot co-transportation task. Impedance-based control strategy and an advanced robot end-effector controller were proposed successively to deal with uncertainties in robot's dynamics. Author of [174] deduced the relative kinematic interaction model of swarms of mobile robots for leader-follower formation control. In spite of these advances, cooperative/ hybrid robotic systems involving mobile robot platforms and fixed-base robotic manipulators have received little attention in the context of part feeding and interaction mode design. By contrast, this work addresses the interaction between a mobile robot and a fixed-base robotic manipulator in a single cooperative robotic system. By establishing a novel interaction mode between the mobile robot and robotic manipulator, the efficiency and flexibility of material detection and grasping can be improved.

This chapter firstly designs an interaction mode between the fixed base robotic manipulator and mobile robot of the proposed Co-MRMS and then introduces a multi-sensor fusion positioning system, containing two different positioning approaches for the robotic manipulator to perceive the positions of mobile robot in an indoor environment. One approach is ultrasonic sensors fused with IMU by EKF. Furthermore, an outlier rejection mechanism is implemented to escape outliers from ultrasonic measurement. Another approach is based on machine vision.

In Chapter 3, the input image is first transformed into a binary image, and then the target is localized through morphological operations. This approach is limited by the requirement of strong differences between the target and background. In this chapter, another machine vision approach for positioning is achieved by detecting the ArUco visual marker, without requiring the strong difference between the target and background. Based on the EKF-based positioning and vision-based positioning, a positioning switching strategy according to the visual sensor state allows the robotic manipulator to reposition the mobile robot seamlessly.

The remaining parts of this chapter are organized as follows: In Section 4.2, the designed interaction mode of the Co-MRMS is presented and validated by simulation-based experiments. In Section 4.3, the coordinate frames in the positioning system are introduced and the transformation between different coordinate frames is derived. Section 4.4 gives a detailed description of the multi-sensor fusion positioning system, involving two different positioning approaches and the seamless positioning switching scheme. Finally, Section 4.5 presents the results of a series of static and dynamic physical experiments, which were conducted to evaluate the performance and behavior of the positioning system, while the summary of this chapter is given in Section 4.6.

4.2 Interaction of Co-MRMS

The objective of designing the interaction mode for the Co-MRMS is to enhance the flexibility and efficiency of part-feeding for the fixed base robotic manipulator by a mobile robot. Given that obtaining the accurate position of an object is the prior target, the interaction model is simplified without considering orientational information. Assume that the state vector is X, which is $\begin{bmatrix} x & y & z \end{bmatrix}^T$. The states of the robotic manipulator and mobile robot are represented as X_R and X_M

respectively. The relative distance between the robotic manipulator and mobile robot denoted by $d_{rel(t)}$, which is

$$d_{rel(t)} = \sqrt{(x_R - x_M)^2 + (y_R - y_M)^2 + (z_R - z_M)^2} \tag{4.1}$$

The interaction mode between the mobile robot and fixed-base robotic manipulator in Co-MRMS has been designed and the framework is shown in Fig. 4.1. The relative distance $d_{rel(t)}$ is calculated and the interaction between two robots can be divided into three stages: If the location of the mobile robot is out-of-scope of the fixed-base robotic manipulator, the robotic manipulator keeps static without movement; If the relative distance is smaller than the value that set for the sake of safety and object identification, both robots stop, waiting for the following operations such as object detection and material grasping; If the mobile robot located in the scope of the robotic manipulator and the relative distance is larger than the set value, the robotic manipulator moves quickly to the mobile robot.

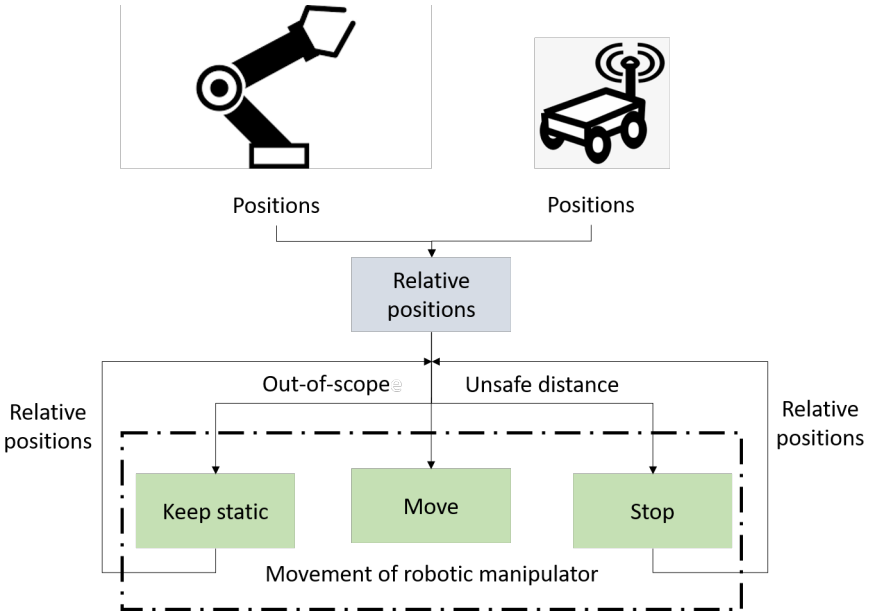

Fig. 4.1. Interaction design of Co-MRMS.

The interaction mode was validated in a simulated environment and the result

is shown in Fig. 4.2. For the convenience of validation, the mobile robot is simplified as a moving point and the fixed-base robotic manipulator is a two-link robotic arm. As is shown in the figure, the fixed-base robotic manipulator keeps static when the moving point is out-of-scope. When the moving point is in the scope and the relative distance between them is larger than the set value, the fixed-base robotic manipulator promptly moves to the moving point. If the relative distance is smaller than the set value, both of the robots stop. Therefore, the feasibility of the designed interaction mode is validated.

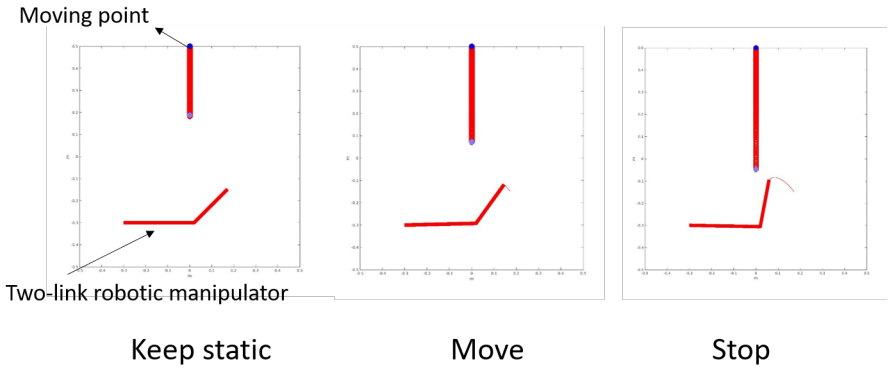

Fig. 4.2. Demonstration of designed interaction.

So far, the interaction mode of the integrated robotic system has been designed and validated. The movement of the fixed-base robotic manipulator depends on the relative distance between the mobile robot and the fixed-base robotic manipulator. To obtain the relative distance, the industrial robotic manipulator needs to continually perceive the positions of the mobile robot. Therefore, positioning the mobile robot accurately and robustly for the robotic manipulator in Co-MRMS is a critical technique and is as well the research focus of this thesis.

4.3 Coordinate Frame Transformation

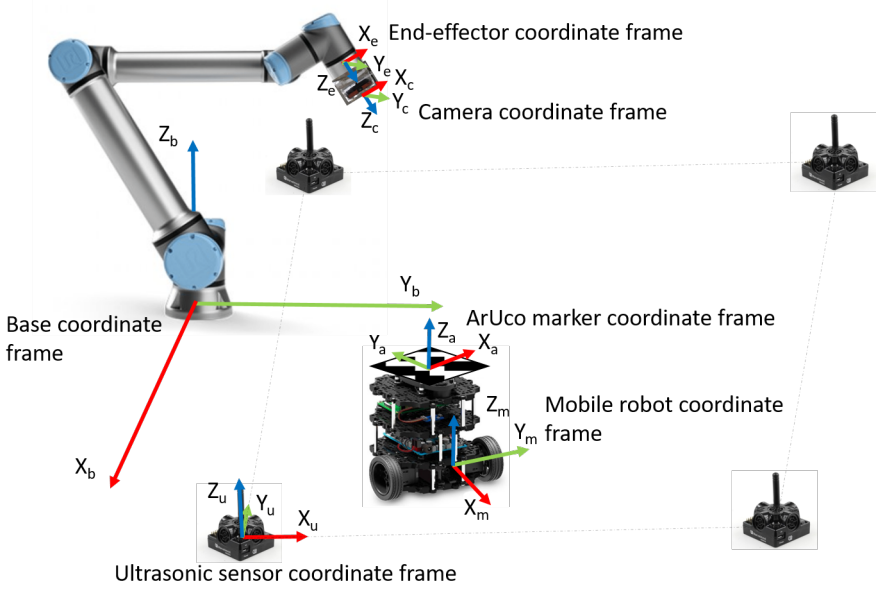

Fig. 4.3. Schematic diagram of the Co-MRMS and coordinate frames.

As is illustrated in Fig. 4.3, five sets of the coordinate frame are defined in the whole system for coordinate transformations to derive the predicted equations and measurement equations for positioning. Here, four stationary ultrasonic sensors are arranged around the workspace and form a positioning system (X_u, Y_u, Z_u). Base coordinate system (X_b, Y_b, Z_b) is defined in the base axis while end-effector coordinate frame (X_e, Y_e, Z_e) is located at the end-effector of robotic manipulator. The mobile robot coordinate frame (X_m, Y_m, Z_m) is fixed orthogonally to the origin located at the centre between the two wheels of the mobile robot. Correspondingly, the obtained raw IMU readings are attached to the mobile robot coordinate frame and are in correspondence with the direction of the mobile robot's motion. To unify the coordinate frames for EKF-based positioning, the accelerations from the accelerometer of IMU are transformed into the ultrasonic sensor coordinate frame. Since the end-effector of the fixed-base robotic manipulator moves along with the mobile robot for tracking, the transformation from the

ultrasonic sensor coordinate frame to the end-effector coordinate frame should be calculated and it can be expressed as

$$X^E = f(\mathbf{q})T_{UB}X^U \tag{4.2}$$

where T_{UB} denotes the transformation matrix from the ultrasonic sensor frame to the base coordinate frame and $\mathbf{q}$ is the vector of joint angles. The joint angles can be obtained by inverse kinematics as the end-effector target position is known. Owing to the dynamics modeling of the fixed-base robotic manipulator, the corresponding torque is calculated and then applied to each joint. Therefore, the trajectory tracking for the end-effector can be fulfilled.

For the visual positioning approach, an eye-in-hand camera is fixed on the end-effector of the robotic manipulator and thus the camera coordinate frame (X_c, Y_c, Z_c) is attached. ArUco marker coordinate frame (X_a, Y_a, Z_a) is attached on the ArUco marker and the marker positions obtained from image processing are relative to the eye-in-hand camera coordinate frame and should be transformed into the end-effector coordinate frame to facilitate the tracking. Therefore, the transformation of the marker position from the camera coordinate frame to the end-effector coordinate frame can be expressed as

$$X^E = T_{CE}X^C \tag{4.3}$$

where T_{CE} denotes the transformation matrix from the eye-in-hand camera frame to the end-effector coordinate frame.

4.4 Development of the Multi-sensor Fusion Positioning Method

In this work, the information fusion includes two meanings: one is the fusion of IMU and ultrasonic sensor based on the EKF algorithm for the position estimation of mobile robots, and another is the fusion of two different kinds of

positioning methods for repositioning. This section first discusses the two kinds of positioning methods that are deployed for localising a mobile robot in an indoor environment. These are EKF-based approach fusing IMU with ultrasonic positioning system and vision-based approach by camera with ArUco marker. Each positioning technique has both limitations and capabilities. The positioning method using camera with ArUco marker has high accuracy and precision but is not robust due to the sudden "blind spots" or distorted captured images, while the EKF-based fusion positioning method with ultrasonic sensor and IMU is robust to the detection distance or views but is not as accurate and precise as the visual positioning method with ArUco marker. Then the seamless switching strategy for relocalising the mobile robot is introduced to deal with the case that the camera becomes unavailable.

4.4.1 EKF-based State Estimation

As a classic sensor fusion approach for nonlinear systems, EKF was employed to estimate the positions of mobile robots. The position prediction is done through IMU readings and the correction comes from the position data of the ultrasonic sensor. The EKF algorithm, taking advantage of specific features with overcoming the limits of standalone sensors, presents a better resulting performance than an individual sensor. The general forms of the prediction model and correction model in discrete-time domain are given, respectively:

$$X_{i+1} = f(X_i, u_{i+1}) + \varepsilon_{i+1}. \tag{4.4}$$

$$Z_{i+1} = h(X_{i+1}) + \upsilon_{i+1}. \tag{4.5}$$

where X is the state vector corresponding to the positions and velocities in X-Y plane, which is $\begin{bmatrix} x & y & v_x & v_y \end{bmatrix}^T$. ε_{i+1} and υ_{i+1} represent the system noise and measurement noise, respectively. Both of the noises are modeled using zero

mean Gaussian distribution with associated covariance matrices:

$$\begin{aligned} \varepsilon_{i+1} &\sim N(0, Q_{i+1}). \\ \upsilon_{i+1} &\sim N(0, R_{i+1}). \end{aligned} \tag{4.6}$$

Control vector u, which corresponds to the mobile robot accelerations along x and y directions, is represented by $\begin{bmatrix} a_x & a_y \end{bmatrix}^T$. The acceleration along x or y axis can be expressed as:

$$\widetilde{a_n} = a + b_a + \varepsilon_a \tag{4.7}$$

where $\widetilde{a_n}$ and a are the nominal and true acceleration respectively. b_a represents the bias and ε_a is the measurement noise. According to the practical measurement, the bias of IMU got minor changes in an hour, which can be assumed that the bias is constant during the short-term tracking. Moreover, the bias can be measured by first recording some readings while the IMU is stationary, then taking those values as 'offsets' when reading the acceleration values in the future.

Let ΔT denotes the sampling time interval. The state prediction of the mobile robot in this work is defined by:

$$X_{i+1} = f(X_i, u_{i+1}) + \varepsilon_{i+1} = \begin{bmatrix} x_i + v_{x(i)}\Delta T + \frac{1}{2}a_{x(i+1)}\Delta T^2 \\ y_i + v_{y(i)}\Delta T + \frac{1}{2}a_{y(i+1)}\Delta T^2 \\ v_{xi} + a_{x(i+1)}\Delta T \\ v_{yi} + a_{y(i+1)}\Delta T \end{bmatrix} + \varepsilon_{i+1} \tag{4.8}$$

4.4.1.1 Positioning by Ultrasonic Sensor System

The ultrasonic positioning system used in this work consists of four stationary beacons, a mobile beacon, a router and the dashboard beacon software. Each beacon has five transceivers. The distance of the mobile beacon that is affixed to the mobile robot is calculated by the router with receiving ultrasonic signals from the stationary beacons. The position of the mobile beacon can be calculated:

$$p_{i+1} = \sqrt{(x_{i+1} - x_s)^2 + (y_{i+1} - y_s)^2 + (z_{i+1} - z_s)^2} \tag{4.9}$$

where $(x_{i+1},\ y_{i+1},\ z_{i+1})$ represents the positions of mobile beacon at time i+1, and $(x_s,\ y_s,\ z_s)$ represents the stationary beacon's coordinates. With position readings from the ultrasonic positioning system, the correction model of EKF can be presented as the following equation:

$$Z_{i+1} = h(X_{i+1}) + \upsilon_{i+1} = \begin{bmatrix} x_{i+1} \\ y_{i+1} \end{bmatrix} + \upsilon_{i+1} \tag{4.10}$$

4.4.1.2 EKF Process

Now, the non-linear system in state-space has been obtained. Then, the EKF procedures can be operated as follows by the given prediction and correction models [175]:

- Initialisation with state X_0 and covariance matrix P_0
- State prediction by motion model:

$$\hat{X}_{i+1|i} = f(\hat{X}_{i|i}, u_{i+1}) + \varepsilon_{i+1} \tag{4.11}$$

where $\hat{X}$ represents the estimate of the state vector X.
Covariance matrix prediction:

$$P_{i+1|i} = F_i P_{i|i} F_i^T + Q_i \tag{4.12}$$

where F_i is the Jacobian matrix of the prediction model and can be written as:

$$F_i = \frac{\partial f}{\partial X} \mid_{\hat{X}_{i|i}, u_{i+1}} \tag{4.13}$$

Outlier rejection:

Since ultrasonic signals may be delayed or reflected by obstacles in real cases, non-updated readings or error values with a drastic change are obtained occasionally from ultrasonic sensors. Thus, a straightforward outlier rejection strategy to

reject outliers from ultrasonic sensor data is proposed. In each iteration, the difference between readings at time i+1 and time i from the ultrasonic sensor is calculated and compared with a constant positive value. If the following equation is satisfied, Z_{i+1} will be considered as an outlier.

$$|Z_{i+1} - Z_i| \geq \rho \times v \times \Delta T \tag{4.14}$$

where v is the driving speed of mobile robot and ΔT is the sampling time interval, and ρ is the adjustment factor. Likewise, if the difference between Z_{i+1} and Z_i is equal to 0, it is taken as no updated reading from the ultrasonic sensor. Then the measurement data at time i+1 is abandoned. Otherwise, the ultrasonic receiver data will be adopted in the correction step of the EKF algorithm if satisfying the formula:

$$0 < |Z_{i+1} - Z_i| < \rho \times v \times \Delta T \tag{4.15}$$

Due to the EKF-based estimation with the outlier rejection method, the effects of error readings from the ultrasonic sensor can be effectively reduced and the distinguished measurement data can be used for the correction model.

- Measurement data update:

$$Z_{i+1} = h(X_{i+1}) + v_{i+1} \tag{4.16}$$

- Calculation of Kalman gain:

$$K_{i+1} = P_{i+1|i} \times H_{i+1}^T \times (H_{i+1} \times P_{i+1|i} H_{i+1}^T + R_{i+1})^{-1} \tag{4.17}$$

where H_i is the Jacobian matrix of the measurement model and can be written as:

$$H_{i+1} = \frac{\partial h}{\partial X} \mid_{\hat{X}_{i+1|i}, u_{i+1}} \tag{4.18}$$

- State update:

$$\hat{X}_{i+1|i+1} = \hat{X}_{i+1|i} + K_{i+1}(Z_{i+1} - \hat{Z}_{i+1|i}) \tag{4.19}$$

where $\hat{Z}_{i+1|i}$ is the estimated measurement and can be written as:

$$\hat{Z}_{i+1|i} = h(\hat{X}_{i+1|i}) \tag{4.20}$$

- Covariance matrix update:

$$P_{i+1|i+1} = (I - K_{i+1}H_{i+1})P_{i+1|i} \tag{4.21}$$

Afterward, by setting the estimated state as the target position X^E defined in Section 3.2, trajectory tracking by the EKF fusion method can be realized and the equation is stated below.

$$\hat{X}_{i+1|i+1} = X^E \tag{4.22}$$

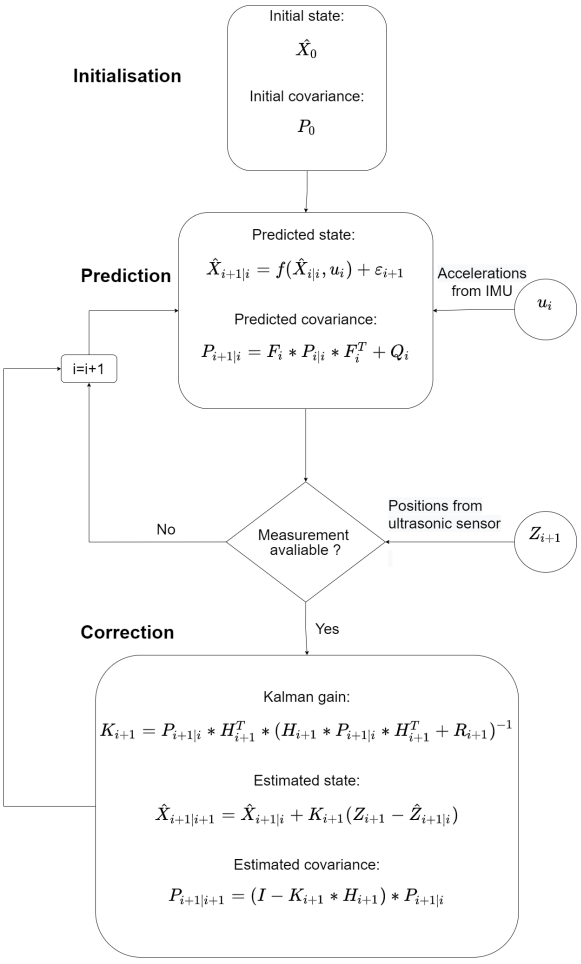

Fig. 4.4. EKF-based algorithm flow chart.

The flow chart of the EKF-based algorithm with the outlier rejection method is shown in Fig. 4.4. It should be noted that the update frequency of IMU is around 200 Hz while the ultrasonic sensor is around 3.65 Hz, which occurs to the data unsynchronization during fusion. To solve this issue, the adopted EKF-based fusion strategy is employed as follows: The predicted state and covariance matrix obtained from the motion model will be corrected if available measurement data is received. Otherwise, the positions of the mobile robot will be estimated with the motion model solely.

4.4.2 Vision-based Estimation

Another positioning approach by aided camera detecting ArUco marker, except EKF-based algorithm fusing ultrasonic sensors and IMU, is utilized in this work. The used marker is generated with OpenCV library and affixed on top of the mobile robot. A standard ArUco marker is defined by a 7x7 square array, where data and fault detection are contained in an inner 5x5 matrix of each row and generate a binary pattern. The marker is identified by the unique pattern that is encoded in each ArUco marker, which is robust with a low failure rate. Additionally, the marker orientation can be detected by the layout of the four corners. Distortion of images occurs commonly in the applications of computer vision, which affects measurement accuracy. To correct the image distortion, the process of camera calibration is conducted with OpenCV to determine the intrinsic and extrinsic parameters of the camera. Intrinsic parameters are related to the camera itself and correspond to its internal characteristics such as focal length and optical centres while extrinsic parameters refer to coordinates transformation between the camera frame and the world frame. As the frame of the marker is identified, multiple computational steps will be performed to obtain the relative pose between the camera and marker and the processes are described in Fig. 4.5.

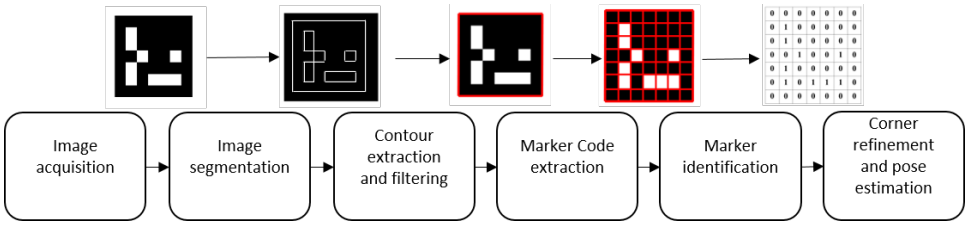

Fig. 4.5. Marker detection process.

The original image is firstly converted to a grey-scale image, then the image binarization is fulfilled through the threshold method. Contours in the image are detected by means of a Canny edge detector [176]. By the Suzuki algorithm [177],

contours in the image are extracted and filtered with discarding and deleting shapes other than square and closely adjacent shapes. Further processed marker is analysed by detecting the black and white pixels and segmenting the marker image into cells. With Otsu's method [178], a binarized image is generated again by setting the threshold value. The pixels of both colours are counted in each cell, and a certain grid map is obtained based on the average binary value of the cell. In order to enhance the accuracy of the ArUco marker detection, corners of the marker are found with sub-pixel interpolation by the cornerSubpixel function in the OpenCV library. Afterward, the pose of the camera with high accuracy is estimated using the optimization method of Levenberg-Marquardt algorithm [179].

4.4.3 Seamless Switching Repositioning Strategy

The design of the proposed localising system enables the robotic manipulator to estimate the auxiliary state of a mobile robot with additional sensors, which allows seamless switching between different sensor suites. On one hand, including additional sensors benefits the enhancement of estimating the robot's state. On the other hand, the elements of the different sensor suites are capable of seamless switching, which improves the fail-safety and versatility of the positioning system.

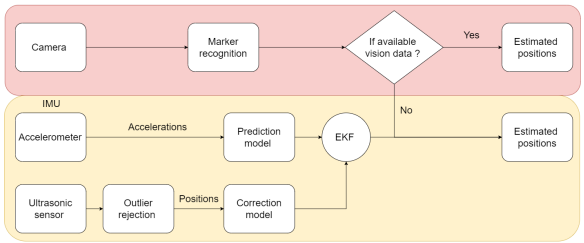

Fig. 4.6. Two-stage seamless switching strategy for repositioning.

As shown in Fig. 4.6, a seamless switching relocalising strategy with two main

stages is proposed for the positioning system. The first stage processes vision data to estimate the positions, while the second stage fuses IMU and ultrasonic sensors by the EKF with the outlier rejection method for seamless switching. As one of the most popular fiducial markers, the ArUco marker presents high accuracy and speed in pose tracking [180]. Therefore, the common case is the change from vision-based position estimation to EKF-based positioning in the case of unavailable vision data. At each time, a judgment statement is performed to determine whether the Aruco marker is detected. If the position outputs from vision are zero, then the vision system is labeled as a disabled state. The positioning system is seamlessly switched to the backup positioning stage, which is the EKF-based positioning method fusing IMU and ultrasonic positioning data. As a result of the seamless switching repositioning strategy, the positioning of the integrated robotic system will be robust against an occluded visual sensor, which can achieve reliable and accurate tracking performance.

4.5 Experimental Evaluations

4.5.1 System Hardware and Experimental Setup

Extensive experiments including static and dynamic state estimation were performed to evaluate the performance of adopted positioning approaches and the proposed switching strategy for repositioning. The overall experiment flowchart is given in Fig. 4.7.

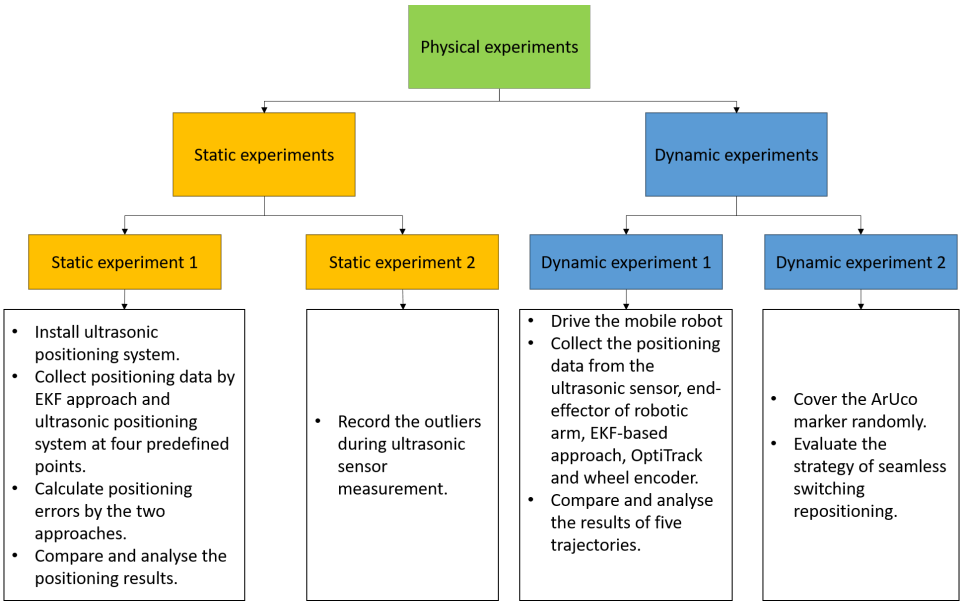

Fig. 4.7. Overall experiment flowchart.

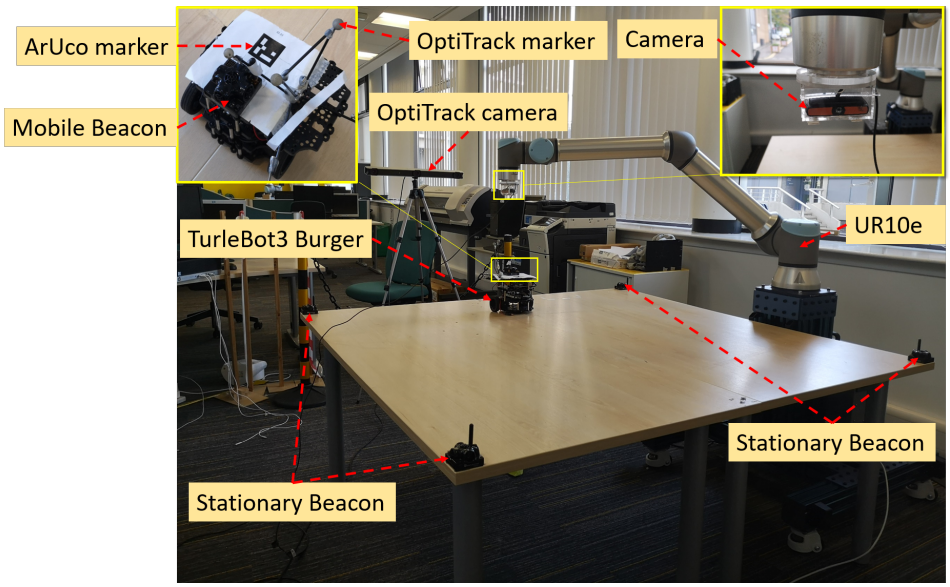

Fig. 4.8. Experiment layout.

The hardware system design for experimental implementation is given in Fig. 4.8, where TurleBot3 Burger and UR10e were used as the mobile robot and robotic manipulator respectively. The four stationary ultrasonic beacons and

a mobile beacon affixed on the mobile robot were supplied by the Starter Set HW v4.9 of Marvelmind. As a high performance optical motion capture system, the OptiTrack Trio camera was utilized and placed on the flat terrain to determine the real-time positions of the mobile robot and the measurement was taken as the ground truth. A low-cost and monocular camera was mounted on the end-effector of the fixed-base robotic manipulator to identify the positions of the ArUco marker. In this work, the large size 1.6m×1.6m experimental table is setup based upon two considerations. On one hand, the beacons in the ultrasonic positioning system can be conveniently arranged at a certain distance from each other to ensure positioning accuracy. On the other hand, sufficient scope is required for mobile robot motion. Robot control and computations were processed on a laptop with an Intel i7-8750H, 8 GB RAM.

4.5.2 Static State Estimation Experiment

The static state estimation experiment aims to compare the EKF-based fusion approach and stand-alone ultrasonic sensor system in positioning accuracy, precision and update frequency. Therefore, the mobile robot was placed at different predefined positions and the data by two positioning approaches were acquired. The root-mean-squared errors (RMSE) of positioning were calculated and quantified by the cumulative distribution function (CDF). In this experiment, the static performances of the EKF-based fusion approach and stand-alone ultrasonic sensor system for positioning a mobile robot were investigated and compared from accuracy, precision and update frequency. Firstly, the four stationary ultrasonic beacons were installed at the four corners of a platform to ensure the mobile robot can be located in the effective coverage area of the ultrasonic positioning system consistently. The IMU is placed statically on the table and 10,000 accelerations are collected. The ground truth of acceleration is zero. Therefore, the bias and

the noise of the IMU data can be obtained by calculating the average and standard variation of collected data, which can be used to get the Q for the EKF algorithm. The bias and the noise of the ultrasonic sensor are tuned by the first recording readings before the experiment, then taking the bias as 'offsets' when reading the values in the future. The noise can be calculated and the variance of the data can be used to obtain the R for the EKF algorithm. Then the mobile robot was placed successively at the predefined four positions and the positioning data by the two approaches were acquired. Next, the RMSE of positions was calculated and quantified by the CDF.

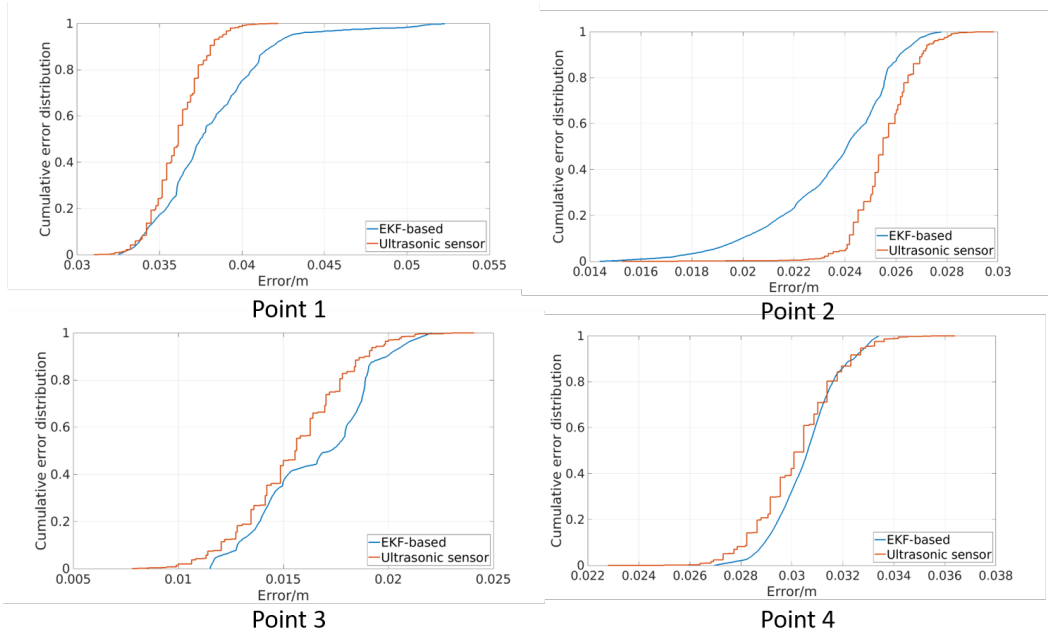

Fig. 4.9. Positioning error CDF comparison.

Fig. 4.9 depicts the comparisons of the position error CDF between the EKF-based approach and stand-alone ultrasonic sensor system at four defined points. The median (p50), 95th percentile (p95) errors and standard deviation (STD) are summarised in Table 4.1. As expected, the ultrasonic sensor reveals high-accuracy in indoor environment positioning as 95th percentile errors are less than 0.04m. It can be observed that median positioning errors of both the EKF-based

approach and ultrasonic sensor system are below 0.04m with a little difference. This suggests that an EKF-based approach attains comparable accuracy to the ultrasonic method. Furthermore, both of the approaches achieve high-precision performance which is reflected by the millimetre-level STD. Additionally, it shows by practical measurement that the positions were updated by ultrasonic sensors with 3.65 HZ while it can reach to 181.9 HZ through the EKF-based position approach. Thus an EKF-based positioning approach fusing IMU with ultrasonic sensors can export high-accuracy and high-precision in positioning while keeping high update frequency in static positioning.

Table 4.1: Positioning errors and STD at four predefined test points.

Point position	Estimator	p50/m	p95/m	STD/m
Point 1 [0.009m, -0.75m]	EKF-based	0.037	0.043	0.0033
	Ultrasonic sensor	0.036	0.039	0.0018
Point 2 [0.775m, -1.49m]	EKF-based	0.024	0.026	0.0025
	Ultrasonic sensor	0.027	0.027	0.0012
Point 3 [1.55m, -0.75m]	EKF-based	0.017	0.016	0.0027
	Ultrasonic sensor	0.020	0.020	0.0026
Point 4 [0.92m, -0.065m]	EKF-based	0.03	0.03	0.0013
	Ultrasonic sensor	0.033	0.033	0.0016

To evaluate the convergence rate of the EKF-based method, a simulation was implemented in Matlab. The initial estimation error was set to 5cm. The update frequency of IMU was set to 200 Hz while the update frequency of ultrasonic sensor was set to 3.65 Hz. The EKF-based positioning process is shown in Fig. 4.10. As can be seen from the figure, the EKF-based positioning method requires around 0.5 seconds to reach the steady state, proving the fast convergence rate of EKF-based positioning method.

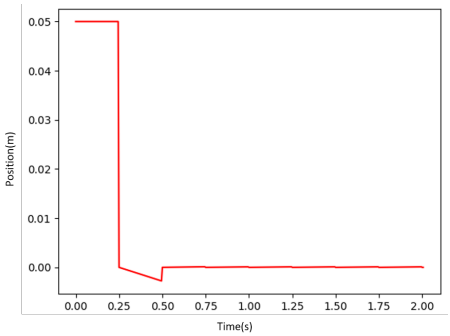

Fig. 4.10. EKF-based positioning process.

As is described in the section of the EKF process, a potential issue of an ultrasonic sensor system is that outliers exist randomly during operation and the measurement reading may be obtained with a drastic change compared to the previous reading, such as positioning in Fig. 4.11. In this work, the outliers of ultrasonic sensor measurement can be effectively eliminated on account of the proposed outlier rejection method in Section 4.1.2, which is another competitive advantage in positioning.

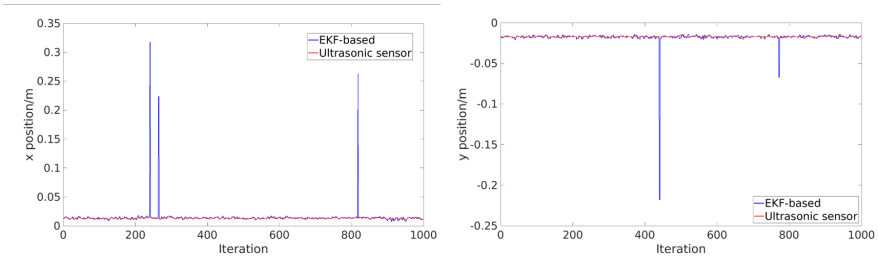

Fig. 4.11. Positioning with outliers of ultrasonic sensor system.

4.5.3 Dynamic State Estimation Experiment

The dynamic experiments were conducted to determine the accuracy and robustness of the proposed positioning system and seamless switching repositioning strategy when the mobile robot moves. The mobile robot was driven along a complex path involving linear motions and a U-turn while the end-effector of the

manipulator kept tracking the mobile robot. While the mobile agent moved along the path, the (x,y) positions of the mobile beacon were determined by the ranges obtained from four stationary beacons and trilateration.

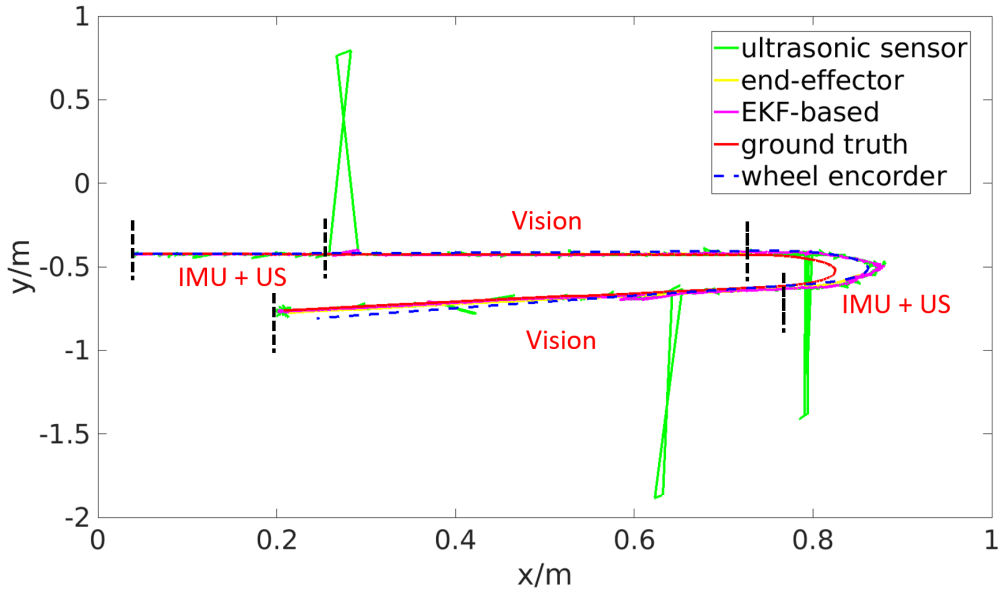

Fig. 4.12. Comparisons of trajectories.

The experimental results of trajectories, x-axis position and y-axis position using different approaches are shown in Figures 4.12, 4.13 and 4.14 respectively, in which the ultrasonic sensor marked as green line represents the ultrasonic receiver data for mobile robot positioning. The end-effector marked as yellow line represents the end-effector positions of the robotic manipulator, EKF-based marked as purple line represents the robot positions after fusing IMU with ultrasonic receiver data by EKF, ground truth marked as red line represents the robot positions obtained from OptiTrack, and wheel encoder marked as blue dash line represents the robot positions using wheel encoder that embedded in a mobile robot.

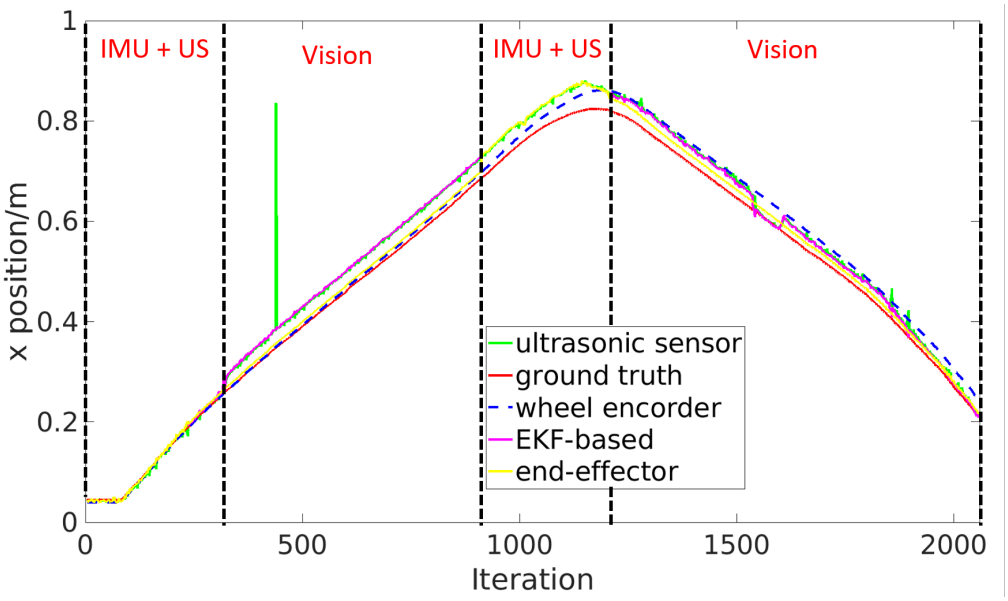

Fig. 4.13. Comparisons of x-axis position.

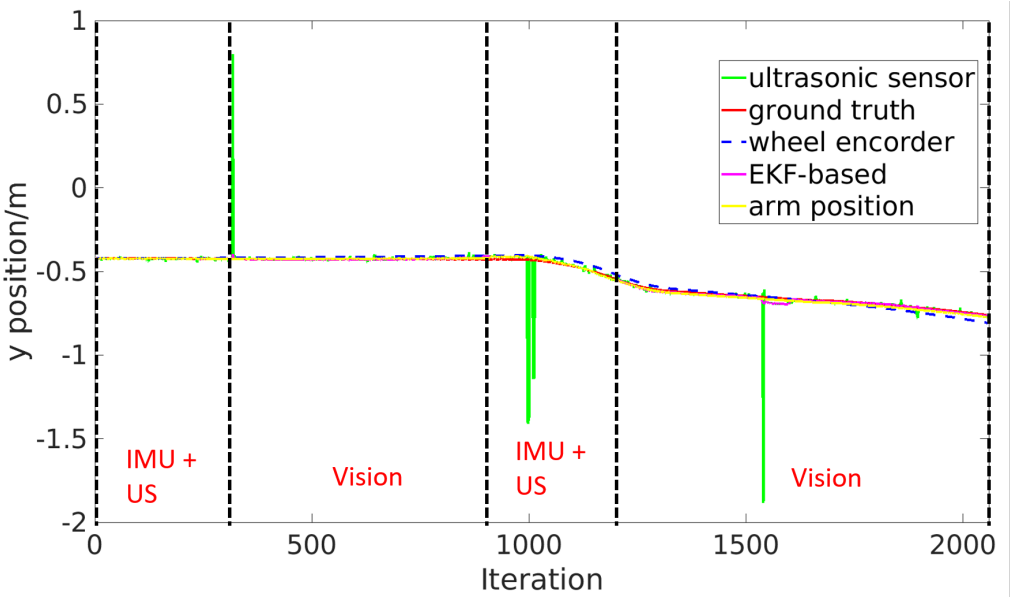

Fig. 4.14. Comparisons of y-axis position.

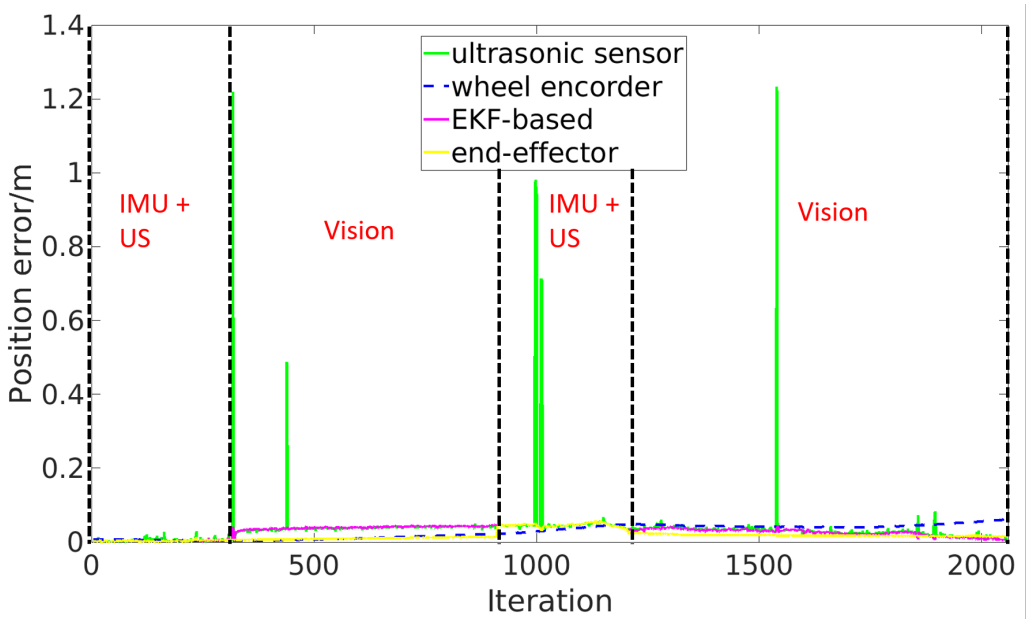

Fig. 4.15. Comparisons of positioning error.

From the results, outliers from an ultrasonic positioning system occur randomly during mobile robot moving, which leads to a dramatic positioning error. While fusing ultrasonic receiver data with IMU by the EKF method, the trajectory is smoothed and the abnormal value is eliminated even when incorrect ultrasonic readings are obtained. Furthermore, comparing the results of five trajectories, the vision system has outstanding stability and accuracy if the ArUco marker can be recognised by the camera while the positioning with wheel encoder gradually deviates from the ground truth with time accumulation over a period. RMSE of different positioning approaches during dynamic motion is shown in Fig. 4.15. At the end point, the RMSE of the wheel encoder is 0.0608m, which is much larger than the vision's 0.015m, the ultrasonic sensor system's 0.0095m and the EKF-based approach's 0.0057m. It is observed that the EKF-based approach with ultrasonic sensor and IMU performs well without accumulated error but got a lower than 0.05m deviation at the U-turn. This is attributed to the variational transceiver and different arrival time of ultrasonic signals. Nevertheless, the EKF-

based approach achieves accurate millimeter level positioning without outlier and accumulative positioning error.

Moreover, to demonstrate the capability of the seamless switching repositioning strategy, the ArUco marker was covered randomly at two phases to cause drop-outs of visual measurements and the dependent sensor suite is indicated in the figures where the US represents the ultrasonic system. As expected, once the dropouts of the visual update occur, the position of end-effector of the robotic manipulator then seamlessly switches to the EKF-based state estimation, which shows the robustness and capability of the proposed seamless switching repositioning strategy.

4.6 Summary

In this chapter, an interaction mode between the mobile robot and fixed-base robotic manipulator has been first designed for the proposed Co-MRMS. Based on the relative distance between the mobile robot and fixed-base robotic manipulator, the proposed Co-MRMS performs different forms of interaction. The simulation-based experiments were conducted to validate the feasibility of the proposed interaction mode.

Then, a multi-sensor fusion positioning system for the fixed industrial manipulator to perceive and interact with a mobile robot was developed. To accurately and robustly acquire the positions of the mobile robot, two different kinds of indoor environment positioning methods, the EKF-based approach fuses ultrasonic sensors with IMU and the vision-based approach with ArUco marker, have been adopted. In addition, with an outlier rejection method strategy, the EKF-based approach can eliminate the outlier of ultrasonic sensor measurement. Furthermore, a two-stage positioning strategy allows the fixed-base robotic manipulator

to reposition the mobile robot seamlessly to deal with the scenario that the visual sensor is occluded.

Through a series of static and dynamic experiments, it has demonstrated that the EKF-based multi-sensor fusion positioning approach can achieve comparative millimetre-sized accuracy as an ultrasonic sensor system while keeping a high update frequency. In contrast to the wheel encoder positioning, the proposed positioning system can suppress the positioning drifts over time through the benefits from the camera and ultrasonic sensor. The fixed-base robotic manipulator achieves desirable robust perceiving, even in the case when the visual sensor fails.

According to the static experiments, the EKF-based positioning approach fusing IMU with an ultrasonic sensor can export high-accuracy (the RMSE is 0.04m) and high-precision (the STD is 0.0033m) in positioning while keeping a high update frequency of 181.9 HZ in static positioning. Evaluations through dynamic experiments demonstrate that the proposed positioning system can suppress the positioning drifts over time when compared with the wheel encoder. The two-stage repositioning strategy can support the robotic manipulator to perceive the positions of the mobile robot robustly, even in the case when the visual sensor is occluded.

This chapter has addressed the problem of intelligent interaction between the fixed-base robotic manipulator and the mobile robot. Thus, the proposed positioning system is confined to a local space, which is not suitable for global positioning in a manufacturing environment. In Chapter 5, the positioning of the mobile robot is extended to the global positioning by using SLAM. This is because SLAM allows the mobile robot to map the dynamic environment and localise itself continuously, enabling higher adaptability, flexibility and capabilities in dealing with change and uncertainty.

Chapter 5

Efficient Image Deblurring Framework for SLAM Enhancement

5.1 Introduction

In modern manufacturing, mobile robots play a major role and boost the automation degree in a manufacturing environment. They are capable of doing tasks such as moving standard-sized goods from one position to another [35]. However, these mobile robots generally perform fixed tasks within a static environment, which is far less autonomous and intelligent. Traditionally, the production line in manufacturing is fixed and invariable, which allows the mobile robot to transport the materials with a predefined route within a static environment. Nevertheless, current manufacturing transforms the environment more frequent and fast, and thus demands highly flexible and adaptive robotic systems to meet the requirements of versatile production systems [19]. Besides, the current localization of mobile robots mostly relies on external setups, such as artificial markers and installing

beacons, which are inflexible to deal with a dynamic environment and incapable of adapting the infrastructure accordingly.

SLAM allows the mobile robot to navigate autonomously in an unknown environment by mapping the surrounding environment and localising itself on the map, which has been increasingly investigated for flexible manufacturing [181]. Compared with other range-finding devices such as radar and laser, visual sensor has a number of advantages including the richness of information acquisition, small volume and low energy consumption. Recently, owing to the abundant texture information provided by the external environment, SLAM system that uses visual sensors has received rising attention, especially applied to the mobile robot. Meanwhile, challenges arise when applying visual-based SLAM in the practices of autonomous manufacturing. Particularly, blurred images that exist in visual SLAM can result in low quality outcomes and are thus studied in this work. Due to the recent advances in CPU and GPU technologies, the major drawback, which is the high computational cost, is no longer an insurmountable problem and thus the real-time implementation of the required sophisticated SLAM algorithms can be performed to process images and extract crucial information. As a matter of fact, various visual sensors such as monoculars and RGB-D cameras have been utilized as promising SLAM solutions. As the literature review in Chapter 2 shows, a large number of fundamental techniques and developments of SLAM systems and image deblurring methods have been proposed. Among numerous SLAM systems, ORB-SLAM3 was proposed on the basis of ORB-SLAM and ORB-SLAM2, proposing the concept of multi-map representation called Atlas and an innovative visual-inertial initialization method. Studies in [125] showed that the accuracy of ORB-SLAM3 greatly exceeds other existing systems and the system allows for both visual and visual-inertial operation modes with different visual sensors such as RGB-D cameras and stereo.

With regards to image deblurring methods, the literature review in Section

2.3.2 shows that learning-based methods require substantial offline training and have poor scalability while traditional methods have been developed for decades and balance well between deblurring effectiveness and efficiency. This Chapter addresses the problem of blurred images which exist in SLAM systems that contain a visual sensor, decreasing the quality of mobile robots' autonomous navigation in a dynamic environment. Thus, an efficient image deblurring framework containing blur detection, image sharpening and image deblurring, is proposed and integrated into ORB-SLAM3 to enhance the accuracy of the SLAM system. The performance of the proposed framework is evaluated on the famous TUM RGB-D dataset and TUM Visual-Inertial dataset, comparing with the benchmarked performance of the original SLAM algorithm. The feasibility of the system is evaluated on a real mobile robot. This work corresponds to Research Questions 4 for autonomous transport by a mobile robot in manufacturing.

The remaining part of this chapter is organised as follows. In Section 5.2, the overall framework of the proposed efficient image deblurring SLAM (EID-SLAM) is presented while Section 5.3 introduces the algorithms in the process of image deblurring. Section 5.4 reports the experimental results conducted to evaluate the system performance on the basis of the trajectory accuracy of SLAM. Finally, a summary of the chapter is provided in Section 5.5.

5.2 Framework of Efficient Image Deblurring SLAM

The proposed EID-SLAM is built on ORB-SLAM3 [125], which is an ORB feature-based SLAM system and can be divided into three main threads, namely tracking, local mapping, and loop and map merging. Feature points are detected and matched by the ORB algorithm at first and then the nonlinear iterative optimisation is performed based on the bundle adjustment (BA) algorithm to

obtain the camera pose and 3D map. As the performance of the ORB-SLAM3 algorithm depends heavily on feature extraction and matching, running rapidly in an environment or dealing with the fast movement of the object will fail to extract sufficient stable matching point pairs, which leads to the inadequacy of input information for the beam adjustment method. In the proposed EID-SLAM, images are pre-processed before feature points extraction of the tracking thread based on a set of algorithms including blur detection, image sharpening and image deblurring.

5.2.1 Overall Framework

The overall framework of the proposed EID-SLAM is shown in Fig. 5.1 in which the image deblurring process and ORB-SLAM3 are both included. The deblurring process is comprised of three steps, which are blur detection, image sharpening and image deblurring. The first step performs blur detection based on the Laplacian method. If the obtained image is determined as a blurred image, then the image sharpening algorithm and image deblurring algorithm based on the Wiener filter are executed sequentially. Otherwise, the image is directly loaded into the following modules of ORB-SLAM3.

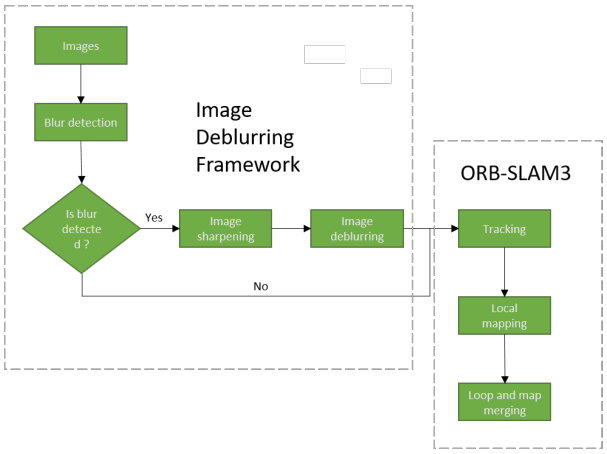

Fig. 5.1. The framework of proposed EID-SLAM.

ORB-SLAM3 system starts with the process of initialisation according to the obtained data from sensors such as camera and IMU. Followed by the tracking thread with inertial and visual data to accomplish a series of operations such as calculating the camera pose with respect to the active map, extracting ORB features from the input image and determining if the current frame is a keyframe. The data obtained from the tracking thread are then passed to the local mapping thread for constructing the environment map. Lastly, the common areas between the active map and the whole Atlas are detected to decide whether to perform loop correction or conduct a map merge. In the proposed EID-SLAM, the image deblurring process is added as the image preprocessing part before the feature detection of ORB-SLAM3.

5.2.2 Tracking Thread

ORB-SLAM3 supports visual mode which uses visual sensors only and visual-inertial mode which uses visual sensors and inertial sensors together [125]. Different modes correspond to different initialisation methods. In visual mode, the same procedure as in ORB-SLAM is used to find the initial motion, where ORB descriptor and FAST points matching are performed between two initial frames. Homography models and fundamental matrix are calculated and scored, then the initial motion is obtained and the features are triangulated by using the one with a higher score. After this, an up-to-scale map that contains several keyframes and hundreds of points is obtained and optimised using BA by the mapping thread. The visual-inertial mode contains three steps for system initilization. Similar to ORB-SLAM, the initial motion is estimated firstly and merely relies on visual frames. But the difference in this step is that IMU preintegration between keyframes with a higher frequency is implemented along with vision-only MAP estimation. The second step of initialisation in visual-inertial mode is optimising

the inertial parameters by using the up-to-scale map and preintegrated IMU data gained from the previous step. In the last step, a joint visual-inertial full bundle adjustment by taking previous visual-only estimation and inertial-only estimation as seed, is accomplished to obtain the final estimated parameters such as scale and camera pose.

Then the system starts tracking thread after completing the initialization. The sensor pose, velocity and IMU bias are obtained in the visual-inertial system whilst only camera position and posture are gained in the visual SLAM system. In the visual SLAM system, an ad-hoc uniform velocity model is adopted first and the keyframe model is used as a substitute in the case of the motion model failure. If both of the types of tracking models are unavailable, the relocation function will be triggered to relocate the keyframes. Then the feature points extracted from frames are used for camera pose calculation and tracking. Image quality is crucial for feature point extraction, which inspires the addition of image deblurring part before the step of image feature point extraction. Meanwhile, the map is projected into the frame and more map point correspondences are searched once an initial set of feature matches and the camera pose are estimated. By using the beam adjustment method, the reprojection error is minimised and the local map points are tracked, which optimizing the camera pose of the current frame. The last step of the tracking thread is to determine whether to generate a new keyframe according to the rules. Specifically, the frame that meets certain criteria is defined as a keyframe and inserted into the constructed map as a map point. In the visual-inertial SLAM system, at first, both the motion model and IMU parameters are used to robustly predict the camera pose. Then the current frame is optimised with the Gauss-Newton algorithm on the basis of feature reprojection error of matched points and IMU error. Followed by an optimization for map update, which links the current frame and the last keyframe and uses prior estimation and Hessian matrix that got from current frame optimisation.

5.2.3 Local Mapping Thread

The Local mapping thread is in charge of the optimisation of keyframes in a local window and all points observed by these keyframes and the management of keyframes. The local BA of visual-inertial ORB-SLAM differs from the local BA of visual ORB-SLAM in that the former includes IMU error terms in cost function and thus additional states of inertial parameters are calculated per keyframe.

For keyframe management, it is reasonable to discard redundant keyframes to restrain the explosive growth of map size in visual ORB-SLAM. But this strategy is not suitable for visual-inertial ORB-SLAM that involves IMU information due to the motion constraints of consecutive keyframes. The keyframe management policy of visual-inertial ORB-SLAM is that two successive keyframes in the local window differ in less than a certain length, are taken as redundant and removed from mapping.

5.2.4 Loop and Map Merging

In the continuous moving, there exists a certain error between the calculated camera pose and map points gained from the triangulation, which leads to the gradual accumulation of errors with the increase of frames. The loop closure thread is responsible for reducing the accumulated drift and is triggered when the system re-enters into the previously mapped scene. The place recognition system is deployed based on the bag-of-words method to achieve long-term data association, especially for relocalization and loop detection. Once the closed loop is detected, global BA optimisation is carried out to reduce the cumulative error in the trajectory. This optimisation shows high robustness and usability but might be very costly when applied to a large-scale scene. Thus, pose-graph optimisation is adopted to reduce the computation requirements as the structure

is ignored. In contrast to the visual ORB-SLAM, the pose-graph optimisation of visual-inertial ORB-SLAM is performed on 6 DoFs since the scale is observed by IMU data. Afterward, a full global BA in a parallel thread is performed to optimise all states, including visual and inertial parameters.

For visual ORB-SLAM, a map merging operation will be launched if the keyframe in the active map and the keyframe from a different map saved in the Atlas are matched, involving an aligning transformation. Since the map contains many elements and requires a long time for merging, the process of merging is divided into two steps. In the first step, the merge is performed in a welding window determined by the neighbors of the matched keyframes in the covisibility graph. The second step uses pose-graph optimization to correct the rest of the merged map. The merging algorithm in visual-inertial ORB-SLAM follows similar steps with pure visual ORB-SLAM but adds the inertial information into the merging process.

5.3 Image Deblurring Algorithm

Motion blur degrades the quality of images and impacts the feature point extraction in the ORB-SLAM3 system, which might cause the insufficiency of feature points and inaccuracy of the pose estimation in the front-end [147]. If the number of extracted feature points is less than a certain value, the back-end of the SLAM system even cannot obtain the data from the front-end and it will lead to failed tracking. In this context, a set of image processing algorithms including blur detection, image sharpening and image deblurring, is presented to improve the image quality before the tracking thread of SLAM module.

5.3.1 Blur Detection

The algorithm of blur detection is based on the Laplacian operator, which is fast to implement. Laplacian operator is defined as a second-order differential operator, which can be deployed to assess the 2nd derivative of an image [182]. Assumed that function f and the Laplacian operator of f is given as:

$$Laplace(f) = \frac{\partial^2 f}{\partial x^2} + \frac{\partial^2 f}{\partial y^2} \tag{5.1}$$

By making a difference on the second derivative of the Laplace operator in x and y directions, the Laplace operator of discrete function can be obtained and the detailed operation is presented as follows.

1) First order difference in x direction:

$$\bigtriangledown f(x) = f(x) - f(x-1) \tag{5.2}$$

2) Second order difference in x direction:

$$\bigtriangledown(\bigtriangledown f(x)) = \bigtriangledown f(x+1) - \bigtriangledown f(x) = (f(x+1) - f(x)) - (f(x) - f(x-1)) \tag{5.3}$$

3) After simplification:

$$\bigtriangledown(\bigtriangledown f(x)) = f(x-1) - 2f(x) + f(x+1) \tag{5.4}$$

4) Extract the previous coefficient: [1, - 2, 1]

Similarly, the coefficients in the y direction can be obtained, which is [1, - 2, 1]. The Laplace kernel matrix is gained by superposition and shown in Fig. 5.2.

0	**1**	**0**
1	**-4**	**1**
0	**1**	**0**

Fig. 5.2. The Laplacian kernel. [182]

The Laplacian operator-based method can be used for blur detection owing to its definition, namely the 2nd derivative of an image. Similar to the Sobel and Scharr operators, the Laplacian highlights regions of an image involving drastic intensity changes. As is known, the image is more likely blurry if there are few responded edges. In case an image contains high variance, which means that there is a wide stretch of edge-like and non-edge-like responses, indicating that the image is a normal and in-focus image. However, if there is very low variance, namely, there is a tiny stretch of responses, indicating that the image is blurred.

By converting the input image into a grey-scale image, the blur detection algorithm can compute the amount of blur in the converted image. If the image is considered not blurred, it will be directly transferred to the tracking thread of SLAM without further process. This measure can reduce the time of deblur procedure and ensure the real-time performance of SLAM system. Fig. 5.3 reveals the process of the blur detection framework based on the Laplacian operator and the process is illustrated as follows. Firstly, the input image is converted into a gray-scale image. Afterward, the single channel of the gray-scale image is convolved with the Laplacian kernel to get a response map. Then the variance of the response map is calculated and compared with the set threshold. The image is regarded as blurred if the variance is less than the set threshold. Otherwise, the image is determined as not blurred.

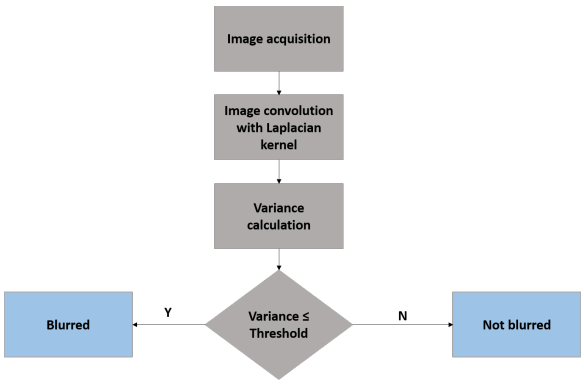

Fig. 5.3. Process of blur detection based on Laplacian operator.

5.3.2 Image Sharpening

Image sharpening is performed if the obtained image is identified as a blurred image. In this process, the sharpness of the image is enhanced. In essence, the detailed edges and target contour in the image are apparent. The policy of feature point extraction is selecting pixels that are largely different from the surrounding pixels. Therefore, the edge information and target contour in the image are required to be extrusive. Consequently, the algorithm of image sharpening is introduced in this work.

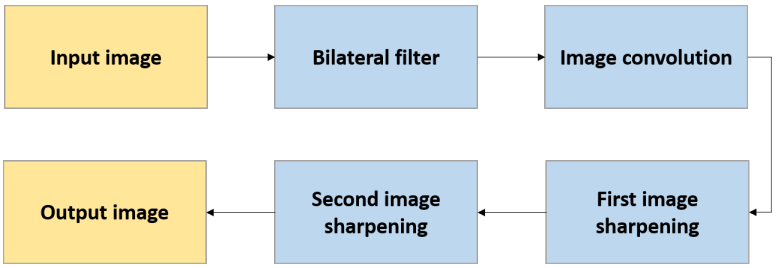

Fig. 5.4. Process of image sharpening.

Generally, image sharpening is beneficial to extract more corner information in the image, especially for blurred images. Depending on this process, extracting ORB features in the tracking thread and detecting the feature points can be easier achieved, which enhances the stability of the system. The process of the adopted image sharpening algorithm is as follows, and the flow chart of the process is shown in Fig. 5.4. The image is firstly converted into a gray-scale image and followed by a bilateral filter to filter the low-pass noise with edge-preserving. Subsequently, the bilateral filtered image is convolved with the sharpness filter shown in Fig. 5.5 to detect the edges in all directions [183]. By adding the detected edges and the original image, the edge information in the image is highlighted, which sharpens the image.

-1	**-1**	**-1**
-1	**8**	**-1**
-1	**-1**	**-1**

Fig. 5.5. The convolution kernel. [183]

5.3.3 Image Deblurring

As Wiener filter can achieve an optimal trade-off between noise smoothing and inverse filtering, it is a simple and efficient algorithm for image deblurring [184]. Therefore, Wiener filter is chosen as the image deblurring tool in this work. For non-blind deblurring, assume that signal, noise spectra and additive noise are known and stationary, Wiener filter can produce an estimation of a target or desired random process by linear time-invariant filtering of an observed noisy process by minimising the mean squared error between the desired process and the estimated random process. In contrast, for a blind deblurring system, the PSF is unknown and needs to be estimated for applying Wiener filter.

Modeling the degradation process mathematically reflects the process of image degradation, which is crucial to restoring the images from blurred images. The process of image degradation is caused by many factors, which makes it difficult to analyze and model individually. Generally, the degradation model can be described as shown in Fig. 5.6.

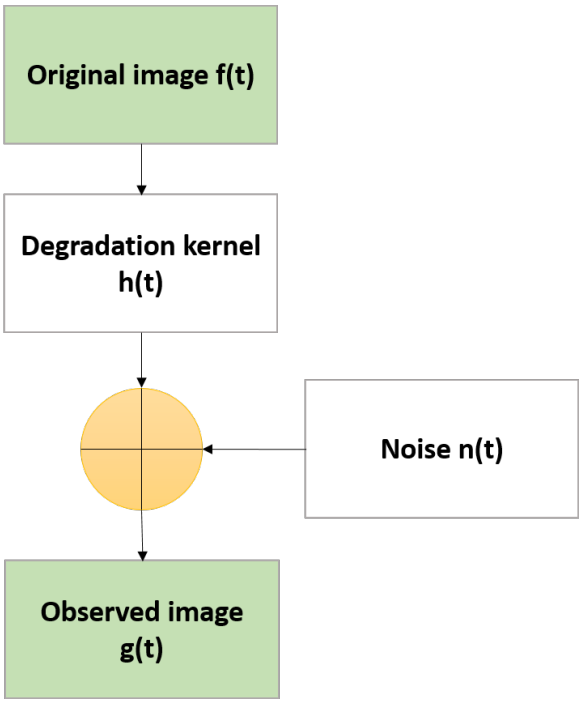

Fig. 5.6. The degradation model.

Correspondingly, the mathematical degradation model in the time domain and frequency domain can be described respectively by [185]:

$$g_b(t) = h_b(t) * f_{d(t)} + n_{(t)} \tag{5.5}$$

$$G_{(f)} = H_{(f)}F_{(f)} + N_{(f)} \tag{5.6}$$

In the Eq. (5.5), $g_b(t)$ corresponds to the observed degraded image, $f_{d(t)}$ represents an original image, $h_b(t)$ is the degradation kernel, which is also known as the PSF. PSF describes the degree of blurring that applies imperfect optics to any given object. $n_{(t)}$ refers to the noise term introduced in the process of image acquisition. Eq. (5.6) represents the mathematical degradation model in the frequency domain.

The goal is to find a convolutional function, namely Wiener filter $w_{(t)}$, where

the estimation of $f_{(t)}$ can be obtained [185]:

$$\hat{f}_{(t)} = w_{(t)} * g_{(t)} \tag{5.7}$$

$$\hat{F}_{(f)} = W_{(f)} * G_{(f)} \tag{5.8}$$

where $\hat{F}_{(f)}$ represents the discrete Fourier transforms (DFT) of $\hat{f}_{(t)}$ [186]. The deconvolutional result, $\hat{f}_{(t)}$, can be obtained by inverse discrete Fourier transforms (IDFT) [186].

As mentioned before, Wiener filter is built on the basis of minimum mean squared error, which can be described as the following form [185]:

$$e_{(f)} = E\left|F(f) - \hat{F}(f)\right|^2 \tag{5.9}$$

From above equation, replacing the $\hat{F}(f)$, the minimum mean squared error can be determined as [185]:

$$\begin{aligned} e_{(f)} &= E\left|F_{(f)} - \hat{F}_{(f)})\right|^2 \\ &= E\left|F_{(f)} - (W_{(f)}G_{(f)})\right|^2 \\ &= E\left|F_{(f)} - (W_{(f)}[H_{(f)}F_{(f)} + N_{(f)}])\right|^2 \\ &= E\left|[1 - W_{(f)}H_{(f)}]F_{(f)} - W_{(f)}N_{(f)}\right|^2 \end{aligned} \tag{5.10}$$

By expanding the Quadratic equation, the following equation can be obtained [185]:

$$\begin{aligned} e_{(f)} = [1 - W(f)H(f)][1 - W(f)H(f)]^* E\left|F_{(f)}\right|^2 \\ -[1 - W(f)H(f)]W^*_{(f)} E\left\{F_{(f)}N^*_{(f)}\right\} \\ -W(f)[1 - W(f)H(f)]^* E\left\{N_{(f)}F^*_{(f)}\right\} \\ +W(f)W^*(f)E\left|N_{(f)}\right|^2 \end{aligned} \tag{5.11}$$

Given that noise and signal are independent, the following equation can be obtained [185]:

$$E\left\{N_{(f)}F^*_{(f)}\right\} = E\left\{F_{(f)}N^*_{(f)}\right\} = 0 \tag{5.12}$$

In addition, the power spectrum can be defined as follows [185]:

$$S_f = E\left|F_{(f)}^2\right| \tag{5.13}$$
$$NO_f = E\left|N_{(f)}^2\right|$$

Then the minimum mean squared error can be represented as [185]:

$$e_{(f)} = [1 - W_{(f)}H_{(f)}][1 - W_{(f)}H_{(f)}]^* S_{(f)} + W_{(f)}W_{(f)}^* NO_{(f)} \tag{5.14}$$

To find the minimum value, $W_{(f)}$ is derived and the equation is set to equal to zero [185].

$$\frac{d_{(f)}}{dW_{(f)}} = W_{(f)}^* NO_{(f)} - H_{(f)}[1 - W_{(f)}H_{(f)}]^* S_{(f)} = 0 \tag{5.15}$$

Then, the Wiener filter is derived as follows [185].

$$\begin{aligned} W_{(f)} &= \frac{H_{(f)}^* S_{(f)}}{H_{(f)}^2 S_{(f)} + NO_{(f)}} \\ &= \frac{H_{(f)}^*}{H_{(f)}^2 + \frac{NO_{(f)}}{S_{(f)}}} \end{aligned} \tag{5.16}$$

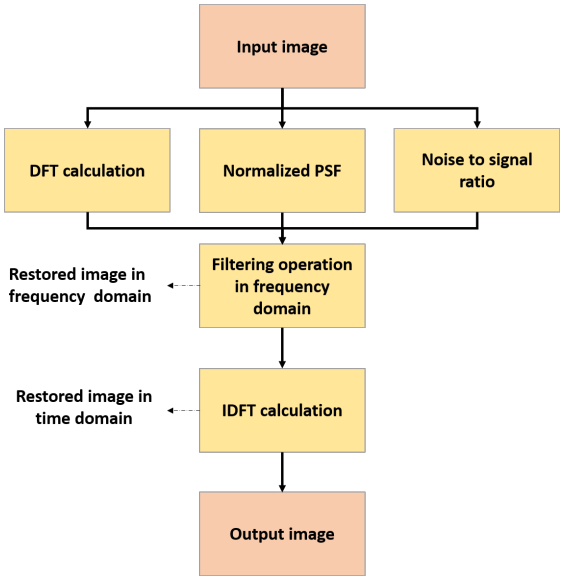

Fig. 5.7. Wiener filter process.

The flow chart of image deblurring applying Wiener filter is shown in Fig.

5.7. Firstly, the observed image in time domain is acquired as input data. Then DFT is applied to transform the input image from time domain to frequency domain [186]. Two crucial parameters, normalised PSF and noise to signal ratio are estimated according to the input information. PSF is firstly initialised and then handled by Wiener filtering. By applying constraints to the filtered PSF, the estimated PSF is obtained. This work estimates the noise variance of image by the method proposed by John Immerkær [187].

$$SNR = \sqrt{\frac{\sum_0^{M_p-1}\sum_0^{N_p-1}\left(g(i,j)\right)^2}{\sum_0^{M_p-1}\sum_0^{N_p-1}\left(g(i,j)-f(i,j)\right)^2}} \tag{5.17}$$

where M_p and N_p are the number of pixels in the length and width of the image respectively. $g(i,j)$ and $f(i,j)$ are the gray values of the original image and the denoised image at (i,j) respectively.

Afterward, the filtering operation is performed based on the previous calculation, and the restored image in frequency domain is gained. To transform the deblurred image from frequency domain to time domain, IDFT is applied. Until now, the image deblurring process using Wiener filter is accomplished and the restored image in time domain is finally obtained from observed blurred images.

5.3.4 ORB Algorithm

As mentioned before, the performance of ORB-SLAM3 is heavily determined by feature point extraction and matching. Thus, running in an environment with blurred images is difficult to get adequate and stable matching point pairs, which causes the failure of positioning and tracking. As a fast and robust feature points detector, Oriented FAST and rotated BRIEF (ORB) was presented in 2011 [188]. It consists of two parts: oriented FAST for feature point detection and rotated BRIEF feature descriptor. The FAST corner detection algorithm

was first proposed in 2006 [189] and represented good performance in robustness and real-time detection when compared with other feature point identification algorithms. Essentially, the gray value of each pixel in the image is compared with the surrounding points. If most of the surrounding pixels are brighter or darker than chosen pixel then it is considered as a feature point.

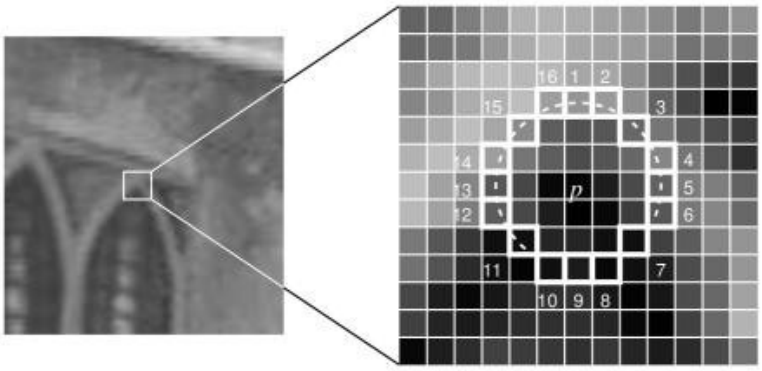

Fig. 5.8. FAST feature point detection. [189]

Taking Fig. 5.8 [189] as an example, the process of FAST feature detection is explained below:

1) Choose a pixel p in the image and set the selected pixel as the centre. The gray value of p is I_p.

2) Set appropriate gray value threshold value t.

3) Regard a Bresenham circle of radius 3 with 16 pixels around the pixel p.

4) Compare the gray value of p with the 16 pixels. If there are a set of consecutive n pixels in the circle which are all greater than $I_p + t$, or all lower than $I_p - t$, then p is determined as a corner.

5) To improve the efficiency of the detection algorithm, the gray values of pixels 1, 5, 9 and 13 are firstly compared. Therein at least three of these four pixels satisfy the above conditions, the remaining 12 points will be continually checked.

Otherwise, if at least three of the four pixels 1, 5, 9 and 13 are not brighter or darker than pixel p, then p is not considered as a possible feature point.

6) Repeat the above procedure until all the pixels in the image are checked.

After obtaining the location of feature points, the method of detecting intensity change around the corner is applied to assign an orientation to each key point and obtain the scale. Assume that a corner's gray value is offset from its centroid which refers to the intensity of the image patch, this vector can be used to compute the orientation of feature point [188]. The specific procedures are shown as follows.

In a small image patch, the moment of the patch is defined as:

$$m_{pq} = \sum_{x,y} x^p y^q I(x, y) \tag{5.18}$$

The centroid of the patch is obtained as:

$$C = \left(\frac{m_{10}}{m_{00}}, \frac{m_{01}}{m_{00}} \right) \tag{5.19}$$

By constructing the vector from the corner's geometric center O to the centroid C, the orientation of the image patch is then given by [188]:

$$\Theta = atan2(m_{01}, m_{10}) \tag{5.20}$$

By implementing the above methods, FAST corners possess the capability of rotation and scale invariance, which is resistant to noise and largely improves the performance of FAST feature point extraction.

The information of extracted feature points needs to be stored to represent an object for matching. In the ORB algorithm, BRIEF descriptor is used to convert the extracted keypoints into a binary feature vector that only contains 0 and 1. Firstly, BRIEF uses a Gaussian kernel to smooth the image and makes the descriptor resists being sensitive to high-frequency noise. Then, in a defined neighborhood, a random pair of pixels are selected and their gray values are

combined into a binary string, which is considered as the descriptor of the feature point.

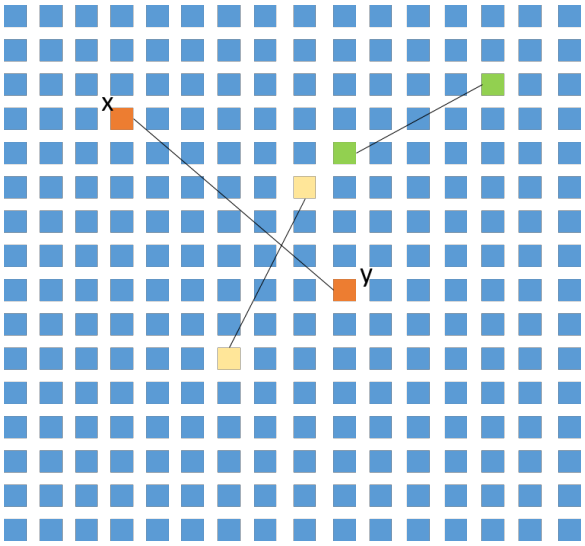

Fig. 5.9. BRIEF description.

By comparing the pair of intensities, the BRIEF binary feature descriptor is determined. As shown in Fig. 5.9, if pixel x is brighter than pixel y, the corresponding bit is assigned as the value of 1, otherwise, it is 0.

A binary test τ is defined by [188]:

$$\tau(p; x, y) = \begin{cases} 1 : I_x < I_y \\ 0 : I_x \geq I_y \end{cases} \tag{5.21}$$

where I_x and I_y are the intensities of image patch p at pixel x and pixel y respectively.

The feature is defined as a vector for n binary test point pairs and the BRIEF descriptor can be obtained by the following equation [188]:

$$f_n(p) = \sum_{1 \leq i \leq n} 2^{i-1} \tau(p; x_i, y_i) \tag{5.22}$$

However, the BRIEF descriptor is not invariant to rotation. ORB algorithm adds the functionality of rotation awareness without losing the speed aspect of BRIEF.

5.4 Evaluations

In this section, experiments were performed to validate the effectiveness of EID-SLAM and the experimental results are presented. All the experiments were processed on a laptop with an Intel i7-8750H, 8 GB RAM. The operating system is Ubuntu 16.04 64bit and the program uses C++ compilation.

5.4.1 Evaluation Using TUM RGB-D Dataset

In this experiment, the famous open dataset TUM RGB-D, which was collected by Microsoft Kinect Sensor in various indoor scenes, is utilized. The collected dataset is mainly comprised of three parts, which are RGB image, depth image and the obtained real trajectory acquired by the high accuracy and precision motion capture system. 7 sequences with regard to dynamic scenes in TUM RGB-D dataset are utilized. The sequences have several motion blur scenes, which is suitable to demonstrate the utility of the proposed image deblurring framework.

At first, it is qualitatively validated that the procedure of image deblurring can improve the performance of feature point extraction. The number of matching pairs was compared quantitatively. In addition, the EID-SLAM system and the original ORB-SLAM3 were compared in blurring scenes to verify the advantage of the proposed image deblurring framework. Specifically, each sequence was operated 10 times to obtain reliable experimental data.

In the process of operation, the adding module of image deblurring in SLAM system detects the blurred images first and the images regarded as blurry are then sent to the processes of sharpening adjustment and image deblurring. Afterward, the preprocessed image is transmitted to the process of feature point extraction.

The feature points extraction between the motion blurred image and deblurred image, were compared and the result is shown in Fig. 5.10. As found at the figure, the left is the image that existed in the sequence with motion blur while the right is the deblurred version. The highlighted key points indicate the main differences in feature point extraction between the two images. It can be clearly seen that much information in the image has been improved and highlighted after image deblurring, which thus extracts more feature points compared with the original blurred image.

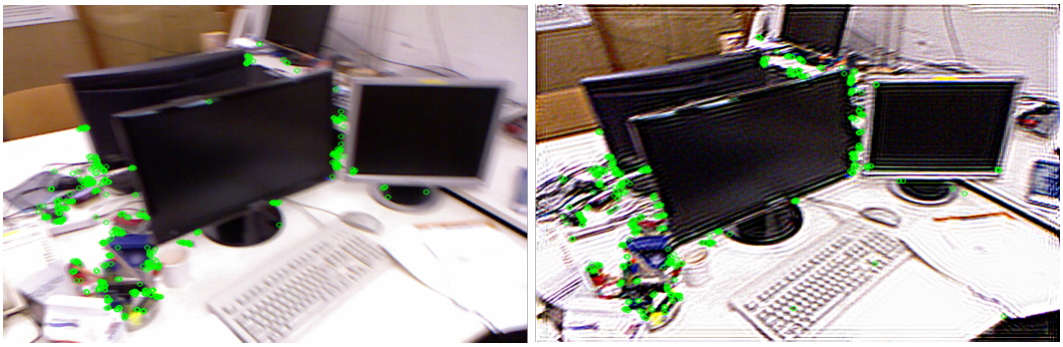

Fig. 5.10. Point extraction comparison between blurred image and deblurred image.

The matching effect of the blurred image and the deblurred image was compared as well and the experimental result is displayed in Fig. 5.11. As shown in the figure, the image deblurring framework improves the feature points matching obviously, which verifies its effectiveness.

Fig. 5.11. Matching comparison between blurred images and deblurred images.

The EID-SLAM system and original ORB-SLAM3 were tested on the 7 sequences of TUM RGB-D dataset. Absolute trajectory error (ATE) is corresponding to the difference between the camera's true pose and the estimated pose. The difference is taken as the benchmark to evaluate the accuracy of SLAM system. To calculate this, the ground truth and the estimated pose are aligned according to the time stamp and then each pair of poses is compared. ATE in frame i is defined by the following equation [190]:

$$F_i = Q_i^{-1} S p_i \tag{5.23}$$

where Q_i is the ground truth of pose in frame i while p_i is the estimated pose obtained from the SLAM system. S represents the similarity transformation matrix from the calculated pose to the ground truth.

The RMSE of ATE is determined as follows [190]:

$$RMSE = \sqrt{\sum_{i=1}^{n} \frac{(\hat{x}_i - x_i)^2}{n}} \tag{5.24}$$

where $\hat{x}_i$ is the estimated pose of the ith image frame in the sequence and x_i represents the ground truth.

The comparison of ATE in both SLAM systems is shown in Fig. 5.12 and the comparison of translational errors is displayed in Fig. 5.13.

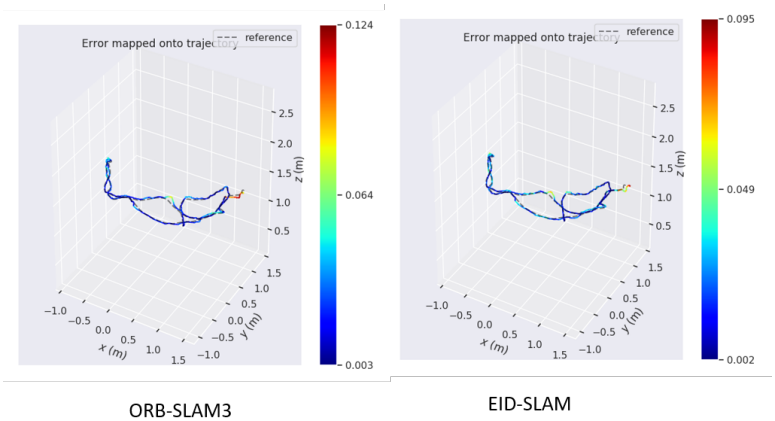

Fig. 5.12. Absolute trajectory error of both SLAM systems.

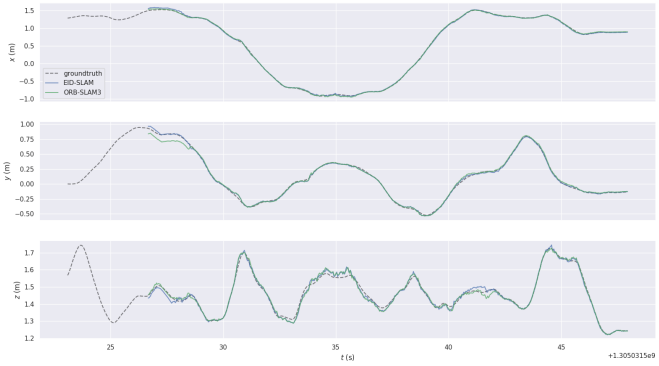

Fig. 5.13. Comparison of translational errors of both SLAM systems.

The RMSEs of both ORB-SLAM3 and proposed EID-SLAM systems in 7 sequences are listed in Table 5.1. The experimental results demonstrate the effectiveness and advantages of EID-SLAM on most of the sequences.

Table 5.1: Evaluation on TUM RGB-D dataset.

Sequences	ORB-SLAM3	EID-SLAM (proposed)
fr1-360	0.200037 m	**0.188247 m**
fr1-desk	0.0179495 m	**0.0303257 m**
fr1-desk2	0.066585 m	**0.0261665 m**
fr1-room	0.069272 m	**0.061698 m**
fr1-rpy	0.0248158 m	**0.0217395 m**
fr3-rpy	0.8140617 m	1.099708 m
fr1-xyz	0.0098497 m	0.0099305 m

The average tracking time on 7 sequences of RGB-D dataset is presented in Table 5.2. It is observed that the average tracking time of EID-SLAM is slightly increased due to the image deblurring. The average percentage of increase is 16.4%.

Table 5.2: Average tracking time on RGB-D dataset.

Sequences	ORB-SLAM3	EID-SLAM (proposed)	Percentage of increase
fr1-360	0.01956531 s	0.02244842 s	0.147358258
fr1-desk	0.02402865 s	0.02795 s	0.16319477
fr1-desk2	0.02466 s	0.02907 s	0.178832117
fr1-room	0.02289 s	0.02634 s	0.150720839
fr1-rpy	0.02306 s	0.02673 s	0.159150043
fr3-rpy	0.02609 s	0.02914 s	0.116903028
fr1-xyz	0.02315 s	0.02852 s	0.231965443

5.4.2 Evaluation Using TUM Visual-Inertial Dataset

TUM Visual-Inertial dataset was collected by an Event-based camera and IMU in a variety of outdoor and indoor scenes. It is resilient to motion blur scenes due to the deployment of expensive Event-based cameras. To validate the proposed image deblurring framework, a number of frames in the sequences were firstly motion blurred with motion length and angle. Then the EID SLAM and ORB-SLAM3 were evaluated based on the blurred sequences. Sequences containing corridors and several offices were chosen to simulate the industrial scene when using mobile robots for transporting materials. As the ground truth of TUM Visual-Inertial dataset is only available in the room where all sequences start and end, the drift at the end of the sequence is consequently measured.

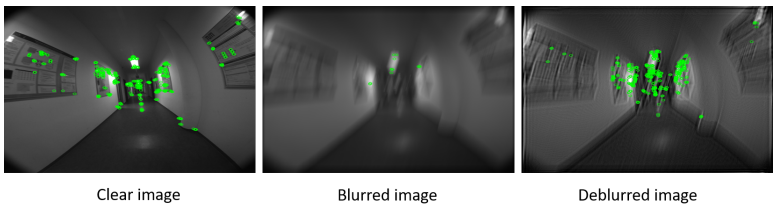

Fig. 5.14. Point extraction comparison among clear image, blurred image and deblurred image.

The comparison of feature points extraction among a clear image, a blurred image and a deblurred image is shown in Fig. 5.14. As can be seen from the figure, the extracted feature points from blurred images have been drastically reduced

compared with the original clear image while getting distinct improvement after image deblurring.

The matching effect among clear image, blurred image and deblurred image is displayed in Fig. 5.15. Compared to a clear image, the number of matches in the blurred image is significantly decreased but the image deblurring framework obviously improves the matching effect of the blurred image, demonstrating the effectiveness of image deblurring.

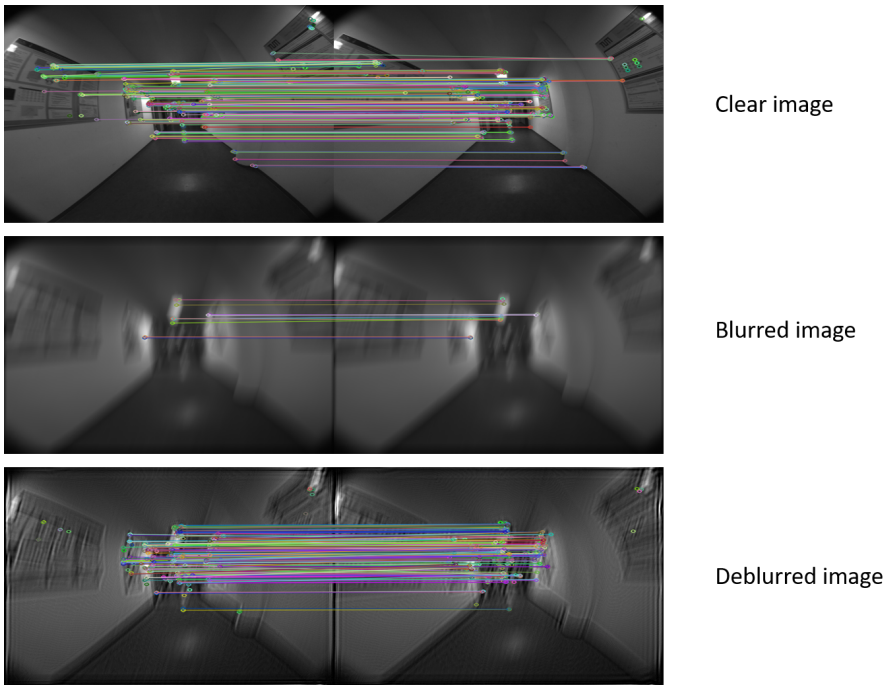

Fig. 5.15. Matching effect comparison among clear image, blurred image and deblurred image.

The RMSEs of ORB-SLAM3 and proposed EID-SLAM on 5 sequences of TUM Visual-Inertial dataset are listed in Table 5.3. The proposed EID-SLAM has less error than ORB-SLAM3 in most sequences, verifying the advantages of image deblurring framework in improving the accuracy of SLAM that existed with blurred images.

Table 5.3: Evaluation on TUM Visual-Inertial dataset.

Sequences	ORB-SLAM3	EID-SLAM (proposed)
corridor1	0.0823986 m	0.0874096 m
corridor2	0.0271294 m	**0.0165418 m**
corridor3	0.2345634 m	**0.1324068 m**
corridor4	0.1498789 m	**0.1376378 m**
corridor5	0.0722924 m	**0.0591188 m**

The comparison of both ORB-SLAM3 and proposed EID-SLAM in average tracking time on TUM Visual-Inertial dataset is presented in Table 5.4. The average percentage of increase is 9.4%. It is observed that the EID-SLAM needs slightly more time than ORB-SLAM3 owing to the image deblurring module.

Table 5.4: Average tracking time on TUM Visual-Inertial dataset.

Sequences	ORB-SLAM3	EID-SLAM (proposed)	Percentage of increase
corridor1	0.03297182 s	0.03461313 s	0.110835423
corridor2	0.03281996 s	0.03472322 s	0.049779174
corridor3	0.0336072 s	0.03366856 s	0.057990735
corridor4	0.03328383 s	0.03697286 s	0.001825837
corridor5	0.0361146428 s	0.04134231 s	0.251015772

5.4.3 Evaluation Using Real-world Robot

The proposed EID-SLAM system was as well tested experimentally in real-world scenarios to evaluate its feasibility. The dataset was collected by the Pepper robot [191] equipped with an Intel RealSense depth camera D435i and the experimental setup is shown in Fig. 5.16. The specific process is as follows. The camera was first calibrated to get the parameters such as intrinsics, extrinsics, and distortion coefficients. Then, the Pepper robot with a camera was driven along a path involving linear motions and turning motions to obtain blurred images for validating the feasibility of the proposed EID-SLAM.

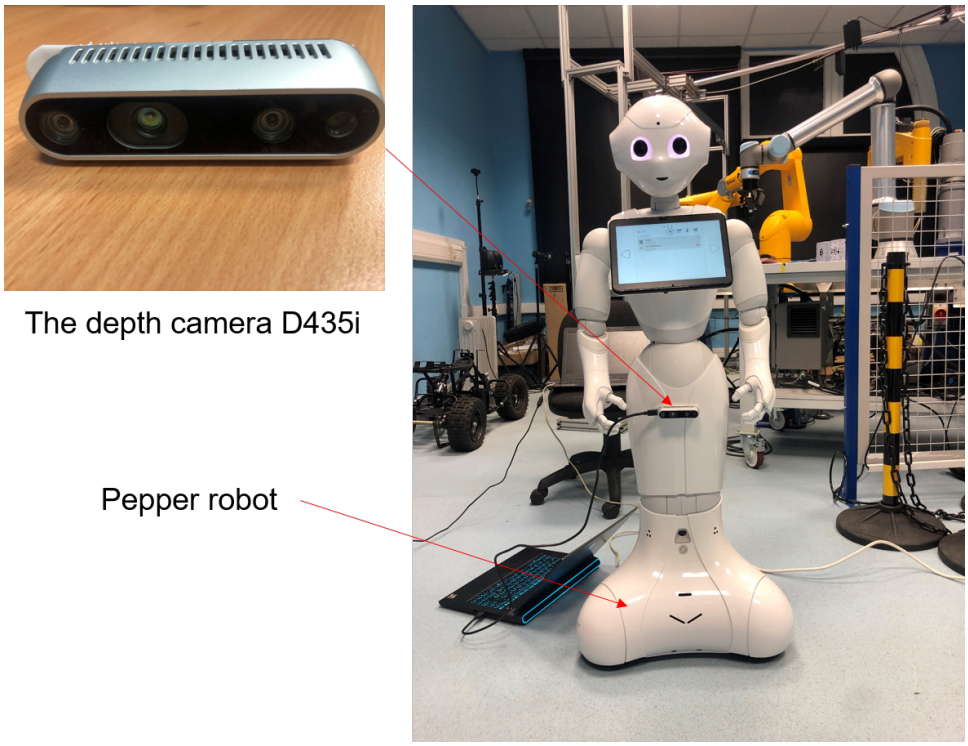

Fig. 5.16. The experimental setup for evaluating EID-SLAM system.

The collected dataset contains a number of blurred frames and was performed by ORB-SLAM3 and EID-SLAM respectively. The comparison of key points detection between a blurred frame and a deblurred frame is displayed in Fig. 5.17, where the deblurred frame detects more key points than the blurred frame.

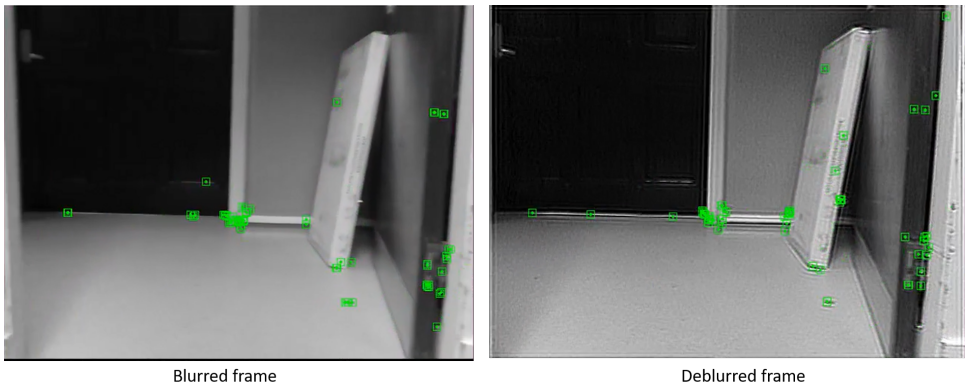

Fig. 5.17. The comparison of key points detection between blurred frame and deblurred frame.

By implementing the EID-SLAM, the trajectory of a robot can be obtained and is shown in Fig. 5.18. The translational positions and rotational angles of trajectory are presented in Fig. 5.19, showing the detailed linear motions and turning motions of the robot. The generated trajectory validates the feasibility of EID-SLAM.

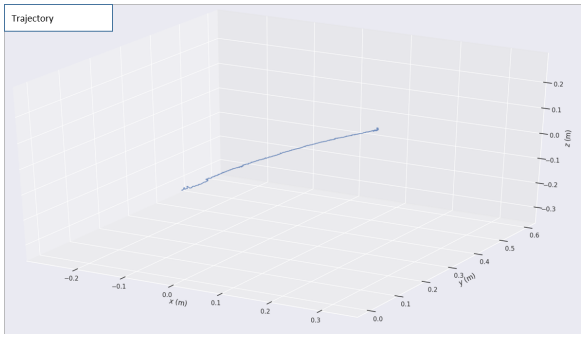

Fig. 5.18. The trajectory of robot.

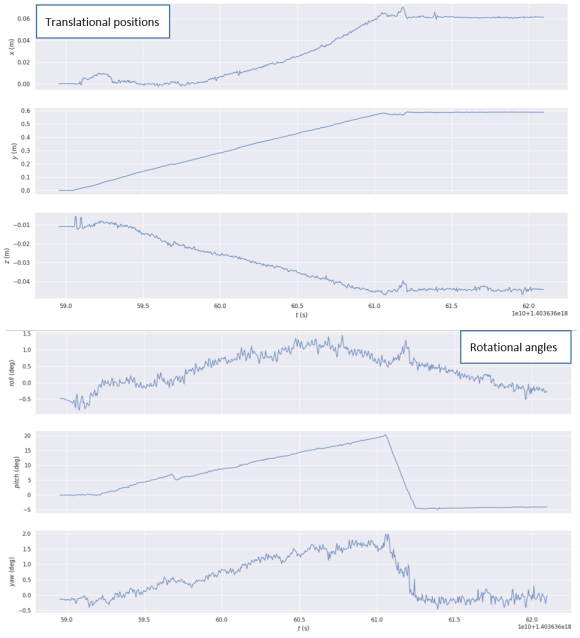

Fig. 5.19. The translational positions and rotational angles of trajectory.

5.5 Summary

In this chapter, the proposed EID-SLAM system has been presented based on ORB-SLAM3 and image deblurring framework. The obtained images are first detected by the Laplacian operator-based blur detection algorithm. If the image is identified as blurred, the image sharpening algorithm is performed to make the detail edges and target contour in the image more apparent. Following this, the sharpened image is handed to the image deblurring module for deblurring the blurred image. Subsequently, the processed images are passed to the tracking thread of ORB-SLAM3 after initialization. Whereas, if the captured image is identified as clear, the image is directly transferred to ORB-SLAM3 for feature point extraction and matching.

The proposed EID-SLAM system has been compared with ORB-SLAM3 in terms of average absolute trajectory error and average tracing time. The experimental results tested on TUM RGB-D dataset and TUM visual-inertial dataset suggested that the EID-SLAM system achieves better performance than ORB-SLAM3 while the experimental results tested on the real-world dataset validate the feasibility of EID-SLAM. Innovatively, the image deblurring framework was combined with ORB-SLAM3, which improves the accuracy of the SLAM system with increasing around 12.9% processing time.

Until now, the proposed Co-MRMS has been modeled in a simulation environment and the performance in fulfilling the transportation and handling task is verified in Chapter 3. Chapter 4 and this chapter have further and deeply explored the local and global positioning approach respectively for the proposed Co-MRMS. In Chapter 6, the combined behavior of the proposed Co-MRMS is validated and the accuracy of machine vision algorithms is assessed in real-world scenes.

Chapter 6

Prototype Verification of the Proposed Co-MRMS through a Case Study on Composite Manufacture

6.1 Introduction

Due to the interesting properties and high strength-to-weight ratio, the applications of composite materials have raised considerably in the last decades [192,193]. They are usually made of multiple plies of fibers (e.g. carbon, glass and/or synthetic fibers), layered up in alternating orientations and held together by resin. Therefore, the laying-up of fiber plies is the fundamental manufacturing phase in the production of composite materials. It is usually performed by human operators, who handle and transport the raw materials, making composite manufacturing time-consuming, labour intensive and prone-to-errors.

The manual lay-up process requires skilled workers with knowledge and experience attained over several years. Common techniques used in manual lay-up and further highlighted the complexity and skills involved in the process were discussed in [194], which indicated that laying up laminators need to be trained before operations. This is a problem for long-term sustainability due to a reducing number of skilled workers [195]. Quality is also going to be dependent on the individual, so it is harder to maintain consistent quality with manual lay-up. Different from manual system, automated composite lay-up by robotic system can be performed 24 hours a day, which is possible to be more time-saving than manual system and is worth investigating as a replacement for manual lay-up.

The demand for the phasing in of robotic solutions to improve process efficiency and increase operator safety has grown significantly in recent years. Automated Tape Laying (ATL) [196] and Automated Fiber Placement (AFP) [197, 198] are two popular automated technologies employed in automotive lay-up of composite material. However, limited by the heavy cost of specialised equipment and low flexibility, they are not suitable for making small composite parts [199]. Up to now, investigations on the use of commercially available robotic platforms for composite lay-up are on the rise in composite manufacturing.

Previous works have investigated the viability of using robotic systems in advanced composite manufacturing by exploiting the flexibility of robots to meet the stringent demands of manufacturing processes. In [200] and [201], complete systems for handling and laying up prepreg on a mould were developed. Robotic workcells were demonstrated with different modules. Bjornsson et al. [202] surveyed pick-and-place systems in automated composite handling with regards to handling strategy, gripping technology and reconfigurability etc. This survey indicated that it is hard to find generic design principle and the best solution for handling raw materials for composite manufacture depends on the specific case study. Schuster et al. [203] demonstrated how cooperative robotic manip-

ulators can execute the automated draping process of large composite plies in physical experiments. Szcesny et al. [204] proposed an innovative approach for automated composite ply placement by employing three industrial manipulators, where two of them were equipped with grippers for material grasping and the third manipulates a mounted compaction roller for layer compression. A comparable hybrid robot cell was developed by Malhan et al. [205, 206], where rapid refinement of online grasping trajectories was studied. Despite these advances, cooperative/hybrid robotic systems involving mobile robot platforms and fixed-base robotic manipulators have received little attention in the context of advanced composite manufacturing.

Due to the requirement of accurate localization and fiber orientation detection, an efficient vision system is of great importance for autonomous robotic systems in advanced composite manufacturing. Fiber orientation detection is challenging due to the high surface reflectivity and fine weaving of the material, and thus it has still predominantly been accomplished manually in practice [207, 208]. Traditional machine vision methods for fiber orientation detection of textiles prefer to utilise diffused lighting [209], such as diffuse dome [210] and flat diffuse [211] illumination measuring techniques. Polarisation model approaches have been particularly popular for measuring fiber orientation, where the contrast between textile features such as fibers and seams are used to identify the structure of the material relative to the camera [212]. However, when considering the specific application of advanced composite manufacturing, changes in lighting conditions are often unavoidable because of the moving shadow of the robot arm cast on the material. The integration of vision systems with robotics was considered by only a few of the previous works. This means systems are inflexible as they are unable to cope with dynamic variations within advanced composite manufacturing processes.

As the above literature review has shown, in composite manufacturing, popular

automated technologies employed in automotive lay-up of composite material are not suitable for making small composite parts owing to the limits of heavy cost of specialised equipment and low flexibility. Additionally, material transport and composite lay-up have not been integrated into a single autonomous robotic system, which is challenging due to the many technologies involved, including path planning, material detection and localization, etc. Achieving this requires the development of a strategy that combines different modules in a flexible system and provides autonomous material transportation and sufficiently-accurate material handling capabilities. This chapter builds up a prototype of the proposed Co-MRMS and presents a physical case study on robotic material transportation and composite lay-up, which is based on a real-world scenario commonly found in advanced composite manufacturing. Compared to previous works, this research addresses specific challenges that arise from the introduction of different robots that must be coordinated along with the complex set of tasks covering transport, detection, grasping and placement of deformable material for composite manufacturing applications. Furthermore, robotic systems without integration of vision systems are inflexible as they are unable to cope with dynamic variations within advanced composite manufacturing processes and this is considered by only a few of the previous works.

Until now, the proposed Co-MRMS has been modeled in a simulation environment and the performance in fulfilling the transportation and handling task is verified in Chapter 3. Chapter 4 and this chapter have further and deeply explored the local and global positioning approach respectively for the proposed Co-MRMS. In Chapter 6, the combined behavior of the proposed Co-MRMS is validated and the accuracy of machine vision algorithms is assessed in real-world scenes.

When the mobile robot drives out of the scope of the fixed-base robotic manipulator, it relies on SLAM for positioning and the performance of SLAM has

been verified separately in Chapter 5. This chapter focuses on the verification of the feasibility and handling performance of the proposed Co-MRMS when the mobile robot drives in the scope of the fixed-base robotic manipulator. To address this, deploying a prototype of the proposed Co-MRMS to perform a series of tasks in composite material manufacturing, is investigated and served as the case study. Therefore, a physical Co-MRMS, which consists of an autonomous mobile robot, a fixed-base manipulator and a machine vision sub-system is expanded from the simulated case study demonstrated in Chapter 3 and presented in this chapter. The mobile robot transports the material autonomously to a predefined position within the working range of the fixed-base manipulator. A machine vision system is designed and integrated with the robotic manipulator to detect the location of the material and estimates the fiber orientation to enable the manipulator to accurately handle the material. This is achieved by employing an ArUco marker detection algorithm [213] to compute the position of the material, and a Fourier transform-based algorithm [214] combined with a least squares line fitting method [215] to calculate the material's fiber orientation. Afterward, the manipulator accurately grasps the material and places it onto a mould. Physical experiments were conducted to verify the cooperation behaviors of the Co-MRMS and quantify the accuracy of the handling.

The rest of this chapter is organised as follows. In Section 6.2, the overall framework of Co-MRMS research and adopted machine vision approaches in physical experiments are presented, while Section 6.3 introduces the robot setup and machine vision system design. Section 6.4 reports the physical experimental results conducted to evaluate the prototype system performance on the basis of the feasibility of laying up fiber plies, how accurately the plies are placed on the mould and how capable the system deals with uncertainty. Finally, a summary of the chapter is provided in Section 6.5.

6.2 Proposed System and Approaches

6.2.1 Further Development of the Proposed Co-MRMS Framework

As a whole, the proposed Co-MRMS consists of three modules covering visual-based SLAM for autonomous transporting, multi-sensor fusion positioning for mobile robot identification and a prototyping Co-MRMS for performance validation. The framework is presented in Fig. 6.1. From a hardware perspective, the proposed Co-MRMS involves four components: a mobile robot, a fixed-base robotic manipulator, a sensing system and a host PC. The four different components are combined and cooperated as a whole robotic system. In this integrated robotic system, the mobile robot is responsible for transporting material from a given starting location within the workshop floor (e.g. the storage area) to the robotic manipulator.

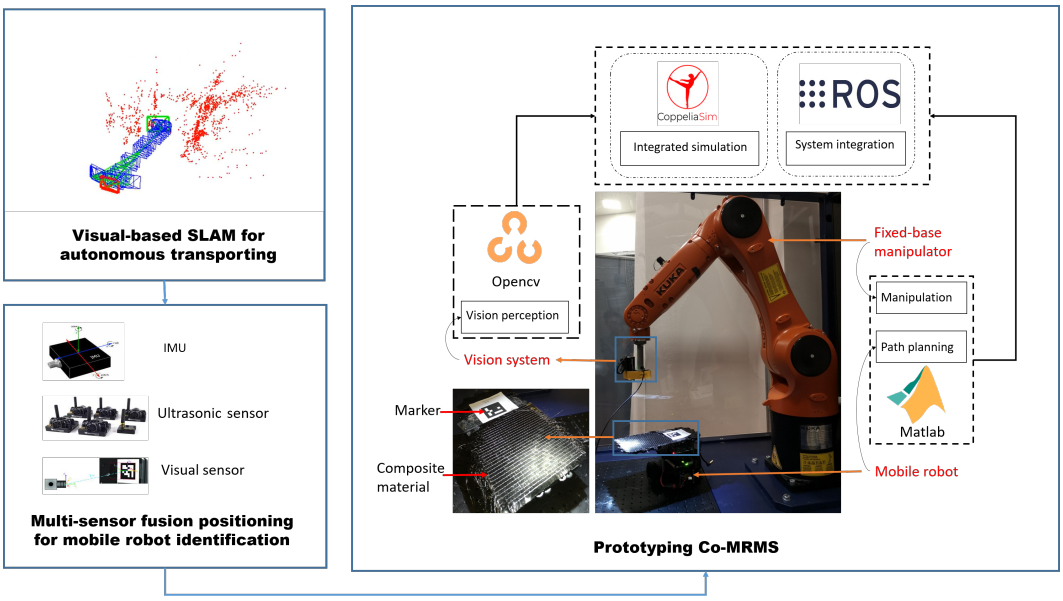

Fig. 6.1. Further development of the proposed Co-MRMS framework.

For this module, the visual-based SLAM has been investigated in Chapter 5 to support the mobile robot conducting autonomous material transport in a dy-

namic manufacturing environment. After arriving at the scope of the fixed-base robotic manipulator, aided by the multi-sensor fusion positioning system proposed in Chapter 4, the estimated positions of the mobile robot are accurately and robustly sent to the fixed-base robot manipulator via the host PC. Finally, the robotic manipulator handles the material from the mobile robot. The prototype system of the proposed Co-MRMS is developed in this chapter to validate the interactive behaviors and material handling ability. Specifically, composite material manufacture is chosen as the case study for investigation. The composite material transport and lay-up are conducted by the Co-MRMS. To achieve this, the fixed manipulator is used for grasping each fiber ply and placing it correctly according to the designed lay-up manufacturing specifications. Robotic path planning for the mobile robot and robotic manipulator was implemented in MATLAB® [155]. Image processing algorithms were developed by using OpenCV, an open-source computer vision and machine vision software library that provides a common infrastructure for computer vision applications and accelerates the development of machine perception capabilities. Being a BSD-licensed product, OpenCV makes it easy for businesses to utilise the library and modify the code. The integration of the Co-MRMS was implemented via ROS.

6.2.2 Localization and Fiber Direction Identification Approach

The aim of the machine vision system is to detect and locate the composite material and identify the orientation of the fiber in the work space according to the requirements of composite material manufacturing processes. The extracted position and orientation of the material are provided to the host PC, which uses the information to plan target coordinates for the robot arm to grasp the composite material transported by the mobile robot. Generally, the position of the material can be approximated continually using wheel encoders of the mobile robot, but

substantial error accumulated over time due to the wheel slippage. This can be compensated by the vision system which provides higher accuracy position information relative to the manipulator end-effector frame and it is necessary to enable accurate localization of composite material. This corrected position estimation can further be used to eliminate the build-up of error within the wheel odometry-based localization system. Thus machine vision plays a crucial role in the proposed Co-MRMS that can be applied to composite material manufacturing. By combining both machine vision and wheel odometry-based data, the proposed localization system can be robust and accurate.

Yet the application requires an approach for object detection that is robust to variations in the size and shape of the material. To overcome these challenges, firstly, a marker-based approach is adopted to enable the proposed Co-MRMS to locate the material accurately. Then, a method for accurate and robust fiber orientation detection is developed. Here it is assumed that the relative position between the marker and the material is fixed. By locating the marker, the position of the material can be inferred from the relative position between the marker and the material. This provides the proposed Co-MRMS with a higher accuracy estimation of the position of the fiber material, which does not accumulate errors over time. Then, the orientation of fiber is detected to support the composite lay-up process. More details will be given in the following sections.

6.2.2.1 Localization Approach

As shown in Fig. 6.2, this work uses a single ArUco vision marker for material localization material. The principle of using a camera to detect and obtain the position of the ArUco vision marker has been described in detail in the section of vision-based estimation in Chapter 4. Therefore, it will not be covered again here.

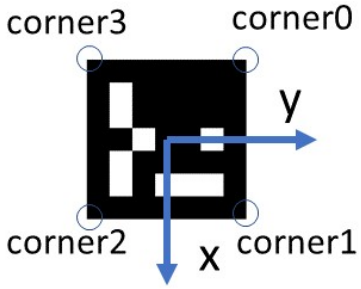

Fig. 6.2. An ArUco marker example.

As shown in Fig. 6.3, the material is placed on the x direction of the marker. Using d_{cc} to denote the distance between the centre of the material and the marker (assumed to be known as a priority), (x_{mar}, y_{mar}) to denote the marker position, and Θ to denote the marker orientation in the x-y plane. The relative position of the material can be calculated by:

$$\begin{cases} x_{mat} = x_{mar} + d_{cc}\cos(\Theta) \\ y_{mat} = y_{mar} + d_{cc}\sin(\Theta) \end{cases} \tag{6.1}$$

Where the final position (x_{mat}, y_{mat}) corresponds to the x and y positions of the material centroid.

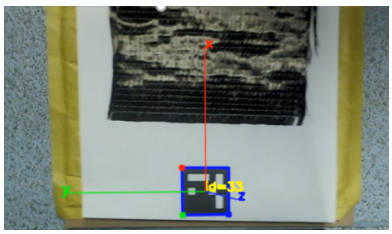

Fig. 6.3. Composite material detection.

Using this approach, the position of the material can be determined robustly regardless of the size and shape of the material. Once the position of the material is detected, target commands are sent to the robot to move the end-effector above this centre position. Additionally, there is no restriction for the size and shape of the material as long as the centre of the fabric is fixed. Thus, this localization

approach is suitable for handling different size and shape of fabric patches.

6.2.2.2 Fiber Orientation Detection Approach

The orientation of the composite material during placement on a mould must be carefully controlled in a composite lay-up process. This is due to the material being anisotropic, meaning it provides varying strength along different directions across the material. In order to make sure that the plies are layered as designed, strict requirements are imposed for the orientation of each layer of fibers to obtain the expected composite parts. The Fourier Transform [216] is a popular image processing tool that has proven to be effective for a variety of image processing applications such as image enhancement and image compression. In this work, the Fourier Transform is applied for fiber orientation analysis, where an image is converted into the frequency domain to obtain its spatial frequency components. The transformed image can be calculated by [216]:

$$F_{(\mu_f,\nu_f)} = \int_{-\infty}^{+\infty}\int_{-\infty}^{+\infty} f_{(x,y)} e^{-i2\pi(\mu x+\nu y)} dxdy \tag{6.2}$$

where μ_f and ν_f are spatial frequencies. In order to robustly detect the orientation of fibers from an image using the Fourier transform, a high gradient image possessing strong directional change in intensity must be acquired. This is achieved through the use of a spotlight mounted together with the camera to produce strong reflections from the fibers of the material.

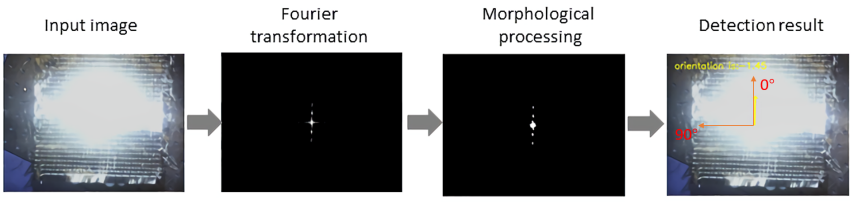

Fig. 6.4. Fiber orientation detection procedure.

The detection process is shown in Fig. 6.4. An image captured by the camera

is first converted to a grey-scale image. Then the Fourier transform is applied to obtain the frequency domain image. A series of morphological procedures are applied to generate several discrete points that lie along the line in the direction of the fibers. The centre of these points can be analysed by contour detection. Finally, a fitted straight line for this set of points is computed and the orientation of this line is calculated according to its slope. Here curve fitting is achieved through the use of the least squares line fitting method. It should be noted that this approach is inspired by the high surface reflectivity and colour difference between yarn and fibers. Therefore, it's suitable for materials like carbon fiber while other methods need to be considered in detecting low surface reflectivity and colour difference materials such as fiberglass.

Assume that the points obtained from the morphological procedures are (x_1, y_1),..., (x_n, y_n), and the fitted straight line equation is $y_i = ax_i + b$. The process for curve fitting is to identify appropriate values for (a, b) that minimises the total squared error E [217]:

$$E = \sum_{i=1}^{n} (y_i - ax_i - b)^2 \tag{6.3}$$

The above equation can be re-expressed as [217]:

$$E = \|Y - XB\|^2, \tag{6.4}$$

where

$$Y = \begin{bmatrix} y_1 \\ \vdots \\ y_n \end{bmatrix}, \; X = \begin{bmatrix} x_1 & 1 \\ \vdots & \vdots \\ x_n & 1 \end{bmatrix}, \; B = \begin{bmatrix} a \\ b \end{bmatrix},$$

The explicit expression of E as a function of Euclidean vector norm is [217]:

$$\begin{aligned} E &= \|Y - XB\|^2 \\ &= (Y - XB)^T (Y - XB) \\ &= Y^T Y - 2(XB)^T Y + (XB)^T (XB). \end{aligned} \tag{6.5}$$

According to the stationary condition of E with respects to B requires

$$\frac{dE}{dB} = 2X^T XB - 2X^T Y = 0, \tag{6.6}$$

which leads to the stationary point

$$B = [X^T X]^{-1} X^T Y. \tag{6.7}$$

Thus the original equation can be represented by a least squares solution, $B = [X^T X]^{-1} X^T Y$ given that $[X^T X]^{-1}$ exists which depends on the data collection. The values for (a, b) are obtained by [217]:

$$\begin{aligned} a &= \frac{\sum x_i^2 \sum y_i - \sum x_i (\sum x_i y_i)}{n \sum x_i^2 - (\sum x_i)^2} \\ b &= \frac{n \sum x_i \sum y_i - \sum x_i (\sum x_i y_i)}{n \sum x_i^2 - (\sum x_i)^2} \end{aligned} \tag{6.8}$$

This provides the fitted line, $y = ax + b$. Using the computed gradient of the line a, the orientation can be calculated by: $\Theta = \arctan(a)$, where Θ is the fiber orientation angle in x-y plane taking x-axis as a reference position. Therefore, as long as the relative orientation of fibers and yarn is known, fiber orientation detection can be adapted to different kinds of prepregs. The prepreg used in this work is carbon fiber reinforced polymer (CFRP) composites. The relative orientation of fibers and sewing yarn is known in advance, which is at 90°.

6.3 Experiment Setup

The composite material used here is a small sheet of fabric prepreg. The physical experiments are described, where the specific robotic layout and designed tools are defined.

6.3.1 Robot Setup

In this work, the Turtlebot3 Burger differential drive mobile robot was chosen as the mobile robot platform in physical experiments due to the unavailability

of industry-standard mobile robots. As the Turtlebot3 Burger is an open-source mobile robot, low-level access to the robot's individual functionalities is possible, providing easy access to wheel odometry-based readings that can be sent to the host PC through a ROS network. For the fixed-base robotic manipulator, the 6 DoFs KUKA KR90 R3100 industrial manipulator was chosen for implementation in the simulation environment to model a realistic industrial environment. In physical experiments, the 6 DoFs KUKA KR6 R900 manipulator was used due to its lower scale and availability. Nevertheless, both robots share the same control scheme, allowing algorithms to transfer without modification between the two systems.

6.3.2 Machine Vision System Design

The machine vision system comprises a commercial low-cost webcam, a spotlight and a customised camera mounting unit. Localization of the material and fiber orientation detection are achieved through the use of a spotlight mounted together with the camera to produce strong reflections from the fibers of the material.In order to attach the camera to the end-effector of the fixed-base manipulator and ensure that the camera is orthogonal to the material plane, a camera mounting unit was designed by CAD (Computer-aided design) software and then 3D printed. The CAD design and mounted 3D-printed piece are presented in Fig. 6.5. During physical experiments, the camera was inserted into the holder facing downwards, while the spotlight was attached to the external surface of the mounting unit facing in the same direction as the camera.

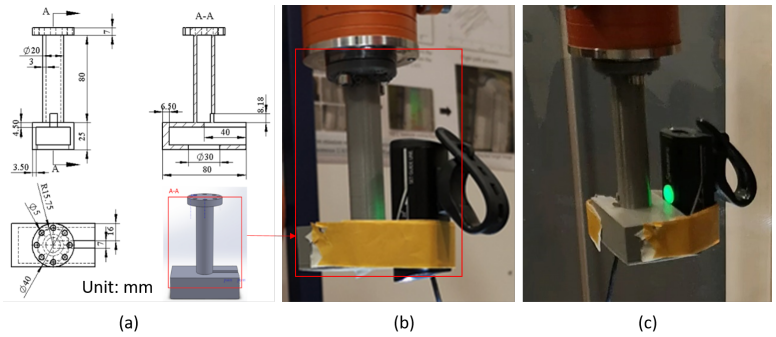

Fig. 6.5. The machine vision system design, (a) CAD model and physical dimensions of the module; (b) and (c) are the camera mount setup during physical experiments.

6.3.3 Host Computer and Related Software

Following the description of the proposed Co-MRMS, Matlab and OpenCV have been used to support the development of crucial robotic capabilities for this work. The path planning routine for the mobile robot, based upon a bi-directional variant of the Rapidly-exploring Random Tree algorithm [157], was implemented on Matlab. Likewise, the planning of manipulator actions for grasping was developed in Matlab, where reasoning is applied on sensory information to identify target positions and complete motions for the end-effector. The robot was actuated using Point-To-Point movement. The Interfacing Toolbox for Robotic Arms (ITRA) toolbox [218], developed for the control of KUKA robots, provided the interface for directly sending actuation commands from Matlab to the KUKA robot controller unit for manipulator control, while ROS provided the interface for the actuation of the Turtlebot3 Burger. The vision system relied upon images captured by a webcam mounted on the end-effector of the manipulator to observe the environment. Then the OpenCV library was used for the development of machine vision algorithms that processed images obtained by the camera.

6.4 Evaluations

The manual lay-up process requires skilled workers with knowledge and experience attained over several years. This is a problem for long-term sustainability due to a reduced number of skilled workers. Quality is also going to be dependent on the individual, so it is harder to maintain consistent quality with manual lay-up. Different from manual system, automated composite lay-up by robotic systems can be performed 24 hours a day, which is possible to be more time-saving than manual system and is worth investigating as a replacement for manual lay-up. System performance is evaluated on the basis of the feasibility of laying up fiber plies, how accurately the plies are placed on the mould and how capable the system deals with uncertainty. To validate the developed system, several experiments were conducted to test the capabilities of the Co-MRMS. Initially, simulation-based experiments were carried out according to the proposed approaches in Section 2 and the accuracy of the vision system was assessed. Subsequently, physical experiments were conducted on an integrated robotic system to validate the combined behavior of the proposed Co-MRMS and assess the accuracy of machine vision algorithms in real-world scenes.

6.4.1 System Interaction Behavior Evaluation

The cooperative system interaction behavior was evaluated by physical experiments, of which a set of execution routines consisting of five active phases and two idle phases were obtained. This corresponds to the complete performance with a duration of approximately 87 seconds, involving approximately 18 seconds idle pauses time. Fig. 6.6 plots the time evolution of the x and y positions of the mobile robot ($odom_x$ and $odom_y$, respectively), and the x, y and z positions of the manipulator end-effector ($kuka_x$, $kuka_y$, and $kuka_z$, respectively) accross

these execution phases recorded from a single trial of the experiment. The first phase consists of the autonomous drive of the mobile robot. The duration of this phase varies according to the start point, goal point and the subsequent path to move between these two points. After the mobile robot arrives at the goal point, it remains stationary to await the machine vision processing phase. This corresponds to a flat curve from the end of phase 1 for $odom_x$ and $odom_y$ in Fig. 6.6. After a brief pause where all systems remain idle to indicate that the mobile robot has reached its destination, the host PC sends the wheel odometry estimation of the mobile robot's position as a target command to drive the manipulator towards the approximate location of the material (phase 2). Here the build-up error in the estimated position arising from wheel slippage causes a misalignment between the centre of the composite material (carried by the mobile robot) and the end-effector of the manipulator. Once the manipulator reaches the target position, both robots remain stationary as the vision system captures an image and runs the localization algorithm to compute a higher accuracy estimate of the mobile robot's true position.

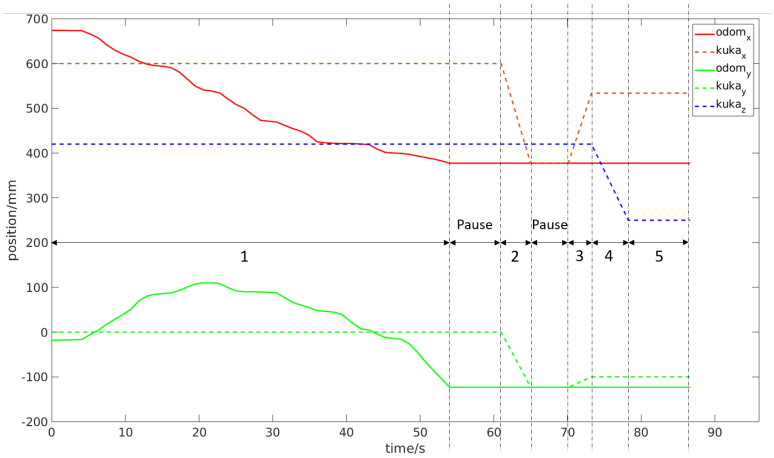

Fig. 6.6. Turtlebot3 Burger and KUKA robot positions during the experiment.

Phase 3 then consists of refining the position of the end-effector using the vision-based estimate of the mobile robot position to reduce the misalignment between

the manipulator and composite material. In the fourth phase, the manipulator lowers the z position of the end-effector from 420 mm to 250 mm (relative to the base frame of the manipulator, which is treated as the world coordinate frame) to provide the camera with a close-up view of the composite material. This is necessary to ensure a satisfactory image can be obtained for accurate fiber orientation detection. In the final phase, machine vision parameters are adjusted for the new image depth and the fiber orientation angle of the material is computed using the algorithm described in Section 2. This information is used to rotate the end-effector to correct for the angular offset between the end-effector and composite material. This facilitates the placement of the material in a controlled orientation during grasping operations by ensuring that the fiber direction is normally aligned with the z-axis rotation of the end-effector.

This experiment demonstrated the capability of the integrated system to correct any manipulator positional offset error that arises from wheel slippage of the mobile robot through higher accuracy estimation provided by machine vision. Compared to the wheel odometry-based localization, the vision system corrected the position in the x and y direction by 156.87 mm and 23.17 mm in this case.

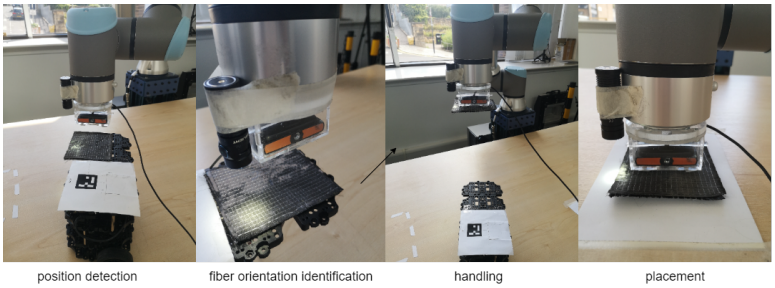

Fig. 6.7. Composite material lay-up experiment.

Due to the high degree of flexibility and wide compatibility of the approach, the fixed-based manipulator can be substituted by other industrial robotic manipulators when considering the availability of equipment. As is shown in Fig. 6.7,

experiments including material detection, fiber orientation identification, handling and placement were implemented in 6 degrees of freedom UR 10e with a handling tool inspired by tapes. The results indicate that the developed system is capable of performing a complete fiber plies lay-up process.

6.4.2 Machine Vision System Accuracy Evaluation

To measure the accuracy of the machine vision algorithms in the real world, additional experiments were conducted.

The first experiment was used to quantify the errors in the measured position of the mobile robot using the vision-based localization algorithm and wheel odometry. The setup for the experiment is shown in Fig. 6.5, where the camera and spotlight are mounted on the end-effector of the KUKA robot positioned above the Turtlebot3 Burger platform. The mobile robot was driven autonomously to a randomly generated goal within the workspace of the manipulator and the wheel odometry-based position reading was obtained. The fixed-base manipulator was then manually controlled to align the end-effector directly above the centroid of the composite material. The feedback position information of the end-effector was obtained from the KUKA controller and used as the ground truth in this experiment. Finally, the vision-based estimate of the material position was obtained by applying the localization algorithm with both robots fixed. This experiment was conducted 20 times for statistical significance. For this reason, the mobile robot drove autonomously to a randomly generated goal within the workspace of the manipulator, of which the travelled distances were different each time. The average travelled distance of the mobile robot was 340.9mm. Table 6.1 reports the MAE and RMSE for both wheel odometry estimation and vision-based estimation relative to the ground truth. It was found that the MAE and RMSE for wheel odometry was 19.88 mm and 24.72 mm, respectively. This was much larger

than the MAE and RMSE for vision-based localization, which was 4.04 mm and 4.75 mm respectively. Evidently, machine vision reduced the wheel odometry-based error by 80%, which significantly improves the accuracy for localization when used in conjunction with wheel odometry.

The systematic lay-up accuracy is quantified by measuring the deviation between the placement center and fiber plies. This work uses a single ArUco vision marker for material localization. As long as the centre of the fabric is fixed, this localization approach is suitable for handling different sizes and shapes of fabric patches which is shown in Fig. 6.8. Here, the RMSE of (i) and (ii) are obtained with little difference, which are 5.10 mm and 5.48 mm respectively.

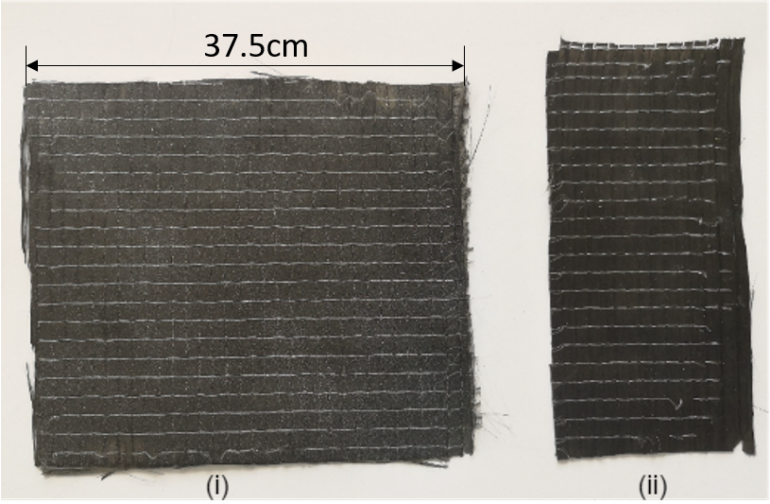

Fig. 6.8. Different size and shape of fabric patches.

Additionally, an experiment was conducted to quantify the accuracy of machine vision for fiber orientation detection. Like the first experiment, a camera and flashlight were mounted on the end-effector of the robotic manipulator. A sample piece of composite material was placed in a fixed position in the workspace of the manipulator while the end-effector was positioned directly above the centre of the material with their rotation axes aligned at 0°. The orientation of the end-effector about the z-axis was incrementally increased by 10° within the range of [0°, 180°].

At each interval the fiber orientation detection algorithm was used to measure the orientation angle of the fiber relative to the camera, which should coincide with the rotation angle of the end-effector under ideal conditions. Thus the measured angle was compared against the end-effector rotation, used as the ground truth, to compute the MAE and RMSE. Moreover, fiber orientation detection accuracy under three different light conditions (no flash light, low flash light, high flash light) were investigated. Fiber orientation readings shown in Fig. 6.9 reveal that the identification is more accurate with stronger flash light. The MAE and RMSE for fiber orientation detection were shown in Table 6.1. Furthermore, manual lay-up was tested by picking and placing the same materials under the same conditions. Table 6.1 shows the accuracy of the developed Co-MRMS and manual system in lay-up. The placement accuracy differs by 1 mm approximately.

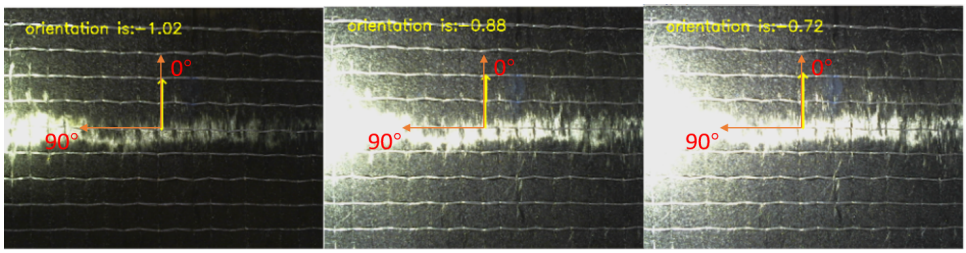

Fig. 6.9. Fiber orientation readings under different light conditions.

Table 6.1: Material localization and fiber orientation detection error.

		MAE	RMSE
Material localization	Wheel odometry/mm	19.88	24.72
	Vision/mm	4.04	4.75
	Manual system/mm	3.08	3.67
Fiber orientation detection	Vision (high flash light)/degree	5.11	5.73
	Vision (low flash light)/degree	5.91	6.70
	Vision (no flash light)/degree	6.59	7.12
	Manual system/degree	2.09	2.61

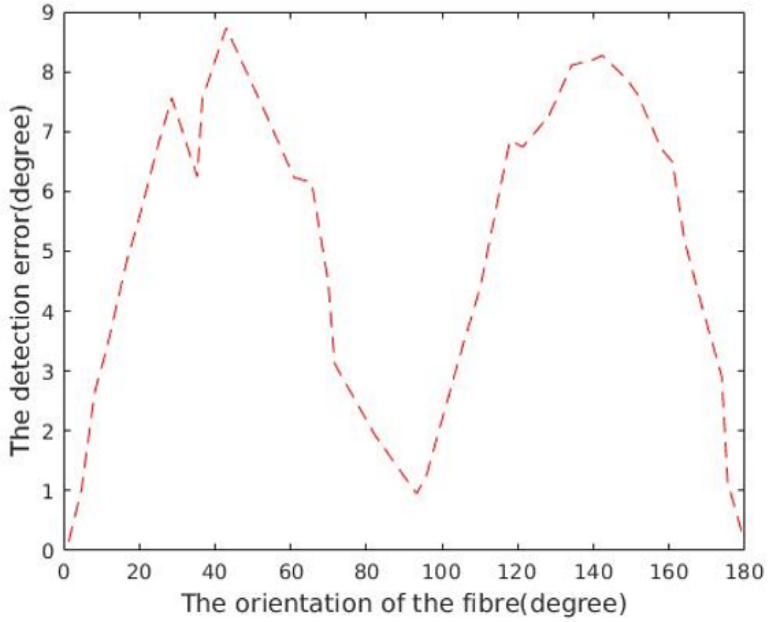

Fig. 6.10. Vision detection error varies with fiber orientation angle.

Furthermore, the error in fiber orientation detection in the real world was greater than the simulation results as the composite material was modelled as a non-rigid body, of which the optical features (high specular reflectivity and high absorption of light) of the material were not simulated and the illumination environment in the real world is far more challenging than the simulated environment. Moreover, the alignment between the camera and the normal of the material was not exact in the physical setup, which introduces additional projection errors when detecting the orientation of the fiber as shown in Fig. 6.10. The investigation shows that the closer the true fiber orientation is to 0°, the higher the accuracy in fiber orientation detection. This can be overcome by applying a two-step detection strategy as follows. The first step consists of computing an approximate rotation angle for the end-effector to roughly align the camera with the fiber orientation which corresponds to the zero degrees region. Subsequently, a finer tuning on the end-effector rotation is performed by applying a second in-

stance of the fiber orientation detection algorithm, which produces an estimate for the fiber orientation angle with minimal error.

The strategy was evaluated in physical experiments. As expected, the performance yielded greater accuracy in fiber orientation detection. The error of the vision system was reduced to 0.23 degrees approximately. In comparison, the detection error was around or below 1 degree by the derived fiber reflection model in [219] and the frequency domain machine vision algorithm in [220] showed around 5 degrees error for braid angle measurement. This indicated that the proposed machine vision system with a two-step strategy can achieve high accuracy in fiber orientation detection. In addition, the systematic error is approximately 1.84 degrees due to the nonalignment between the camera and fiber orientation and is lower than the manual system's 2.61 degrees. Nevertheless, the system is capable of meeting the high accuracy orientation detection requirements in composite material manufacturing.

6.5 Summary

In this chapter, the overall framework of the proposed Co-MRMS research has been presented and introduced. Three modules, which are visual-based SLAM for autonomous transporting, multi-sensor fusion positioning for mobile robot identification and a prototyping Co-MRMS for performance validation, have been included in the framework. Since multi-sensor fusion positioning and visual-based SLAM have been investigated in Chapter 4 and Chapter 5 respectively, this chapter addresses the validation of cooperative and handling behaviors of proposed Co-MRMS. Therefore, a prototype of the proposed Co-MRMS, which comprised of a fixed-base manipulator, an autonomous mobile robot and a sensing sub-system, has been developed for validation. Through a case study of

autonomous material transfer and handling in advanced composite manufacturing, the feasibility and handling ability of the proposed Co-MRMS have been verified. Additionally, the experimental results also verify that the prototype of the proposed Co-MRMS can achieve high accuracy in localization (the root mean squared error is 4.04 mm) and fiber orientation detection (the root mean squared error is 1.84 degrees) and enable dealing with uncertainties such as the shape and size of fiber plies.

Chapter 7

Discussion, Conclusion and Recommendations for Future Work

Owing to the fast growing deployment of modern robotics in recent decades, a great deal of new challenges to the advancement of robotic techniques have been arising. As manufacturing has developed rapidly over the decades, there has been a great drive for the development of advanced robotic systems to cope with changeable manufacturing environments. Greater emphasis on flexible and autonomous robotic systems has been placed for both safety and productivity reasons. Although robotic systems have been extensively researched and the research has led to a great boost in manufacturing efficiency, there is still much to be improved in terms of system autonomy and flexibility.

In this chapter, the research findings from each chapter are discussed collectively in the broader context of robotic systems. Then, the contributions to knowledge presented in this thesis are summarised. Finally, the limitations of the proposed system and relevant applied methods are discussed and views on the

future perspectives based on this research are presented.

7.1 Key Research Findings

This thesis has presented investigations on a Co-MRMS that is composed of both a mobile robot and a fixed-base robotic manipulator for manufacturing applications. During the study process, a number of research findings have been obtained as well as the literature review in Chapter 2. The four research questions introduced in Section 1.2.2, which had initially set out to address in this research, are reviewed here to respond to the original aim of this research.

1 What is the current situation of using cooperative robotic manipulators and mobile robot systems in advanced manufacturing?

In Chapter 2, it is observed that despite advanced manufacturing has deployed different forms of robotic systems, the flexibility and fast adaptability to rapidly changing manufacturing environment are still insufficient. Robotic manipulators and mobile robots are robots commonly used in advanced manufacturing. Cooperative robotic manipulator and mobile robot system, generally refer to a single robotic system, namely mobile manipulator, where the robotic manipulator is mounted on the mobile robot and these two distinct robots are coupled as a whole. To date, mobile manipulators have been substantially investigated and widely used in industry but the tasks performed by this system are limited due to the light load of robots.

In advanced manufacturing, there are a large number of robotic manipulators in manufacturing, consisting of multi-linked manipulators and end-effectors, which are statically attached to a fixed surface and continuously repeat a delicately predefined sequence of actions without changes for decades. Mobile robots are used as intermediates to supply the materials for the fixed-base robotic manipulator.

In this case, the fixed-base robotic manipulator and the mobile robot can be regarded as a whole cooperative robotic manipulator and mobile robot system, where two robots are loosely coupled in the same robotic framework. This form of Co-MRMS has received little attention, lacking sufficient investigations.

Additionally, these two distinct robots are generally taken as independent units with little interaction, hampering the autonomy and flexibility of production in manufacturing. The interaction mode of the Co-MRMS that contains a fixed-base robotic manipulator and a mobile robot, and the information of mobile robots obtained through sensing technologies have been studied in Chapter 4 for operations.

Furthermore, the cooperative robotic manipulator and mobile robot system is traditionally deployed in fixed, structured environments with a weak ability to deal with challenging environments. SLAM enables the robotic system to map the environment dynamically and localise itself simultaneously, which is investigated in Chapter 5 to enhance the autonomy and flexibility of the robotic system.

2 How to use the cooperative fixed-base robotic manipulator and mobile robot system to realize both autonomous material transport and flexible handling?

Looking at the current state-of-the-art, material transport and flexible handling are two separate tasks and are usually operated by independent robotic systems without correlation. Hence, to realise both autonomous material transport and flexible handling in a single robotic system, a mobile robot that is responsible for material transport and a fixed-base robotic manipulator that is responsible for material handling, are the basic components of an integrated robotic system. In Chapter 2, the framework of a typical cooperative robotic manipulator and mobile robot system, namely mobile manipulator, has been presented with covering the fundamental hardware and software modules. Founded on this, the proposed Co-MRMS, which comprised of a fixed-base manipulator and a mobile

robot, is presented and validated through simulation-based experiments in Chapter 3. For this research, composite material manufacture is chosen as the case study for investigation. The procedures using the proposed Co-MRMS system for composite material transport and handling can be divided into several phases. Firstly, the mobile robot carrying material is driven autonomously by the planning algorithm to the scope of a fixed-base robotic manipulator. Then, aided by the sensing system, the fixed-base robotic manipulator accurately identifies the location of material for handling and fiber orientation for lay-up. Following this, the fixed-base robotic manipulator with a designed handling mechanism handles the composite material and completes the process of lay-up. The physical experiments that demonstrate the feasibility and efficiency of the integrated robotic system, are displayed in Chapter 5.

3 How to achieve accurate and robust positioning in the proposed Co-MRMS?

Assisted by various sensing technologies, the fixed-base robotic manipulator can obtain the positions of the mobile robot, thereby prompting the interaction between two robots. That is, in the proposed Co-MRMS, accurately and robustly positioning the mobile robot by the fixed-base robotic manipulator is critical for achieving the interaction. Until now, single sensor positioning methods that used single sensor and multi-sensor fusion positioning methods that used multiple sensors, have been extensively investigated.

Owing to the rapid development of machine vision techniques, visual-based system using cameras has been developed as a promising solution for various industrial applications, as well as robot positioning [166]. For example, in the case study of material transport and flexible handling in advanced composite manufacturing that was introduced in Chapter 3 and Chapter 5, vision systems are indispensable to performing optimum fiber orientation identification, material localization and quality monitoring. In [221], a camera was mounted on the end-

effector of a robotic manipulator to effectively localise and handle raw material while an external camera was adopted to monitor the draping quality. Nevertheless, vision systems have not been well integrated with robotic systems in advanced composite manufacturing, which demands high accuracy and real-time processing capabilities.

Recall in Chapter 3 the machine vision sub-system is involved in the proposed Co-MRMS. The conducted simulation tests validated that material localization can be drastically reduced by using machine vision to correct odometry errors. The fiber orientation can be accurately estimated as well. In addition, visual-based positioning system can provide accurate and reliable information of the mobile robot through the artificial marker ArUco. However, compared with the single sensor positioning methods, multi-sensor fusion positioning methods can improve the robustness of positioning greatly by collecting and fusing the environmental information from different types of sensors. Considering the case that the visual-based positioning is disabled, IMU and ultrasonic sensors are included as complementary sensors and the multi-sensor positioning method EKF is used for sensor fusion. This design allows for seamless sensor suite switching. Experimental results in Chapter 4 showed that the positioning approach is capable of accurately obtaining the positions of the mobile robot, yet is able to continually and robustly maintain a high quality positioning solution even in the case when the vision sensor is disabled.

4 How can the proposed Co-MRMS transports the material in a fast-changing environment?

Conventionally, in the manufacturing industry, mobile robots are deployed in a stable and controlled environment and driven along the predefined path for material transport. In this case, the working environment is required to remain static and unchanged over time. However, to adapt to the rapid development and

changing environment in manufacturing, robots are required to not only work in a stable environment but also enable to adapt to the complex, uncertain, dynamic and unstructured environment, which is identified as autonomy as well as one of the important objectives that Industry 4.0 pursue.

Without the intrinsic information provided by the controlled environment, achieving autonomous transport is difficult. Existing techniques in literature have already demonstrated the employment of SLAM to overcome such problems. For example, Campos et al. [125] showed that ORB-SLAM3 greatly exceeds other existing systems and the system allows for both visual and visual-inertial operation modes with different visual sensors such as RGB-D cameras and stereo. However, this required high-quality captured images for feature point extraction and distorted captured images may cause a failure of the tracking. For instance, motion blur degrades the quality of the image and impacts the feature point extraction, which might cause the insufficiency of feature points and inaccuracy of the pose estimation of visual SLAM. Adding an image pre-processing module before the tracking thread of the SLAM module can improve the image quality and thus enhance the performance of the SLAM system. This concept of image pre-processing is adopted in Chapter 6 and focuses on the image deblurring such that the accuracy was refined as the effect of a blurred image can be reduced. Thus, the proposed image pre-processing module can be combined with the SLAM system and used for autonomous material transport by mobile robots in dynamic and incompletely controlled environments.

7.2 Contributions to Knowledge

In this section, a number of developments that advance the state-of-the-art in Co-MRMS within manufacturing environment are presented. In the following,

the major contributions to knowledge of this thesis are summarised.

Limitations of Co-MRMS in manufacturing: A literature review of existing research in the area of robotic systems within the context of manufacturing has been presented, covering the fundamental system framework of cooperative robotic manipulator and mobile robot system, and the state-of-the-art in methods of robotic positioning and SLAM. The knowledge gaps have been discussed thoroughly based on an analysis of the literature and the limitations of the reviewed work have been identified.

Novel Co-MRMS: A Co-MRMS, which is basically comprised of a fixed-base manipulator and an autonomous mobile robot has been proposed, and a prototype has been built up for material transport and handling tasks. The system has been verified on a case study of material transport and lay-up in advanced composite manufacturing. To enable the system to work, a machine vision system integrated with the robots for accurate material detection, localization and fiber orientation identification has also been developed. Through the simulation-based and physical experimental results, the efficient interaction and high performance of the proposed Co-MRMS for autonomous material transportation, material localization, fiber orientation detection and grasping of deformable material have been demonstrated. Thereinto, the presented machine vision approach can achieve high accuracy in localization (the root mean squared error is 4.04 mm) and fiber orientation detection (the root mean squared error is 1.84 degrees) and enable dealing with uncertainties such as the shape and size of fiber plies.

Flexible interaction mode for the proposed Co-MRMS: The interaction mode between a fixed-base robotic manipulator and a mobile robot has been designed for flexible and efficient part-feeding. The robotic manipulator responds quickly to the mobile robot, rather than waiting for the mobile robot to stop at the predefined position, enhancing the efficiency and flexibility of part-feeding.

Multi-sensor fusion positioning system for the proposed Co-MRMS: The positioning framework for the fixed-base robotic manipulator perceiving the positions of the mobile robot has been designed for the interaction between two agents. A positioning system contains two different kinds of localization approaches which are ultrasonic sensors fused with IMU by filtered EKF algorithm and vision-based method by camera identifying ArUco marker, has been proposed. Taking into consideration that the visual sensor fails, the two positioning methods are allowed to switch seamlessly as a repositioning strategy.

Efficient image pre-processing module for SLAM: An efficient image deblurring framework against the problem of blurred images has been introduced for enhancing the performance of the SLAM system which is used for the autonomous navigation of mobile robots in dynamic environments. Before the feature points extraction in the tracking thread of SLAM, the captured images are processed based on a set of algorithms including Laplacian-based blur detection, image sharpening and Wiener filter-based image deblurring.

7.3 Limitations

In this work, a wide range of considerations of the proposed Co-MRMS have been covered. Nevertheless, as is shown in the literature review of the state-of-the-art in Chapter 2, the Co-MRMS involves multiple modules and achieving autonomous control for manufacturing tasks is a hard problem. Although a number of developments have been presented in this thesis, there are still several limitations that have not been addressed in the range of this research.

Chapter 3 and Chapter 5 used the educational mobile robot platform Turtlebot 3 Burger rather than an industrial standard mobile robot for the conducted investigations. This meant experiments and evaluations were limited to small-scale

setups due to the small size of the Turtlebot3 platform. Additionally, it should be noted that the trials in Chapter 5 incorporate the manipulation actions for grasping the material in physical trials with tapes rather than vacuum suction hardware. Nevertheless, in both the simulation-based and physical experiments, autonomous material transportation, localization, fiber orientation detection and handling capabilities were achieved. However, additional development work is necessary to implement the proposed system framework onto an industrial standard set of hardware to validate the proposed system.

7.4 Future Perspectives Based on Co-MRMS

This work investigated the challenges of addressing inflexible robotic systems in manufacturing environment and developed a novel Co-MRMS that can adapt to multiple tasks while achieving high performance. Until now, the research on the Co-MRMS that involved both a mobile robot and a fixed-base robotic manipulator has remained lacking.

Accordingly, this research developed a number of techniques that advance the state-of-the-art in Co-MRMS within manufacturing environment by demonstrating the feasibility to perform both material transport and handling tasks while remaining high accuracy. Evaluations were conducted thoroughly through a number of simulation-based and physical experiments to quantify and validate the advantages of the proposed robotic system and associated approaches.

This thesis carried out a number of tasks such as material transport and draping within composite manufacturing as the case study to validate the feasibility of the proposed Co-MRMS. However, wrinkles and gaps are commonly generated during the process of composite material draping and are mainly eliminated by human operators. Thus, one interesting research direction for investigation is

the feasibility of developing a method to correct any creases or poor contacts between the composite material and the mould in the composite draping process through the use of the manipulator(s), which can maximise the quality of draping process when performed autonomously using a cooperative robotic system. One potentially viable approach to correcting the defect in draping involves applying hybrid position-force control to achieve both precise movement and consistent pressure on the material surface.

Another interesting avenue to examine is the investigation into the feasibility and potential of non-stopping grasping in the proposed Co-MRMS, where the fixed base robotic manipulator can accurately handle the material on a moving mobile robot. To date, the performance of material supplement by mobile robots has been limited to fixed stoppage positions and stoppage intervals that are predefined for the fixed-base robotic manipulator to handle material, yet the strategy of non-stopping grasping offers the adaptability and flexibility to perform material handling task that will otherwise be impossible to achieve within a changeable and dynamic environment due to the limited interaction between two robots. The dynamics modelling between the mobile robot and fixed-base robotic manipulator can be further derived and combined with the interaction modelling deduced in Chapter 4 to design an adaptive controller for this problem.

In Chapter 5, I have proposed an EID-SLAM system based on ORB-SLAM3 and image deblurring framework to improve the robustness of ORB-SLAM3. However, the adopted blind image deblurring algorithm needs to estimate the PSF first and then implement Wiener filter for image deblurring, which is time-consuming. Therefore, to overcome this drawback, further development is needed.

This thesis has also conducted a preliminary study of a cooperative robotic system that consists of a fixed-base robotic manipulator and a mobile robot. In advanced manufacturing, different parts need to be distributed to the fixed-base

robotic manipulator by multiple mobile robots in some cases such as assembly and disassembly. Consequently, other forms of cooperative robotic systems such as a cooperative robotic system consisting of a fixed-base robotic manipulator and multiple mobile robots are worth studying and the investigations presented in this thesis pave the way for this research direction.

References

[1] Z. Liu, Q. Liu, W. Xu, L. Wang, and Z. Zhou, "Robot learning towards smart robotic manufacturing: A review," *Robotics and Computer-Integrated Manufacturing*, vol. 77, pp. 1–21, 2022.

[2] M. Javaid, A. Haleem, R. P. Singh, and R. Suman, "Substantial capabilities of robotics in enhancing industry 4.0 implementation," *Cognitive Robotics*, vol. 1, pp. 58–75, 2021.

[3] "Execution summary world robotics 2017 industrial robots." International Federation of Robotics, Tech. Rep., 2022.

[4] G. Fragapane, H.-H. Hvolby, F. Sgarbossa, and J. O. Strandhagen, "Autonomous mobile robots in sterile instrument logistics: an evaluation of the material handling system for a strategic fit framework," *Production Planning & Control*, vol. 34, no. 1, pp. 53–67, 2023.

[5] J. Hu, W. Liu, H. Zhang, J. Yi, and Z. Xiong, "Multi-robot object transport motion planning with a deformable sheet," *IEEE Robotics and Automation Letters*, vol. 7, no. 4, pp. 9350–9357, 2022.

[6] D. Johnson, G. Chen, and Y. Lu, "Multi-agent reinforcement learning for real-time dynamic production scheduling in a robot assembly cell," *IEEE Robotics and Automation Letters*, vol. 7, no. 3, pp. 7684–7691, 2022.

[7] J. Arents and M. Greitans, "Smart industrial robot control trends, challenges and opportunities within manufacturing," *Applied Sciences*, vol. 12, no. 2, pp. 937–957, 2022.

[8] B. Wang, F. Tao, X. Fang, C. Liu, Y. Liu, and T. Freiheit, "Smart manufacturing and intelligent manufacturing: A comparative review," *Engineering*, vol. 7, no. 6, pp. 738–757, 2021.

[9] S. Phuyal, D. Bista, and R. Bista, "Challenges, opportunities and future directions of smart manufacturing: a state of art review," *Sustainable Futures*, vol. 2, p. 100023, 2020.

[10] K. Cheng, Z.-C. Niu, R. C. Wang, R. Rakowski, and R. Bateman, "Smart cutting tools and smart machining: development approaches, and their implementation and application perspectives," *Chinese Journal of Mechanical Engineering*, vol. 30, pp. 1162–1176, 2017.

[11] L. Sanneman, C. Fourie, J. A. Shah *et al.*, "The state of industrial robotics: Emerging technologies, challenges, and key research directions," *Foundations and Trends® in Robotics*, vol. 8, no. 3, pp. 225–306, 2021.

[12] A. Cherubini, R. Passama, B. Navarro, M. Sorour, A. Khelloufi, O. Mazhar, S. Tarbouriech, J. Zhu, O. Tempier, A. Crosnier *et al.*, "A collaborative robot for the factory of the future: Bazar," *The International Journal of Advanced Manufacturing Technology*, vol. 105, no. 9, pp. 3643–3659, 2019.

[13] M. Hvilshøj, S. Bøgh, O. Madsen, and M. Kristiansen, "The mobile robot "Little Helper": concepts, ideas and working principles," in *IEEE Conference on Emerging Technologies & Factory Automation*, 2009, pp. 1–4.

[14] K. Zhou, G. Ebenhofer, C. Eitzinger, U. Zimmermann, C. Walter, J. Saenz, L. P. Castaño, M. A. F. Hernández, and J. N. Oriol, "Mobile manipulator is

coming to aerospace manufacturing industry," in *IEEE International Symposium on Robotic and Sensors Environments (ROSE) Proceedings*, 2014, pp. 94–99.

[15] D. Bourne, H. Choset, H. Hu, G. Kantor, C. Niessl, Z. Rubinstein, R. Simmons, and S. Smith, "Mobile manufacturing of large structures," in *IEEE International Conference on Robotics and Automation (ICRA)*, 2015, pp. 1565–1572.

[16] H. N. Ghafil and K. Jármai, "Research and application of industrial robot manipulators in vehicle and automotive engineering, a survey," in *Vehicle and Automotive Engineering 2: Proceedings of the 2nd VAE*, 2018, pp. 611–623.

[17] G. S. Tewolde, C. Wu, Y. Wang, and W. Sheng, "Distributed multi-robot work load partition in manufacturing automation," in *IEEE International Conference on Automation Science and Engineering*, 2008, pp. 504–509.

[18] C. Smith, Y. Karayiannidis, L. Nalpantidis, X. Gratal, P. Qi, D. V. Dimarogonas, and D. Kragic, "Dual arm manipulation—A survey," *Robotics and Autonomous systems*, vol. 60, no. 10, pp. 1340–1353, 2012.

[19] I. Nielsen, Q.-V. Dang, G. Bocewicz, and Z. Banaszak, "A methodology for implementation of mobile robot in adaptive manufacturing environments," *Journal of Intelligent Manufacturing*, vol. 28, pp. 1171–1188, 2017.

[20] C. C. Kemp, A. Edsinger, H. M. Clever, and B. Matulevich, "The design of stretch: A compact, lightweight mobile manipulator for indoor human environments," in *International Conference on Robotics and Automation (ICRA)*, 2022, pp. 3150–3157.

[21] R. Abebe and M. Gopal, "Optimization and simulation of arc welding robot parameters based on offline programming," *Materials Today: Proceedings*, 2023.

[22] W. Chen, G. Shang, A. Ji, C. Zhou, X. Wang, C. Xu, Z. Li, and K. Hu, "An overview on visual slam: From tradition to semantic," *Remote Sensing*, vol. 14, no. 13, pp. 3010–3057, 2022.

[23] J. F. Hair, A. H. Money, P. Samouel, and M. Page, "Research methods for business," *Education+ Training*, vol. 49, no. 4, pp. 336–337, 2007.

[24] M. Easterby-Smith, R. Thorpe, and P. R. Jackson, *Management research*. Sage, 2012.

[25] W. Rowell, "Characterisation of the engineering change management process and relationship with artefact knowledge within the product lifecycle," 2013.

[26] J. Wilson, "Essentials of business research: A guide to doing your research project," *Essentials of business research*, pp. 1–376, 2014.

[27] D. P. Andrew, P. M. Pedersen, and C. D. McEvoy, *Research methods and design in sport management*. Human Kinetics, 2019.

[28] C. Robson, *Real world research*. John Wiley & Sons, 2024.

[29] M. D. Myers, "Qualitative research in business and management," 2019.

[30] C. R. Kothari, *Research methodology: Methods and techniques*. New Age International, 2004.

[31] J. Sturm, N. Engelhard, F. Endres, W. Burgard, and D. Cremers, "A benchmark for the evaluation of rgb-d slam systems," in *IEEE/RSJ International Conference on Intelligent Robots and Systems (IROS)*, 2012, pp. 573–580.

[32] D. Schubert, T. Goll, N. Demmel, V. Usenko, J. Stückler, and D. Cremers, "The tum vi benchmark for evaluating visual-inertial odometry," in *IEEE/RSJ International Conference on Intelligent Robots and Systems (IROS)*, 2018, pp. 1680–1687.

[33] K. Schwab, "The fourth industrial revolution," in *World Economic Forum*, 2017.

[34] P. Osterrieder, L. Budde, and T. Friedli, "The smart factory as a key construct of industry 4.0: A systematic literature review," *International Journal of Production Economics*, vol. 221, p. 107476, 2020.

[35] M. Schneier, M. Schneier, and R. Bostelman, *Literature review of mobile robots for manufacturing*. US Department of Commerce, 2015.

[36] M. Hvilshøj, S. Bøgh, O. Skov Nielsen, and O. Madsen, "Autonomous industrial mobile manipulation (aimm): past, present and future," *Industrial Robot: An International Journal*, vol. 39, no. 2, pp. 120–135, 2012.

[37] C. Eppner, S. Höfer, R. Jonschkowski, R. Martín-Martín, A. Sieverling, V. Wall, and O. Brock, "Lessons from the amazon picking challenge: Four aspects of building robotic systems." in *Robotics: Science and Systems*, 2016, pp. 4831–4835.

[38] G. Michalos, N. Kousi, S. Makris, and G. Chryssolouris, "Performance assessment of production systems with mobile robots," *Procedia CIRP*, vol. 41, pp. 195–200, 2016.

[39] Q. Chang, X. Liu, W. Xu, L. Yan, and B. Yang, "The design and experiments of a small wheel-legged mobile robot system with two robotic arms," in *IEEE/RSJ International Conference on Intelligent Robots and Systems (IROS)*, 2016, pp. 2590–2595.

[40] J. Saenz, C. Vogel, F. Penzlin, and N. Elkmann, "Safeguarding collaborative mobile manipulators-evaluation of the VALERI workspace monitoring system," *Procedia Manufacturing*, vol. 11, pp. 47–54, 2017.

[41] M. Chen, C. Liu, and G. Du, "A human-robot interface for mobile manipulator," *Intelligent Service Robotics*, vol. 11, no. 3, pp. 269–278, 2018.

[42] Y. Xiong, P. J. From, and V. Isler, "Design and evaluation of a novel cable-driven gripper with perception capabilities for strawberry picking robots," in *IEEE International Conference on Robotics and Automation (ICRA)*, 2018, pp. 7384–7391.

[43] T. Kot, M. Mihola, J. Bajak, and P. Novák, "Gripper with precisely adjustable gripping force," in *18th International Carpathian Control Conference (ICCC)*, 2017, pp. 555–559.

[44] S. Hernandez-Mendez, A. Marin-Hernandez, E. R. Palacios-Hernandez, and K. L. Luna-Gallegos, "A switching position/force controller for two independent finger gripper over ROS," in *International Conference on Electronics, Communications and Computers (CONIELECOMP)*, 2017, pp. 1–6.

[45] I. T. Ćirić, Ž. M. Ćojbašić, D. D. Ristić-Durrant, V. D. Nikolić, M. V. Ćirić, M. B. Simonović, and I. R. Pavlović, "Thermal vision based intelligent system for human detection and tracking in mobile robot control system," *Thermal Science*, vol. 20, no. suppl. 5, pp. 1553–1559, 2016.

[46] S. M. Rahman and Y. Wang, "Mutual trust-based subtask allocation for human-robot collaboration in flexible lightweight assembly in manufacturing," *Mechatronics*, vol. 54, pp. 94–109, 2018.

[47] H. Liu, N. Stoll, S. Junginger, J. Zhang, M. Ghandour, and K. Thurow, "Human-Mobile robot interaction in laboratories using Kinect Sensor and

ELM based face feature recognition," in *9th International Conference on Human System Interactions (HSI)*, 2016, pp. 197–202.

[48] J. Bai, S. Lian, Z. Liu, K. Wang, and D. Liu, "Deep learning-based robot for automatically picking up garbage on the grass," *IEEE Transactions on Consumer Electronics*, vol. 64, no. 3, pp. 382–389, 2018.

[49] F. Gao, F. Ma, J. Wang, J. Sun, E. Yang, and H. Zhou, "Visual saliency modeling for river detection in high-resolution SAR imagery," *IEEE Access*, vol. 6, pp. 1000–1014, 2017.

[50] M. Schwarz, D. Droeschel, C. Lenz, A. S. Periyasamy, E. Y. Puang, J. Razlaw, D. Rodriguez, S. Schüller, M. Schreiber, and S. Behnke, "Team NimbRo at MBZIRC 2017: Autonomous valve stem turning using a wrench," *Journal of Field Robotics*, vol. 36, no. 1, pp. 170–182, 2019.

[51] P. Amayo, T. Bruls, and P. Newman, "Semantic classification of road markings from geometric primitives," in *21st International Conference on Intelligent Transportation Systems (ITSC)*, 2018, pp. 387–393.

[52] M. Cefalo and G. Oriolo, "A general framework for task-constrained motion planning with moving obstacles," *Robotica*, vol. 37, no. 3, pp. 575–598, 2019.

[53] F. F. A. Silva and B. V. Adorno, "Whole-body control of a mobile manipulator using feedback linearization based on dual quaternions," in *XIII Latin American Robotics Symposium and IV Brazilian Robotics Symposium (LARS/SBR)*, 2016, pp. 293–298.

[54] Y. He, M. Wu, and S. Liu, "Decentralised cooperative mobile manipulation with adaptive control parameters," in *IEEE Conference on Control Technology and Applications (CCTA)*, 2018, pp. 82–87.

[55] J. Peng, J. Yu, and J. Wang, "Robust adaptive tracking control for nonholonomic mobile manipulator with uncertainties," *ISA transactions*, vol. 53, no. 4, pp. 1035–1043, 2014.

[56] B. Navarro, A. Cherubini, A. Fonte, G. Poisson, and P. Fraisse, "A framework for intuitive collaboration with a mobile manipulator," in *IEEE/RSJ International Conference on Intelligent Robots and Systems (IROS)*, 2017, pp. 6293–6298.

[57] C. Pérez-D'Arpino and J. A. Shah, "Fast target prediction of human reaching motion for cooperative human-robot manipulation tasks using time series classification," in *IEEE International Conference on Robotics and Automation (ICRA)*, 2015, pp. 6175–6182.

[58] A. Cherubini, R. Passama, A. Crosnier, A. Lasnier, and P. Fraisse, "Collaborative manufacturing with physical human-robot interaction," *Robotics and Computer-Integrated Manufacturing*, vol. 40, pp. 1–13, 2016.

[59] O. Madsen, "Robotics-enabled logistics and assistive services for the transformable factory of the future (TAPAS)," 2009.

[60] O. Madsen, S. Bøgh, C. Schou, R. S. Andersen, J. S. Damgaard, M. R. Pedersen, and V. Krüger, "Integration of mobile manipulators in an industrial production," *Industrial Robot: An International Journal*, vol. 42, no. 1, pp. 11–18, 2015.

[61] D. Pavlichenko, G. M. García, S. Koo, and S. Behnke, "Kittingbot: A mobile manipulation robot for collaborative kitting in automotive logistics," in *International Conference on Intelligent Autonomous Systems*, 2018, pp. 849–864.

[62] A. Dömel, S. Kriegel, M. Kaßecker, M. Brucker, T. Bodenmüller, and M. Suppa, "Toward fully autonomous mobile manipulation for industrial

environments," *International Journal of Advanced Robotic Systems*, vol. 14, no. 4, p. 1729881417718588, 2017.

[63] P. J. Koch, M. K. van Amstel, P. Debska, M. A. Thormann, A. J. Tetzlaff, S. Bogh, and D. Chrysostomou, "A skill-based robot co-worker for industrial maintenance tasks," *Procedia Manufacturing*, vol. 11, pp. 83–90, 2017.

[64] P. Štibinger, G. Broughton, F. Majer, Z. Rozsypálek, A. Wang, K. Jindal, A. Zhou, D. Thakur, G. Loianno, T. Krajník *et al.*, "Mobile manipulator for autonomous localization, grasping and precise placement of construction material in a semi-structured environment," *IEEE Robotics and Automation Letters*, vol. 6, no. 2, pp. 2595–2602, 2021.

[65] K. Schmid, F. Ruess, M. Suppa, and D. Burschka, "State estimation for highly dynamic flying systems using key frame odometry with varying time delays," in *IEEE/RSJ International Conference on Intelligent Robots and Systems*, 2012, pp. 2997–3004.

[66] W. Seo and K.-R. Baek, "Indoor dead reckoning localization using ultrasonic anemometer with IMU," *Journal of Sensors*, vol. 2017, 2017.

[67] C. De Farias, M. Adjigble, B. Tamadazte, R. Stolkin, and N. Marturi, "Dual quaternion-based visual servoing for grasping moving objects," in *IEEE 17th International Conference on Automation Science and Engineering (CASE)*, 2021, pp. 151–158.

[68] N. P. Papanikolopoulos, P. K. Khosla, and T. Kanade, "Visual tracking of a moving target by a camera mounted on a robot: A combination of control and vision," *IEEE Transactions on Robotics and Automation*, vol. 9, no. 1, pp. 14–35, 1993.

[69] J. Ding, Z. Yan, and X. We, "High-accuracy recognition and localization of moving targets in an indoor environment using binocular stereo vision,"

ISPRS International Journal of Geo-Information, vol. 10, no. 4, p. 234, 2021.

[70] P. K. Allen, A. Timcenko, B. Yoshimi, and P. Michelman, "Automated tracking and grasping of a moving object with a robotic hand-eye system," *IEEE Transactions on Robotics and Automation*, vol. 9, no. 2, pp. 152–165, 1993.

[71] S. Mane and S. Mangale, "Moving object detection and tracking using convolutional neural networks," in *Second International Conference on Intelligent Computing and Control Systems (ICICCS)*, 2018, pp. 1809–1813.

[72] M. Shahjalal, M. Hossan, M. Hasan, M. Z. Chowdhury, N. T. Le, Y. M. Jang *et al.*, "An implementation approach and performance analysis of image sensor based multilateral indoor localization and navigation system," *Wireless Communications and Mobile Computing*, vol. 2018, 2018.

[73] M. Diop, L. Y. Ong, T. S. Lim, and C. H. Lim, "A computer vision-aided motion sensing algorithm for mobile robot's indoor navigation," in *IEEE 14th International Workshop on Advanced Motion Control (AMC)*, 2016, pp. 400–405.

[74] S. Igarashi, Y. Kaizu, T. Tsutsumi, K. Furuhashi, and K. Imou, "Autonomous driving control of a robotic mower on slopes using a low-cost two-frequency GNSS compass and an IMU," *Journal of the ASABE*, vol. 65, no. 6, pp. 1179–1189, 2022.

[75] A. Rojo, R. Raya, and J. C. Moreno, "Virtual reality application for real-time pedalling cadence estimation based on hip ROM tracking with inertial sensors: a pilot study," *Virtual Reality*, vol. 27, no. 1, pp. 3–17, 2023.

[76] E. Kabuye, P. LeDuc, and J. Cagan, "A mixed reality system combining augmented reality, 3D bio-printed physical environments and inertial measurement unit sensors for task planning," *Virtual Reality*, pp. 1–14, 2023.

[77] G. Santaera, E. Luberto, A. Serio, M. Gabiccini, and A. Bicchi, "Low-cost, fast and accurate reconstruction of robotic and human postures via imu measurements," in *2015 IEEE International Conference on Robotics and Automation (ICRA)*, 2015, pp. 2728–2735.

[78] P. Neto, J. N. Pires, and A. P. Moreira, "3-D position estimation from inertial sensing: Minimizing the error from the process of double integration of accelerations," in *39th Annual Conference of the IEEE Industrial Electronics Society*, 2013, pp. 4026–4031.

[79] H. Hellmers, A. Norrdine, J. Blankenbach, and A. Eichhorn, "An imu/magnetometer-based indoor positioning system using kalman filtering," in *International Conference on Indoor Positioning and Indoor Navigation*, 2013, pp. 1–9.

[80] M. Shen, Y. Wang, Y. Jiang, H. Ji, B. Wang, and Z. Huang, "A new positioning method based on multiple ultrasonic sensors for autonomous mobile robot," *Sensors*, vol. 20, no. 1, p. 17, 2019.

[81] J. Borenstein, H. R. Everett, L. Feng, and D. Wehe, "Mobile robot positioning: Sensors and techniques," *Journal of Robotic Systems*, vol. 14, no. 4, pp. 231–249, 1997.

[82] M. Elsanhoury, P. Mäkelä, J. Koljonen, P. Välisuo, A. Shamsuzzoha, T. Mantere, M. Elmusrati, and H. Kuusniemi, "Precision positioning for smart logistics using ultra-wideband technology-based indoor navigation: A review," *IEEE Access*, vol. 10, pp. 44 413–44 445, 2022.

[83] H. Nomura and T. Naito, "Integrated visual servoing system to grasp industrial parts moving on conveyer by controlling 6DOF arm," in *IEEE International Conference on Systems, Man and Cybernetics,*, vol. 3, 2000, pp. 1768–1775.

[84] F. Ebner, T. Fetzer, F. Deinzer, L. Köping, and M. Grzegorzek, "Multi sensor 3D indoor localisation," in *International Conference on Indoor Positioning and Indoor Navigation (IPIN)*, 2015, pp. 1–11.

[85] Y. Xu, H. Yu, and J. Zhang, "Fusion of inertial and visual information for indoor localisation," *Electronics Letters*, vol. 54, no. 13, pp. 850–851, 2018.

[86] M. Kozłowski, R. Santos-Rodriguez, and R. Piechocki, "Sensor modalities and fusion for robust indoor localisation," *EAI Endorsed Transactions on Ambient Systems*, vol. 6, no. 18, 2019.

[87] Y. Dobrev, S. Flores, and M. Vossiek, "Multi-modal sensor fusion for indoor mobile robot pose estimation," in *IEEE/ION Position, Location and Navigation Symposium (PLANS)*, 2016, pp. 553–556.

[88] M. B. Alatise and G. P. Hancke, "Pose estimation of a mobile robot based on fusion of IMU data and vision data using an extended Kalman filter," *Sensors*, vol. 17, no. 10, p. 2164, 2017.

[89] X. Chen, Y. Xu, Q. Li, J. Tang, and C. Shen, "Improving ultrasonic-based seamless navigation for indoor mobile robots utilizing EKF and LS-SVM," *Measurement*, vol. 92, pp. 243–251, 2016.

[90] F. O. Coelho, J. P. Carvalho, M. F. Pinto, and A. L. Marcato, "EKF and computer vision for mobile robot localization," in *13th APCA International Conference on Automatic Control and Soft Computing (CONTROLO)*, 2018, pp. 148–153.

[91] H. Gao, X. Zhang, C. Li, X. Chen, Y. Fang, and X. Chen, "Directional endpoint-based enhanced EKF-SLAM for indoor mobile robots," in *IEEE/ASME International Conference on Advanced Intelligent Mechatronics (AIM)*, 2019, pp. 978–983.

[92] O. Kaltiokallio, R. Hostettler, N. Patwari, and R. Jäntti, "Recursive Bayesian filters for RSS-based device-free localization and tracking," in *International Conference on Indoor Positioning and Indoor Navigation (IPIN)*, 2018, pp. 1–8.

[93] C. Smaili, M. E. El Najjar, and F. Charpillet, "Multi-sensor fusion method using dynamic Bayesian network for precise vehicle localization and road matching," in *19th IEEE International Conference on Tools with Artificial Intelligence*, vol. 1, 2007, pp. 146–151.

[94] L. Rabiner and B.-H. Juang, "Fundamentals of speech processing," 1993.

[95] X. He, D. N. Aloi, and J. Li, "Probabilistic multi-sensor fusion based indoor positioning system on a mobile device," *Sensors*, vol. 15, no. 12, pp. 31 464–31 481, 2015.

[96] N. Yang, W. F. Tian, Z. H. Jin, and C. B. Zhang, "Particle filter for sensor fusion in a land vehicle navigation system," *Measurement science and technology*, vol. 16, no. 3, p. 677, 2005.

[97] M. Pham, D. Yang, and W. Sheng, "A sensor fusion approach to indoor human localization based on environmental and wearable sensors," *IEEE Transactions on Automation Science and Engineering*, vol. 16, no. 1, pp. 339–350, 2018.

[98] P. Wei, L. Cagle, T. Reza, J. Ball, and J. Gafford, "LiDAR and camera detection fusion in a real-time industrial multi-sensor collision avoidance system," *Electronics*, vol. 7, no. 6, p. 84, 2018.

[99] B. Hua, D. Hossain, G. Capi, M. Jindai, and I. Yoshida, "Human-like artificial intelligent wheelchair robot navigated by multi-sensor models in indoor environments and error analysis," *Procedia Computer Science*, vol. 105, pp. 14–19, 2017.

[100] L. Vargas-Meléndez, B. L. Boada, M. J. L. Boada, A. Gauchía, and V. Díaz, "A sensor fusion method based on an integrated neural network and Kalman filter for vehicle roll angle estimation," *Sensors*, vol. 16, no. 9, p. 1400, 2016.

[101] X. Wang, L. Gao, S. Mao, and S. Pandey, "CSI-based fingerprinting for indoor localization: A deep learning approach," *IEEE Transactions on Vehicular Technology*, vol. 66, no. 1, pp. 763–776, 2016.

[102] F. Jamil, N. Iqbal, S. Ahmad, and D.-H. Kim, "Toward accurate position estimation using learning to prediction algorithm in indoor navigation," *Sensors*, vol. 20, no. 16, p. 4410, 2020.

[103] K. Hausman, S. Weiss, R. Brockers, L. Matthies, and G. S. Sukhatme, "Self-calibrating multi-sensor fusion with probabilistic measurement validation for seamless sensor switching on a UAV," in *IEEE International Conference on Robotics and Automation (ICRA)*, 2016, pp. 4289–4296.

[104] A. I. Mourikis and S. I. Roumeliotis, "A multi-state constraint Kalman filter for vision-aided inertial navigation," in *Proceedings of the IEEE International Conference on Robotics and Automation*, 2007, pp. 3565–3572.

[105] S. Lynen, M. W. Achtelik, S. Weiss, M. Chli, and R. Siegwart, "A robust and modular multi-sensor fusion approach applied to MAV navigation," in *IEEE/RSJ International Conference on Intelligent Robots and Systems*, 2013, pp. 3923–3929.

[106] S. Leutenegger and R. Y. Siegwart, "A low-cost and fail-safe inertial navigation system for airplanes," in *IEEE International Conference on Robotics and Automation*, 2012, pp. 612–618.

[107] A. Lampe and R. Chatila, "Performance measure for the evaluation of mobile robot autonomy," in *IEEE International Conference on Robotics and Automation*, 2006, pp. 4057–4062.

[108] R. Chai, H. Niu, J. Carrasco, F. Arvin, H. Yin, and B. Lennox, "Design and experimental validation of deep reinforcement learning-based fast trajectory planning and control for mobile robot in unknown environment," *IEEE Transactions on Neural Networks and Learning Systems*, 2022.

[109] R. Raj and A. Kos, "A comprehensive study of mobile robot: history, developments, applications, and future research perspectives," *Applied Sciences*, vol. 12, no. 14, p. 6951, 2022.

[110] J. J. Leonard and H. F. Durrant-Whyte, "Simultaneous map building and localization for an autonomous mobile robot." in *IEEE/RSJ International Conference on Intelligent Robots and Systems (IROS)*, vol. 3, 1991, pp. 1442–1447.

[111] R. C. Smith and P. Cheeseman, "On the representation and estimation of spatial uncertainty," *The International Journal of Robotics Research*, vol. 5, no. 4, pp. 56–68, 1986.

[112] D. Cole and P. Newman, "Using laser range data for 3D SLAM in outdoor environments," in *IEEE International Conference on Robotics and Automation*, 2006, pp. 1556–1563.

[113] L. Kleeman, "Advanced sonar and odometry error modeling for simultaneous localisation and map building," in *IEEE/RSJ International Conference on Intelligent Robots and Systems*, vol. 1, 2003, pp. 699–704.

[114] J. Cheng, L. Zhang, Q. Chen, X. Hu, and J. Cai, "A review of visual SLAM methods for autonomous driving vehicles," *Engineering Applications of Artificial Intelligence*, vol. 114, p. 104992, 2022.

[115] A. J. Davison, I. D. Reid, N. D. Molton, and O. Stasse, "MonoSLAM: Real-time single camera SLAM," *IEEE Transactions on Pattern Analysis and Machine Intelligence*, vol. 29, no. 6, pp. 1052–1067, 2007.

[116] J. Shi *et al.*, "Good features to track," in *Proceedings of IEEE Conference on Computer Vision and Pattern Recognition*, 1994, pp. 593–600.

[117] R. A. Newcombe, S. J. Lovegrove, and A. J. Davison, "DTAM: Dense tracking and mapping in real-time," in *International Conference on Computer Vision*, 2011, pp. 2320–2327.

[118] R. Mur-Artal, J. M. M. Montiel, and J. D. Tardos, "ORB-SLAM: a versatile and accurate monocular SLAM system," *IEEE Transactions on Robotics*, vol. 31, no. 5, pp. 1147–1163, 2015.

[119] R. Mur-Artal and J. D. Tardós, "ORB-SLAM2: An Open-Source SLAM System for Monocular, Stereo, and RGB-D Cameras," *IEEE Transactions on Robotics*, vol. 33, no. 5, pp. 1255–1262, 2017.

[120] P. Henry, M. Krainin, E. Herbst, X. Ren, and D. Fox, "RGB-D mapping: Using Kinect-style depth cameras for dense 3D modeling of indoor environments," *The International Journal of Robotics Research*, vol. 31, no. 5, pp. 647–663, 2012.

[121] F. Endres, J. Hess, N. Engelhard, J. Sturm, D. Cremers, and W. Burgard, "An evaluation of the RGB-D SLAM system," in *IEEE International Conference on Robotics and Automation*, 2012, pp. 1691–1696.

[122] T. Qin, P. Li, and S. Shen, "Vins-mono: A robust and versatile monocular visual-inertial state estimator," *IEEE Transactions on Robotics*, vol. 34, no. 4, pp. 1004–1020, 2018.

[123] M. Bloesch, S. Omari, M. Hutter, and R. Siegwart, "Robust visual inertial odometry using a direct EKF-based approach," in *IEEE/RSJ International Conference on Intelligent Robots and Systems (IROS)*, 2015, pp. 298–304.

[124] R. Mur-Artal and J. D. Tardós, "Visual-inertial monocular SLAM with map reuse," *IEEE Robotics and Automation Letters*, vol. 2, no. 2, pp. 796–803, 2017.

[125] C. Campos, R. Elvira, J. J. G. Rodríguez, J. M. Montiel, and J. D. Tardós, "ORB-SLAM3: An Accurate Open-Source Library for Visual, Visual–Inertial, and Multimap SLAM," *IEEE Transactions on Robotics*, vol. 37, no. 6, pp. 1874–1890, 2021.

[126] O. Seiskari, P. Rantalankila, J. Kannala, J. Ylilammi, E. Rahtu, and A. Solin, "HybVIO: Pushing the Limits of Real-time Visual-inertial Odometry," in *Proceedings of the IEEE/CVF Winter Conference on Applications of Computer Vision*, 2022, pp. 701–710.

[127] A. Merzlyakov and S. Macenski, "A comparison of modern general-purpose visual slam approaches," in *IEEE/RSJ International Conference on Intelligent Robots and Systems (IROS)*, 2021, pp. 9190–9197.

[128] P. Satish, M. Srikantaswamy, and N. K. Ramaswamy, "A comprehensive review of blind deconvolution techniques for image deblurring." *Traitement du Signal*, vol. 37, no. 3, 2020.

[129] S. H. Umale and A. M. Sahu, "A review on various techniques for image debluring," *International Journal of Computer Science and Mobile Computing*, vol. 3, no. 4, pp. 263–268, 2014.

[130] K. Zhang, W. Ren, W. Luo, W.-S. Lai, B. Stenger, M.-H. Yang, and H. Li, "Deep image deblurring: A survey," *International Journal of Computer Vision*, vol. 130, no. 9, pp. 2103–2130, 2022.

[131] P. Liu, X. Zuo, V. Larsson, and M. Pollefeys, "MBA-VO: Motion blur aware visual odometry," in *Proceedings of the IEEE/CVF International Conference on Computer Vision*, 2021, pp. 5550–5559.

[132] Y. Zhang, C. Wang, S. J. Maybank, and D. Tao, "Exposure trajectory recovery from motion blur," *IEEE Transactions on Pattern Analysis and Machine Intelligence*, vol. 44, no. 11, pp. 7490–7504, 2021.

[133] S. Yadav, C. Jain, and A. Chugh, "Evaluation of image deblurring techniques," *International Journal of Computer Applications*, vol. 139, no. 12, pp. 32–36, 2016.

[134] N. Wiener, N. Wiener, C. Mathematician, N. Wiener, N. Wiener, and C. Mathématicien, *Extrapolation, interpolation, and smoothing of stationary time series: with engineering applications*. MIT press Cambridge, MA, 1949.

[135] W. H. Richardson, "Bayesian-based iterative method of image restoration," *JoSA*, vol. 62, no. 1, pp. 55–59, 1972.

[136] L. B. Lucy, "An iterative technique for the rectification of observed distributions," *The Astronomical Journal*, vol. 79, p. 745, 1974.

[137] J.-J. Ding, W.-D. Chang, Y. Chen, S.-W. Fu, C.-W. Chang, and C.-C. Chang, "Image deblurring using a pyramid-based Richardson-Lucy algorithm," in *19th International Conference on Digital Signal Processing*, 2014, pp. 204–209.

[138] X. Y. Qi, L. Zhang, and C. L. Tan, "Motion deblurring for optical character recognition," in *Eighth International Conference on Document Analysis and Recognition (ICDAR'05)*, 2005, pp. 389–393.

[139] I. Rekleitis, "Visual motion estimation based on motion blur interpretation," 1995.

[140] I. Goodfellow, J. Pouget-Abadie, M. Mirza, B. Xu, D. Warde-Farley, S. Ozair, A. Courville, and Y. Bengio, "Generative adversarial nets," *Advances in Neural Information Processing Systems*, vol. 27, 2014.

[141] O. Kupyn, V. Budzan, M. Mykhailych, D. Mishkin, and J. Matas, "DeblurGAN: blind motion deblurring using conditional adversarial networks," in *Proceedings of the IEEE Conference on Computer Vision and Pattern Recognition (CVPR)*, June 2018.

[142] O. Kupyn, T. Martyniuk, J. Wu, and Z. Wang, "Deblurgan-v2: Deblurring (orders-of-magnitude) faster and better," in *Proceedings of the IEEE/CVF International Conference on Computer Vision*, 2019, pp. 8878–8887.

[143] X. Tao, H. Gao, X. Shen, J. Wang, and J. Jia, "Scale-recurrent network for deep image deblurring," in *Proceedings of the IEEE Conference on Computer Vision and Pattern Recognition*, 2018, pp. 8174–8182.

[144] S. Park, T. Schöps, and M. Pollefeys, "Illumination change robustness in direct visual slam," in *IEEE International Conference on Robotics and Automation (ICRA)*, 2017, pp. 4523–4530.

[145] O. Roesler and V. P. Ravindranath, "Evaluation of slam algorithms for highly dynamic environments," in *Fourth Iberian Robotics Conference: Advances in Robotics, Volume 2*, 2020, pp. 28–36.

[146] M. Bujanca, X. Shi, M. Spear, P. Zhao, B. Lennox, and M. Luján, "Robust SLAM systems: Are we there yet?" in *IEEE/RSJ International Conference on Intelligent Robots and Systems (IROS)*, 2021, pp. 5320–5327.

[147] J. Guo, R. Ni, and Y. Zhao, "DeblurSLAM: A novel visual SLAM system robust in blurring scene," in *IEEE 7th International Conference on Virtual Reality (ICVR)*, 2021, pp. 62–68.

[148] K. Luo, M. Lin, P. Wang, S. Zhou, D. Yin, and H. Zhang, "Improved orb-slam2 algorithm based on information entropy and image sharpening adjustment," *Mathematical Problems in Engineering*, vol. 2020, pp. 1–13, 2020.

[149] J. Mustaniemi, J. Kannala, S. Särkkä, J. Matas, and J. Heikkilä, "Fast motion deblurring for feature detection and matching using inertial measurements," in *24th International Conference on Pattern Recognition (ICPR)*, 2018, pp. 3068–3073.

[150] K. Yamaguchi and K. Inaba, "Intelligent and collaborative robots," in *Springer Handbook of Automation*. Springer, 2023, pp. 335–356.

[151] S. Bøgh, M. Hvilshøj, M. Kristiansen, and O. Madsen, "Identifying and evaluating suitable tasks for autonomous industrial mobile manipulators (AIMM)," *The International Journal of Advanced Manufacturing Technology*, vol. 61, no. 5, pp. 713–726, 2012.

[152] M. Fathi, V. Rodríguez, D. B. Fontes, and M. J. Alvarez, "A modified particle swarm optimisation algorithm to solve the part feeding problem at assembly lines," *International Journal of Production Research*, vol. 54, no. 3, pp. 878–893, 2016.

[153] R. Christensen, "Mechanics of composite materials. Courier Corporation," *Massachusetts: USA*, 2012.

[154] S. V. Hoa, *Principles of the manufacturing of composite materials*. DEStech Publications, Inc, 2009.

[155] D. J. Higham and N. J. Higham, *MATLAB guide*. SIAM, 2016.

[156] G. Bradski and A. Kaehler, "OpenCV," *Dr. Dobb's Journal of Software Tools*, vol. 3, 2000.

[157] C. Wong, E. Yang, X.-T. Yan, and D. Gu, "Optimal path planning based on a multi-tree T-RRT* approach for robotic task planning in continuous cost spaces," in *12th France-Japan and 10th Europe-Asia Congress on Mechatronics*, 2018, pp. 242–247.

[158] M. Quigley, K. Conley, B. Gerkey, J. Faust, T. Foote, J. Leibs, R. Wheeler, and A. Y. Ng, "ROS: an open-source Robot Operating System," in *ICRA Workshop on Open Source Software*, vol. 3, 2009, p. 5.

[159] D. E. Breen, D. H. House, and M. J. Wozny, "A particle-based model for simulating the draping behavior of woven cloth," *Textile Research Journal*, vol. 64, no. 11, pp. 663–685, 1994.

[160] J. Flusser, S. Farokhi, C. Höschl, T. Suk, B. Zitova, and M. Pedone, "Recognition of images degraded by Gaussian blur," *IEEE Transactions on Image Processing*, vol. 25, no. 2, pp. 790–806, 2015.

[161] M. Young, "Pinhole optics," *Applied Optics*, vol. 10, no. 12, pp. 2763–2767, 1971.

[162] Z. Xu, B.-S. Shin, and R. Klette, "Accurate and robust line segment extraction using minimum entropy with Hough transform," *IEEE Transactions on Image Processing*, vol. 24, no. 3, pp. 813–822, 2014.

[163] J. Brownlee, "Train neural networks with noise to reduce overfitting," *Machine Learning Mastery*, 2019.

[164] K. Vallons, I. Duque, S. Lomov, and I. Verpoest, "Fibre orientation effects on the tensile properties of biaxial carbon/epoxy ncf composites," in *Proceedings of the ICCM International Conference on Composite Materials, Edinburgh, UK*, 2009, pp. 27–31.

[165] A. Björnsson, "Automated layup and forming of prepreg laminates," Ph.D. dissertation, Linköping University Electronic Press, 2017.

[166] R. Mautz and S. Tilch, "Survey of optical indoor positioning systems," in *International Conference on Indoor Positioning and Indoor Navigation*, 2011, pp. 1–7.

[167] S. Garrido-Jurado, R. Muñoz-Salinas, F. J. Madrid-Cuevas, and M. J. Marín-Jiménez, "Automatic generation and detection of highly reliable fiducial markers under occlusion," *Pattern Recognition*, vol. 47, no. 6, pp. 2280–2292, 2014.

[168] A. Babinec, L. Jurišica, P. Hubinskỳ, and F. Duchoň, "Visual localization of mobile robot using artificial markers," *Procedia Engineering*, vol. 96, pp. 1–9, 2014.

[169] A. Ben-Afia, L. Deambrogio, D. Salós, A.-C. Escher, C. Macabiau, L. Soulier, and V. Gay-Bellile, "Review and classification of vision-based localisation techniques in unknown environments," *IET Radar, Sonar & Navigation*, vol. 8, no. 9, pp. 1059–1072, 2014.

[170] C. Liu and M. Tomizuka, "Modeling and controller design of cooperative robots in workspace sharing human-robot assembly teams," in *IEEE/RSJ International Conference on Intelligent Robots and Systems*, 2014, pp. 1386–1391.

[171] Z. Li, X. Li, Q. Li, H. Su, Z. Kan, and W. He, "Human-In-the-Loop control of soft exosuits using impedance learning on different terrains," *IEEE Transactions on Robotics*, vol. 38, no. 5, pp. 2979–2993, 2022.

[172] X. Yu, W. He, Q. Li, Y. Li, and B. Li, "Human-robot co-carrying using visual and force sensing," *IEEE Transactions on Industrial Electronics*, vol. 68, no. 9, pp. 8657–8666, 2020.

[173] X. Yu, B. Li, W. He, Y. Feng, L. Cheng, and C. Silvestre, "Adaptive-constrained impedance control for human–robot co-transportation," *IEEE Transactions on Cybernetics*, vol. 52, no. 12, pp. 13 237–13 249, 2021.

[174] A. Loria, J. Dasdemir, and N. A. Jarquin, "Leader-follower formation and tracking control of mobile robots along straight paths," *IEEE Transactions on Control Systems Technology*, vol. 24, no. 2, pp. 727–732, 2015.

[175] D. Simon, *Optimal state estimation: Kalman, H infinity, and nonlinear approaches*. John Wiley & Sons, 2006.

[176] J. Canny, "A computational approach to edge detection," *IEEE Transactions on Pattern Analysis and Machine Intelligence*, no. 6, pp. 679–698, 1986.

[177] S. Suzuki *et al.*, "Topological structural analysis of digitized binary images by border following," *Computer Vision, Graphics, and Image Processing*, vol. 30, no. 1, pp. 32–46, 1985.

[178] N. Otsu, "A threshold selection method from gray-level histograms," *IEEE Transactions on Systems, Man, and Cybernetics*, vol. 9, no. 1, pp. 62–66, 1979.

[179] D. W. Marquardt, "An algorithm for least-squares estimation of nonlinear parameters," *Journal of The Society for Industrial and Applied Mathematics*, vol. 11, no. 2, pp. 431–441, 1963.

[180] H. C. Kam, Y. K. Yu, and K. H. Wong, "An improvement on Aruco marker for pose tracking using Kalman filter," in *IEEE/ACIS International Conference on Software Engineering, Artificial Intelligence, Networking and Parallel/Distributed Computing (SNPD)*, 2018, pp. 65–69.

[181] D. S. Schueftan, M. J. Colorado, and I. F. M. Bernal, "Indoor mapping using SLAM for applications in Flexible Manufacturing Systems," in *IEEE 2nd Colombian Conference on Automatic Control (CCAC)*, 2015, pp. 1–6.

[182] R. Bansal, G. Raj, and T. Choudhury, "Blur image detection using Laplacian operator and Open-CV," in *International Conference System Modeling & Advancement in Research Trends (SMART)*, 2016, pp. 63–67.

[183] R. C. Gonzalez, *Digital image processing*. Pearson Education India, 2009.

[184] C. Cai, A. Liu, and B. Zhang, "Motion deblurring from a single image," in *IEEE 20th International Conference on Computer Supported Cooperative Work in Design (CSCWD)*, 2016, pp. 406–410.

[185] H. Papasaika-Hanusch, "Digital image processing using matlab," *Institute of Geodesy and Photogrammetry*, vol. 63, 1967.

[186] M. F. Wahab, F. Gritti, and T. C. O'Haver, "Discrete fourier transform techniques for noise reduction and digital enhancement of analytical signals," *TrAC Trends in Analytical Chemistry*, vol. 143, p. 116354, 2021.

[187] J. Immerkaer, "Fast noise variance estimation," *Computer vision and image understanding*, vol. 64, no. 2, pp. 300–302, 1996.

[188] E. Rublee, V. Rabaud, K. Konolige, and G. Bradski, "ORB: An efficient alternative to SIFT or SURF," in *International Conference on Computer Vision*, 2011, pp. 2564–2571.

[189] E. Rosten and T. Drummond, "Machine learning for high-speed corner detection," in *European Conference on Computer Vision*, 2006, pp. 430–443.

[190] D. Prokhorov, D. Zhukov, O. Barinova, K. Anton, and A. Vorontsova, "Measuring robustness of visual slam," in *International Conference on Machine Vision Applications (MVA)*, 2019, pp. 1–6.

[191] A. K. Pandey and R. Gelin, "A mass-produced sociable humanoid robot: Pepper: The first machine of its kind," *IEEE Robotics & Automation Magazine*, vol. 25, no. 3, pp. 40–48, 2018.

[192] J. Fleischer, R. Teti, G. Lanza, P. Mativenga, H.-C. Möhring, and A. Caggiano, "Composite materials parts manufacturing," *CIRP Annals*, vol. 67, no. 2, pp. 603–626, 2018.

[193] R. K. Malhan, A. V. Shembekar, A. M. Kabir, P. M. Bhatt, B. Shah, S. Zanio, S. Nutt, and S. K. Gupta, "Automated planning for robotic layup of composite prepreg," *Robotics and Computer-Integrated Manufacturing*, vol. 67, p. 102020, 2021.

[194] M. Elkington, D. Bloom, C. Ward, A. Chatzimichali, and K. Potter, "Hand layup: understanding the manual process," *Advanced Manufacturing: Polymer & Composites Science*, vol. 1, no. 3, pp. 138–151, 2015.

[195] V. A. Prabhu, M. Elkington, D. Crowley, A. Tiwari, and C. Ward, "Digitisation of manual composite layup task knowledge using gaming technology," *Composites Part B: Engineering*, vol. 112, pp. 314–326, 2017.

[196] M. N. Grimshaw, "Automated tape laying," 2001.

[197] G. Marsh, "Automating aerospace composites production with fibre placement," *Reinforced Plastics*, vol. 55, no. 3, pp. 32–37, 2011.

[198] L. Zhang, X. Wang, J. Pei, and Y. Zhou, "Review of automated fibre placement and its prospects for advanced composites," *Journal of Materials Science*, vol. 55, no. 17, pp. 7121–7155, 2020.

[199] A. C. Long, *Composites forming technologies*. Elsevier, 2014.

[200] R. Buckingham and G. Newell, "Automating the manufacture of composite broadgoods," *Composites Part A: Applied Science and Manufacturing*, vol. 27, no. 3, pp. 191–200, 1996.

[201] D. E. Ruth and P. Mulgaonkar, "Robotic lay-up of prepreg composite plies," in *IEEE International Conference on Robotics and Automation*, 1990, pp. 1296–1300.

[202] A. Björnsson, M. Jonsson, and K. Johansen, "Automated material handling in composite manufacturing using pick-and-place systems-a review," *Robotics and Computer-Integrated Manufacturing*, vol. 51, pp. 222–229, 2018.

[203] A. Schuster, M. Kupke, and L. Larsen, "Autonomous manufacturing of composite parts by a multi-robot system," *Procedia Manufacturing*, vol. 11, pp. 249–255, 2017.

[204] M. Szcesny, F. Heieck, S. Carosella, P. Middendorf, H. Sehrschön, and M. Schneiderbauer, "The advanced ply placement process-an innovative direct 3D placement technology for plies and tapes," *Advanced Manufacturing: Polymer & Composites Science*, vol. 3, no. 1, pp. 2–9, 2017.

[205] R. K. Malhan, A. M. Kabir, A. V. Shembekar, B. Shah, S. K. Gupta, and T. Centea, "Hybrid cells for multi-layer prepreg composite sheet layup," in *IEEE 14th International Conference on Automation Science and Engineering (CASE)*, 2018, pp. 1466–1472.

[206] R. K. Malhan, R. J. Joseph, A. V. Shembekar, A. M. Kabir, P. M. Bhatt, and S. K. Gupta, "Online grasp plan refinement for reducing defects during robotic layup of composite prepreg sheets," in *IEEE International Conference on Robotics and Automation (ICRA)*, 2020, pp. 11 500–11 507.

[207] M. Schöberl, K. Kasnakli, and A. Nowak, "Measuring strand orientation in carbon fiber reinforced plastics (CFRP) with polarization," in *World Conference on Non-Destructive Testing*, 2016.

[208] L. Nelson and R. Smith, "Fibre direction and stacking sequence measurement in carbon fibre composites using Radon transforms of ultrasonic data," *Composites Part A: Applied Science and Manufacturing*, vol. 118, pp. 1–8, 2019.

[209] L. Shi and S. Wu, "Automatic fiber orientation detection for sewed carbon fibers," *Tsinghua Science and Technology*, vol. 12, no. 4, pp. 447–452, 2007.

[210] R. Schmitt, T. Fürtjes, B. Abbas, P. Abel, W. Kimmelmann, P. Kosse, and A. Buratti, "Real-time machine-vision-system for an automated quality monitoring in mass production of multiaxial non-crimp fabrics," in *Automation, Communication and Cybernetics in Science and Engineering 2015/2016*. Springer, 2016, pp. 769–782.

[211] P. Kosse, E. Soemer, R. Schmitt, B. Engel, and J. Deitmerg, "Optical detection and analysis of the fiber waviness of bent fiber-thermoplastic composites," *Technical Measurement*, vol. 83, no. 1, pp. 43–52, 2016.

[212] R. Schmitt, C. Mersmann, and A. Schoenberg, "Machine vision industrialising the textile-based FRP production," in *Proceedings of 6th International Symposium on Image and Signal Processing and Analysis*, 2009, pp. 260–264.

[213] F. J. Romero-Ramirez, R. Muñoz-Salinas, and R. Medina-Carnicer, "Speeded up detection of squared fiducial markers," *Image and Vision Computing*, vol. 76, pp. 38–47, 2018.

[214] C. E. Ayres, B. S. Jha, H. Meredith, J. R. Bowman, G. L. Bowlin, S. C. Henderson, and D. G. Simpson, "Measuring fiber alignment in electrospun scaffolds: a user's guide to the 2D fast Fourier transform approach," *Journal of Biomaterials Science, Polymer Edition*, vol. 19, no. 5, pp. 603–621, 2008.

[215] D. York, "Least-squares fitting of a straight line," *Canadian Journal of Physics*, vol. 44, no. 5, pp. 1079–1086, 1966.

[216] R. N. Bracewell and R. N. Bracewell, *The Fourier transform and its applications*. McGraw-Hill New York, 1986, vol. 31999.

[217] D. E. Wells and E. J. Krakiwsky, *The method of least squares*. Department of Surveying Engineering, University of New Brunswick Canada, 1971, vol. 18.

[218] C. Mineo, M. Vasilev, B. Cowan, C. N. MacLeod, S. G. Pierce, C. Wong, E. Yang, R. Fuentes, and E. J. Cross, "Enabling robotic adaptive behaviour capabilities for new Industry 4.0 automated quality inspection paradigms," *Insight-Non-Destructive Testing and Condition Monitoring*, vol. 62, no. 6, pp. 338–344, 2020.

[219] S. Zambal, W. Palfinger, M. Stöger, and C. Eitzinger, "Accurate fibre orientation measurement for carbon fibre surfaces," *Pattern Recognition*, vol. 48, no. 11, pp. 3324–3332, 2015.

[220] A. J. Hunt and J. P. Carey, "A machine vision system for the braid angle measurement of tubular braided structures," *Textile Research Journal*, vol. 89, no. 14, pp. 2919–2937, 2019.

[221] B. Corves, J. Brinker, I. Prause, M. Hüsing, B. Abbas, H. Krieger, and P. Kosse, "AutoHD—Automated handling and draping of reinforcing textiles," in *Mechanisms, Transmissions and Applications*. Springer, 2015, pp. 301–309.

Appendix A

Hardware Specifications

Table A.1: Hardware used in this thesis.

Hardware	Quantity	Specification
Robotic manipulator	3	The Universal Robots UR10e KUKA KR90 R3100 KUKA KR90
Mobile robot	2	Turtlebot3 Burger Pepper Robot
Ultrasonic sensor system	1	Starter Set Super-MP-3D
IMU	1	MPU9250
Camera	3	Webcam OptiTrack V120: Trio Intel® RealSense™ depth camera D435i

Appendix B

Model Parameters for Composite Material Deformation

One important factor in modeling deformable objects is the stiffness level of the material. The adopted method for modeling deformable objects in CoppeliaSim enables this stiffness to be adjusted by tweaking two different types of model parameters: the x and y dimensions of each individual primitive cuboid (represented by L_x and L_y respectively) and the principle moments of inertia along the x, y and z axes (represented by I_x, I_y and I_z respectively). The primitive cuboid dimensions and principle moments of inertia are presented in the table below, where the height of each cuboid represents the thickness of the composite material.

Table B.1: Model parameters for composite material deformation.

Model parameters	**Value**
Principle moment of inertia I_x $/mm^2$	1.25
Principle moment of inertia I_y $/mm^2$	4.25
Principle moment of inertia I_z $/mm^2$	15.00
Length L_x $/mm$	12.00
Width L_y $/mm$	6.00
Height L_z $/mm$	1.00